

**THE IMPACT OF COMMON LABORATORY CONTAMINATION ON THE  
STABILITY OF A COLLOIDAL GRAPHENE SOLUTION**

by

**Christopher J. Kurpiel**

Bachelor of Science, Chemistry, United States Air Force Academy, 2004

Master of Aeronautical Science, Embry-Riddle Aeronautical University, 2011

Submitted to the Graduate Faculty of the  
Kenneth P. Dietrich School of Arts and Sciences in partial fulfillment  
of the requirements for the degree of  
Master of Science in Chemistry

University of Pittsburgh

2015

UNIVERSITY OF PITTSBURGH  
KENNETH P. DEITRICH SCHOOL OF ARTS AND SCIENCES

This thesis was presented

by

Christopher J. Kurpiel

It was defended on

November 24, 2015

and approved by

Dr. Alexander Star, Professor, Department of Chemistry

Dr. Jill Millstone, Assistant Professor, Department of Chemistry

Thesis Advisor: Dr. Haitao Liu, Assistant Professor, Department of Chemistry

**THE IMPACT OF COMMON LABORATORY CONTAMINATION ON THE  
STABILITY OF A COLLOIDAL GRAPHENE SOLUTION**

Christopher J. Kurpiel, M.S.

University of Pittsburgh, 2015

Copyright © by Christopher J. Kurpiel

2015

# **THE IMPACT OF COMMON LABORATORY CONTAMINATION ON THE STABILITY OF A COLLOIDAL GRAPHENE SOLUTION**

Christopher J. Kurpiel, M.S.

University of Pittsburgh, 2015

Since its isolation in 2004, graphene has captured the imagination of the scientific community with its unique physical and chemical properties. These properties hold promise in revolutionizing many industries with applications in electronics and protective coatings. However, the ability to produce graphene with homogeneous properties on the industrial scale has been elusive and delayed the material's wide scale use. One method of graphene synthesis that has shown promise in producing large amounts of graphene is solvent-based exfoliation. Graphene produced through solvent-based exfoliation is often manipulated in a colloidal solution where the stability of the suspension can impact the quality of the graphene. In this study, the solvent-based exfoliation of graphene in the solvent N-methyl-2-pyrrolidone was explored and the graphene produced characterized through UV-Vis, AFM, and Raman spectroscopy. Additionally the identity of a suspected laboratory contaminant observed to stabilize the colloidal solution was investigated through analytical techniques and identified as a low molecular weight copolymer consisting of mostly polyisoprene. Finally, the effect of the contaminant on the stability of the colloidal graphene suspension was confirmed through observation and UV-Vis kinetic studies. The experimental results were then compared to current literature and mechanisms of colloidal stability to understand the stabilization effect that was observed and quantify it for future use.

## TABLE OF CONTENTS

<b>LIST OF TABLES .....</b>	<b>IX</b>
<b>LIST OF FIGURES .....</b>	<b>X</b>
<b>LIST OF EQUATIONS.....</b>	<b>XII</b>
<b>ABRREVIATIONS.....</b>	<b>XIII</b>
<b>PREFACE.....</b>	<b>XV</b>
<b>1.0 INTRODUCTION.....</b>	<b>1</b>
<b>1.1 WHAT IS GRAPHENE? .....</b>	<b>1</b>
<b>1.2 GRAPHENE SYNTESIS METHODS.....</b>	<b>5</b>
<b>1.2.1 Top-down Methods.....</b>	<b>7</b>
<b>1.2.2 Bottom-up Methods.....</b>	<b>11</b>
<b>1.3 GRAPHENE CHARACTERIZATION.....</b>	<b>13</b>
<b>1.3.1 Ultraviolet-Visible Spectroscopy .....</b>	<b>14</b>
<b>1.3.2 Atomic Force Microscopy .....</b>	<b>15</b>
<b>1.3.3 Raman Spectroscopy .....</b>	<b>18</b>
<b>1.4 OTHER CHARACTERIZATION TECHNIQUES .....</b>	<b>22</b>
<b>1.4.1 High-Performance Liquid Chromatography .....</b>	<b>22</b>
<b>1.4.2 Mass Spectroscopy.....</b>	<b>25</b>
<b>1.4.3 Nuclear Magnetic Resonance .....</b>	<b>28</b>
<b>1.5 COLLOIDAL STABALIZATION.....</b>	<b>30</b>
<b>1.5.1 Electrostatic Stabilization .....</b>	<b>33</b>
<b>1.5.2 Steric Stabilization.....</b>	<b>34</b>

1.5.3	Stabilization of Solvent-Exfoliated Graphene in NMP .....	34
1.6	SPECIFIC AIMS .....	39
2.0	EXPERIMENTAL .....	41
2.1	MATERIALS .....	41
2.1.1	Graphene Synthesis .....	41
2.1.2	Colloidal Stabilization .....	42
2.2	SAMPLE PREPARATION .....	43
2.2.1	Graphene Synthesis .....	43
2.2.1.1	UV-Vis Spectroscopy .....	44
2.2.1.2	Atomic Force Microscopy .....	44
2.2.1.3	Raman Spectroscopy.....	45
2.2.2	Solvent Exchange.....	45
2.2.3	Colloidal Stabilization .....	46
2.2.3.1	Benchtop Observations.....	46
2.2.3.2	HPLC – MS.....	46
2.2.3.3	Nuclear Magnetic Resonance Spectroscopy .....	47
2.2.4	Colloidal Stabilization – Isoprene .....	47
2.2.4.1	Benchtop Observations.....	47
2.2.4.2	UV-Vis Spectroscopy – Kinetic.....	48
2.2.5	Colloidal Stabilization – Polyisoprene .....	48
2.3	CHARACTERIZATION METHODS.....	49
2.3.1	Graphene Synthesis .....	49
2.3.1.1	UV-Vis Spectroscopy .....	49

2.3.1.2	Atomic Force Microscopy .....	49
2.3.1.3	Raman Spectroscopy.....	49
2.3.2	Laboratory Contamination Studies .....	50
2.3.2.1	Benchtop Observations.....	50
2.3.2.2	High-Performance Liquid Chromatography .....	50
2.3.2.3	Mass Spectroscopy .....	51
2.3.2.4	Nuclear Magnetic Resonance Spectroscopy .....	51
2.3.3	Colloidal Stabilization - Isoprene.....	51
2.3.3.1	Benchtop Observations.....	51
2.3.3.2	UV-Vis Spectroscopy – Kinetic.....	52
<b>3.0</b>	<b>RESULTS AND DISCUSSION .....</b>	<b>53</b>
3.1.1	Graphene Synthesis .....	53
3.1.1.1	UV-Vis Spectroscopy .....	53
3.1.1.2	Atomic Force Microscopy .....	54
3.1.1.3	Raman Spectroscopy.....	55
3.1.2	Laboratory Contamination Studies .....	58
3.1.2.1	Benchtop Observations.....	60
3.1.2.2	High-Performance Liquid Chromatography .....	62
3.1.2.3	Mass Spectroscopy .....	64
3.1.2.4	Nuclear Magnetic Resonance Spectroscopy .....	66
3.1.3	Colloidal Stabilization – Isoprene .....	67
3.1.3.1	Benchtop Observations.....	69
3.1.3.2	UV-Vis Spectroscopy – Kinetic.....	71

<b>4.0</b>	<b>CONCLUSION AND FUTURE DIRECTIONS .....</b>	<b>74</b>
	<b>REFERENCES.....</b>	<b>80</b>

## LIST OF TABLES

Table 1. Surface Coverage ( $\Theta$ ) of Graphene Flakes with Isoprene .....	69
---	----

## LIST OF FIGURES

Figure 1. Allotropes of Carbon .....	2
Figure 2. Band Structure of Graphene .....	4
Figure 3. Graphene Synthesis Methods .....	6
Figure 4. Atomic Force Microscope .....	16
Figure 5. AFM Image of Graphene on Silicon Oxide Substrate.....	18
Figure 6. Raman Spectrum of a Graphene Edge.....	20
Figure 7. Comparison of the Raman Spectra of Graphite and Graphene .....	21
Figure 8. Block Diagram of a High Performance Liquid Chromatograph .....	24
Figure 9. Block Diagram of a Mass Spectrometer.....	26
Figure 10. Lennard-Jones Potential .....	33
Figure 11. Potential Mean Force Between Two Graphene Flakes .....	37
Figure 12. Predicted Distribution of Graphene Sheet Thickness.....	39
Figure 13. Experimental Set-up for Graphene Synthesis.....	43
Figure 14. Experimental UV-Vis Spectrum of Graphene.....	53
Figure 15. Experimental AFM Images of Graphene .....	55
Figure 16. Experimental Raman Spectrum of Graphene .....	57
Figure 17. Shape of the Raman 2D Band in Bi-Layer Graphene .....	58
Figure 18. Solvents Miscible with NMP.....	59
Figure 19. Solvent Exchange .....	60
Figure 20. Benchtop Observations.....	61
Figure 21. HPLC Chromatograms of Contaminants .....	63

Figure 22. Mass Spectrum of Contaminant .....	64
Figure 23. <sup>1</sup> H NMR of Contaminants .....	66
Figure 24. Solvent Accessible Area.....	69
Figure 25. Colloidal Stability Observation – 2.5 Hours .....	70
Figure 26. UV-Vis Kinetics Study – “Clean” Vial.....	71
Figure 27. UV-Vis Kinetics Study – “Clean” Vial with 1000 μL Isoprene .....	71
Figure 28. UV-Vis Kinetics Study – Absorbance at 660 nm.....	72
Figure 29. Graphene and Solvent Surface Energies .....	78

## LIST OF EQUATIONS

Equation 1. Beer – Lambert Law .....	15
Equation 2. Primary Reaction of Electron – Impact Ionization.....	27
Equation 3. Fick’s First Law.....	31
Equation 4. Estimation of the London Discursion Force.....	32
Equation 5. Simplification of the London Dispursion Force for Two Like Molecules .....	32
Equation 6. Lennard-Jones Potential .....	32
Equation 7. Gibbs Energy .....	34
Equation 8. Surface Energy .....	35
Equation 9. Enthalpy of Mixing per Unit Volume .....	35
Equation 10. Collision Frequency Between Two Graphene Sheets .....	38

## ABBREVIATIONS

AFM	Atomic Force Microscopy
CNTs	Carbon Nanotubes
CVD	Chemical Vapor Deposition
DMF	N,N-dimethylformamide
GNRs	Graphene Nanoribbons
HOPG	Highly Ordered Pyrolytic Graphite
HPLC	High Performance Liquid Chromatography
IUPAC	International Union of Pure and Applied Chemistry
MS	Mass Spectroscopy
MWCNTs	Multi-Walled Carbon Nanotubes
NMP	N-methyl-2-pyrrolidone
NMR	Nuclear Magnetic Resonance
PAH	Polycyclic Aromatic Hydrocarbon
PMF	Potential of Mean Force
RAFT	Reversible Addition-Fragmentation Chain Transfer
SiC	Silicon Carbide
SEM	Scanning Electron Microscopy
STM	Scanning Tunneling Microscopy
TEM	Transmission Electron Microscopy
UHV	Ultrahigh Vacuum
UV-Vis	Ultraviolet-Visible Spectroscopy

vdW	van der Waals
XPS	X-ray Photoelectron Microscopy

## PREFACE

I would like to thank Dr. Haitao Liu and the members of the Liu Research Group as well as the faculty and staff of the University of Pittsburgh's Department of Chemistry for their mentorship, knowledge, and guidance that helped this project advance. Additionally I would like to thank the United States Air Force Academy's Department of Chemistry for their sponsorship of my position in the Academy's Faculty Pipeline and the Air Force Institute of Technology's Civilian Institutions Program for administering the program that made my studies possible. Finally, I would like to thank all of my family and friends, too numerous to mention here, who without their support during the 18-month program, this would not be possible.

*A note to the reader:* There are multiple references to the unit "dram" (abbreviated dr or  $\mathfrak{D}$ ) in this text. The dram is a unit of volume from an outdated system of measure known as the "apothecaries" system. Many manufacturers still list and sell glass vials using this unit of measure instead of listing its volume in SI units (cubic meters,  $\text{m}^3$ ) or more a commonly used unit (milliliters, mL). A dram is defined as  $\frac{1}{8}$  fluid ounce and is equivalent to 3.696691 mL.<sup>1</sup> For reference, the 8 dram vials utilized during the course of this investigation have the capacity of approximately 29.6 mL.

## 1.0 INTRODUCTION

### 1.1 WHAT IS GRAPHENE?

Carbon, the sixth element on the periodic table, has been intertwined with human history like no other substance in history. Accounting for 18% of the human body,<sup>2</sup> carbon is not only the basis for all known life but has also played an important role in virtually every technological advancement made by mankind. First utilized as a tool approximately 300,000 to 400,000 years ago when humans harnessed fire,<sup>3</sup> carbon has been indispensable in the smelting of metals and the development of tools that has helped mankind advance through each epoch of history.<sup>4</sup> Later used by Avogadro to define the mole<sup>5</sup> and define the organic branch of chemistry, carbon has helped to shape the modern world by fueling the world's energy demands from the industrial revolution through the space age. Now firmly in the digital age carbon is once again reshaping the modern world through advanced materials that are turning ideas once only science fiction into reality.<sup>6</sup> Now in the first quarter of the 21<sup>st</sup> century a new allotrope of carbon, graphene, has again captured the imagination of the scientific community and continues to impact the advancement of mankind.

Carbon's discovery by man has been lost to antiquity but its origin in the cosmos has been traced to the fusion of alpha particles ( $\alpha$ ) in the interior of a star in a process that naturally forms carbon in a collection of allotropes.<sup>2</sup> Each allotrope of carbon boasts its own unique physical and chemical properties. The first allotropes of carbon known to mankind were the 3D allotropes; graphite, diamonds, and amorphous carbon. Used throughout history graphite has found countless industrial applications while diamonds have been valued not only for their beauty but also their

physical properties such as hardness. In the opening days of the digital age, the 0D allotrope of carbon came to the forefront of the scientific community with the discovery of the buckminsterfullerene ( $C_{60}$ ).<sup>7</sup> The buckminsterfullerene became the most visible member of a family of closed carbon cages in an  $sp^2$  network that saw considerable interest and research efforts.<sup>8</sup> The next allotrope of carbon to capture the spotlight was the 1D allotrope, the carbon nanotube (CNTs), after Iijima announced its isolation and characterization in *Nature*.<sup>9</sup> The unique physical and chemical properties of CNTs sparked countless research efforts resulting in over 24,000 journal articles and proposed diverse applications from antifouling maritime paint<sup>6</sup> to a space elevator.<sup>10</sup> However, despite the recent discoveries of fullerenes and CNTs along with the research surrounding them, the 2D allotrope of carbon remained a scientific mystery at end of the 20<sup>th</sup> century.

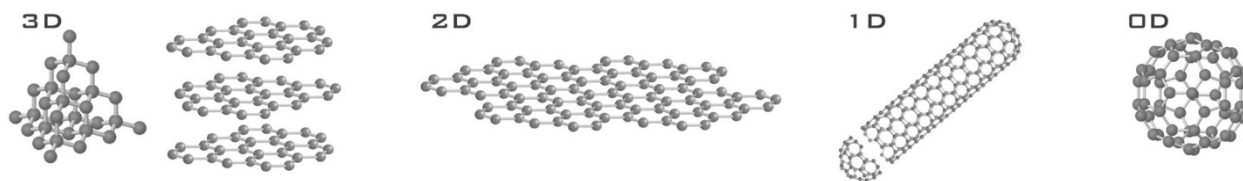


**Figure 1.** Allotropes of Carbon. The allotropes of carbon consist of 3D: diamond and graphite; 2D: graphene; 1D: CNTs; 0D fullerenes.<sup>11</sup>

Reprinted from *Mater. Today*, 10 (1-2), Katsnelson, M. I., Graphene: carbon in two dimensions, 21, **2007**, with permission from Elsevier.

Graphene did not remain a scientific mystery for so long due to a lack of scientific interest in the 2D allotrope. Studies related to graphene can be traced back as far as the 1840s when Schafhaeutl reported the exfoliation of graphite with sulfuric and nitric acids.<sup>12</sup> His work exemplified many of the early investigations related to graphene as the focus was centered on graphite oxide and the intercalation of graphite compounds. While much was learned about the structure of graphite, it was not until 1947 that some of the physical properties of the still to be isolated allotrope were first described by Philip R. Wallace as he investigated the unique electronic

properties of graphite.<sup>13</sup> Hanns-Peter Boehm made noteworthy contributions through the thermal exfoliation of graphite oxide and theoretically introduced the modern scientific community to the expected properties of the 2D allotrope.<sup>14</sup> Additionally, the nomenclature used to describe the 2D allotrope, “graphene,” was coined by Boehm and co-workers in 1986<sup>15</sup> and adopted by IUPAC in 1995.<sup>16</sup> According to the adopted definition;

“The suffix -ene is used for fused polycyclic aromatic hydrocarbons, even when the root of the name is of trivial origin, e.g. naphthalene, anthracene, coronene, etc. A single carbon layer of the graphitic structure can be considered as the final member of this series and the term graphene should therefore be used to designate the individual carbon layers in graphite intercalation compounds.”<sup>16</sup>

Despite advances with graphite oxide and identification of the theoretical properties of graphene it was not until 2004 that the isolation of pristine graphene by Konstantin Novoselov and Andre Geim at Manchester University occurred through micromechanical cleavage.<sup>17</sup> For their “groundbreaking experiments regarding the two-dimensional material graphene” the pair was awarded the 2010 Nobel Prize in Physics<sup>18</sup> and sparked the interest of the scientific community in a way unseen since the discovery of CNTs.

Part of the excitement around the isolation of pristine graphene has been the electrical, optical, and mechanical properties that have been reported. The unique electrical properties of graphene stem from its molecular structure that produces a zero band gap (Figure 2). Novoselov, Geim *et al.* first introduced the research community to the electrical properties by reporting that the electrons in graphene mimic relativistic particles with zero mass and can be modeled by Dirac’s (relativistic) equation.<sup>19</sup> Continued research has uncovered many more favorable properties including a high carrier mobility ( $>10^3 \text{ cm}^2 \text{ V}^{-1} \text{ s}^{-1}$ ) and high carrier density ( $>10^{12} \text{ cm}^{-2}$  for doped

samples).<sup>20</sup> These values of graphene make the material attractive for use in electronics as flexible electrodes and a possible replacement for the present industry standard, indium tin oxide.<sup>20</sup> Additionally, the theoretical surface area ( $2,630 \text{ m}^2 \text{ g}^{-1}$ ) eclipses that of traditional activated carbon (below  $1,500 \text{ m}^2 \text{ g}^{-1}$ ) and has generated interest in graphene for energy storage applications.<sup>21</sup>

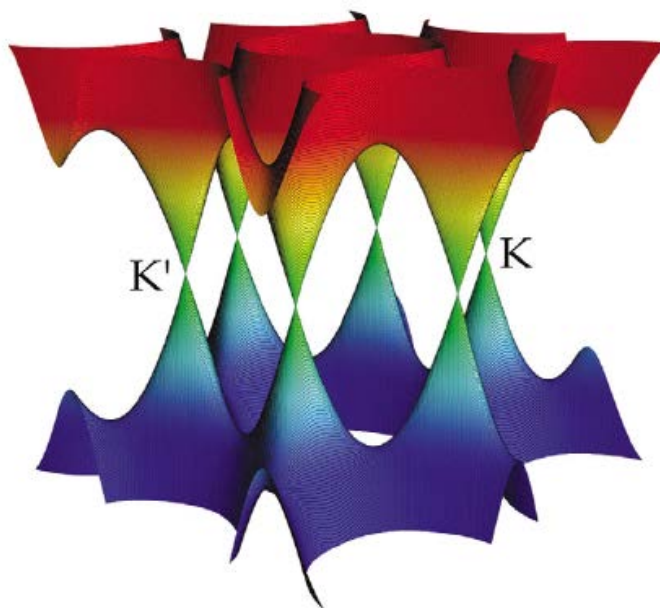


**Figure 2.** Band structure of graphene.<sup>11</sup>

Reprinted from *Mater. Today*, 10 (1-2), Katsnelson, M. I., Graphene: carbon in two dimensions, 22, 2007, with permission from Elsevier.

The optical and mechanical properties of graphene have also sparked considerable interest. With a reported optical conductivity of up to  $10^4 \text{ S m}^{-1}$ <sup>22</sup> and an absorbance of 2.3%<sup>23</sup> graphene is actively being pursued for a variety of electro-optical devices. The orientation of the carbon atoms bonded through  $\text{sp}^2$  hybridized orbitals in a graphene lattice contribute a considerable inherent strength along the carbon bonds ( $0.142 \text{ N m}$ ).<sup>24</sup> This arrangement results in an ultimate tensile strength of 103 GPa and a Young's modulus of 1 TPa, making it the strongest material ever discovered.<sup>24</sup> In addition to incredible strength, the structure of graphene produces an electron mobility of up to  $2.5 \times 10^5 \text{ cm}^2 \text{ V}^{-1} \text{ s}^{-1}$  and a thermal conductivity of more than  $3,000 \text{ W m K}^{-1}$ .<sup>24</sup>

Furthermore, the arrangement of  $sp^2$  carbon atoms in a hexagon pattern allows the material, even as a monolayer, to act as a perfect membrane to atomic species.<sup>25</sup> A property actively being explored for water filtration<sup>26</sup>, desalination<sup>27</sup>, and anticorrosion<sup>24</sup> applications.

Due to the unique properties of graphene, considerable interest from both researchers and industry have been shown to the 2D allotrope of carbon. The electrical, optical, and mechanical properties reported for graphene make it a unique material with considerable promising applications. However despite a promising future, the scientific community is only beginning to understand the mysteries surrounding the production and processing of graphene. Through continued research and innovation graphene may achieve its full potential in flexible electronics,<sup>20</sup> biomedical,<sup>28</sup> and aerospace<sup>29</sup> applications.

## 1.2 GRAPHENE SYNTHESIS METHODS

One of the defining physical properties of bulk graphite is that it is a highly anisotropic material. As such it is composed of individual graphene sheets stacked along the graphitic crystal's c-axis.<sup>30</sup> Each graphene sheet is made-up of carbon atoms oriented in a planer  $sp^2$ -hybridized structure with an interatomic distance of 1.42 Å.<sup>30</sup> To form the bulk material, the stacked graphene sheets are held together by relatively weak van der Waals (vdW) forces at a distance of 3.35 Å, the disruption of which has enabled the isolation of graphene.<sup>30</sup> Since Novoselov and Geim first reported a reliable method for disrupting the attraction between layers of highly oriented pyrolytic graphite (HOPG) through micromechanical cleavage,<sup>17</sup> researchers have discovered a plethora of methods capable of disrupting the van der Waals forces of graphite to isolate graphene.<sup>30</sup>

The synthetic routes used to prepare graphene are divided into two basic methodologies: top-down methods and bottom-up methods (Figure 3).<sup>30</sup> Top-down refers to a family of methods that use another allotrope of carbon as the starting material for the synthesis and manipulate it to isolate the more fundamental component of graphene.<sup>30</sup> Top down methods include mechanical exfoliation of graphite,<sup>17</sup> solution-based exfoliation of graphite,<sup>31</sup> electrochemical exfoliation of graphite,<sup>32</sup> chemical oxidation of graphite,<sup>33</sup> and unzipping CNTs.<sup>34</sup> Bottom-up methods in contrast use a catalytic process to build graphene sheets from small organic molecules.<sup>30</sup> The most common bottom-up methods include chemical synthesis,<sup>35</sup> epitaxial growth on silicon carbide (SiC),<sup>36</sup> and chemical vapor deposition (CVD) techniques.<sup>37-38</sup> Each method has its own advantages and disadvantages that contribute to the throughput and scalability of the method as well as its reproducibility, quality, and physical properties. Solution based exfoliation was the technique chosen to prepare graphene for this research.

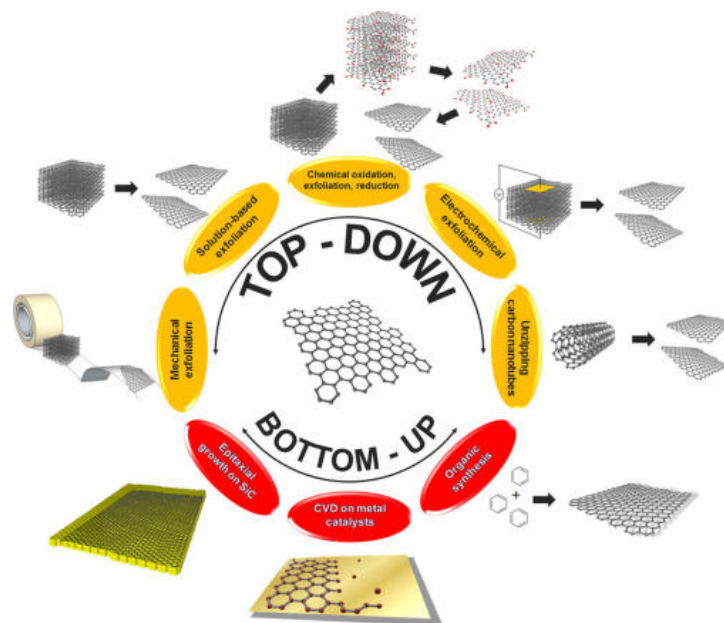


**Figure 3.** Graphical display of graphene synthesis methods. Top-Down methods include mechanical exfoliation, solution based exfoliation, chemical oxidation, electrochemical exfoliation, and unzipping CNTs. Bottom-up methods include epitaxial growth on SiC, chemical vapor deposition, and organic synthesis.<sup>30</sup>

Reprinted with permission from *Chem. Rev.*, **2014**, 114 (14), pp 7150-7188.  
Copyright (2014) American Chemical Society.

### 1.2.1 Top-down Methods

Top-down synthetic routes for the preparation of graphene typically focus on methods capable of weakening the van der Waals' interactions holding the stacked graphene sheets of graphite together. Methods to break the vdW forces include mechanical exfoliation,<sup>17</sup> solution-based exfoliation,<sup>31</sup> electrochemical exfoliation,<sup>32</sup> and the chemical oxidation of graphite.<sup>33</sup> In addition to using bulk graphite as the starting material, CNTs have also been used in the top-down synthesis of graphene through unrolling CNTs into graphene sheets.<sup>34</sup> Despite the different synthetic routes all top-down methods are commonly focused on isolating the more fundamental graphene sheets that compose the 3D and 1D allotropes of carbon.

The first reported method of isolating pristine graphene was pioneered by Novoselov and Geim in 2004.<sup>17</sup> Their technique known as micromechanical cleavage, colloquially called the “scotch tape method,” is a mechanical method of graphene exfoliation.<sup>30</sup> To isolate graphene flakes, a piece of adhesive tape was pressed against a prepared piece of HOPG and used to peel off layers of the graphitic crystal by overcoming the inter-layer vdW forces between graphene sheets.<sup>17</sup> This technique reliably produced flakes up to 10  $\mu\text{m}$  in size and were subsequently transferred to a Si substrate for characterization.<sup>17</sup> Mechanical exfoliation is considered to produce the most pristine graphene of any synthetic method and exhibits many of the physical and chemical properties that have generated the scientific interest around graphene.<sup>30</sup> Despite the pristine nature of the graphene prepared through this technique, mechanical exfoliation has a very low throughput and lacks the defects needed for certain electronic applications.<sup>30</sup>

Solution-based exfoliation is a method that has been developed to disrupt the vdW forces between graphene layers in bulk graphite through the exposure of graphite to certain chemicals in solution. Many organic solvents have been used in solution-based exfoliation methods with

NMP<sup>39</sup> and DMF<sup>40</sup> being two of the most widely used. Solvents with a Hildebrand solubility parameter of  $\delta T \sim 23 \text{ MPa}^{1/2}$  and Hansen solubility parameters of  $\delta D \sim 18 \text{ MPa}^{1/2}$ ,  $\delta P \sim 9.3 \text{ MPa}^{1/2}$ , and  $\delta H \sim 7.7 \text{ MPa}^{1/2}$  have been reported as suitable for solution-based exfoliation with dispersibility decreasing as the values vary from these ideal values.<sup>41</sup> In solution-based exfoliation methods, ultra-sonication is often used as a driving force in weakening the attractive forces with the time of sonication greatly effecting the concentration of graphene obtained.<sup>31</sup> Variations in the experimental conditions utilized have resulted in reported graphene concentrations of up to  $63 \text{ mg mL}^{-1}$  using ultra-sonication.<sup>42</sup> A possibly undesirable side-effect of sonication is the splintering of the graphene sheets into small inhomogeneous flakes. Methods of solution-based exfoliation have been reported that do not use sonication but instead include a preparation step in which the graphite is intercalated with potassium prior to exfoliation with NMP, a method that has reported concentrations up to  $2 \text{ mg mL}^{-1}$ .<sup>43</sup> Furthermore, another method of disrupting the vdW forces in the presence of a solvent called “turbulence-assisted shear exfoliation of graphene” has been reportedly accomplished using a kitchen blender<sup>44</sup> and shows the robustness and simplicity of this method of exfoliation to disrupt the vdW forces between graphene layers. For certain uses, solution-based exfoliation methods often include the use of a surfactant, such as sodium cholate,<sup>45</sup> to prevent aggregation and contribute to the stability of the graphene suspension. The surfactants however bind tightly to the graphene and have been shown to affect the electrical properties of the graphene produced. Surfactant free methods have therefore been studied to address the potentially undesirable presence of surfactant on graphene flakes.<sup>42, 46</sup> With a wide variety of solution-based methods of exfoliation reported, the technique has been widely studied due to its relative simplicity, scalability, and the quality of graphene produced. However, graphene produced through solution-based exfoliation is often multi-layer graphene and hard to separate.<sup>47</sup>

Furthermore, sonication can alter the electronic properties of graphene making it undesirable for certain uses.<sup>48</sup> A surfactant free, solution-based exfoliation of graphene based on a method developed by Khan *et al.* was used in this research study.<sup>42</sup>

The electrochemical exfoliation of graphene is a two-step process that involves the intercalation of ions within graphite followed by exfoliation in the presence of an electrical bias.<sup>30</sup> The intercalation of graphite is carried out in an electrochemical cell with a graphitic working electrode, a platinum counter electrode, and a reference electrode (Ag/AgCl is commonly used).<sup>30</sup> The electrolyte can be either aqueous or organic with both sulfuric acid<sup>32</sup> and poly(styrenesulfonate)<sup>49</sup> electrolytes being reported in the literature. Either a cathodic (reduction) or anodic (oxidation) potential can be applied to the cell to intercalate ions in the graphite.<sup>30</sup> The choice of potential will influence the properties of the graphene produced. For instance, an anodic current will produce graphene oxide characterized by structural defects and oxygen functional groups.<sup>30</sup> During this step, a positive potential will cause negatively charged ions to be formed<sup>30</sup> and is followed by the exfoliation step that involves the application of a negative potential to yield a stable colloidal graphene solution.<sup>50</sup> Advantages of electrochemical exfoliation are its relatively limited environmental impact, speed, and moderate reaction conditions.<sup>51</sup> The technique also allows the reaction conditions to be closely controlled through manipulation of the electrochemical cell if certain properties are desired.<sup>30</sup> The electrochemical exfoliation method is irreversible and the structural damage along with the presence of oxygen functional groups has a large impact on the electrochemical properties of the graphene produced.<sup>30</sup>

The preparation of graphene from the chemical oxidation of graphite is a multistep process that involves the oxidation, exfoliation, and reduction of a graphitic sample.<sup>30</sup> This method seeks to disrupt the vdW forces between graphene layers by a chemical species intercalating between

the layers and then expanding to weaken the attractive forces. One method of introducing a chemical species to the graphite network is through oxidative intercalation which exposes a strong oxidizing agent to concentrated sulfuric and nitric acids.<sup>30</sup> This effect was first observed in 1859 as Brodie generated highly oxidized graphite in an effort to determine the exact formula of graphite.<sup>52</sup> The technique has since been refined by the work of Staudenmaier (1898),<sup>53</sup> Hummers (1958),<sup>54</sup> and Tour (2010).<sup>33</sup> Brodie and Staudenmaier used potassium chlorate as the oxidizing agent while the modern method of preparing graphite oxide pioneered by Hummers uses potassium permanganate to eliminate the formation of hazardous  $\text{ClO}_2$  gas.<sup>30</sup> Through the oxidation of graphite, the inter-plane distance between layers of graphene is increased from 3.35 Å to more than 6 Å.<sup>30</sup> The vdW forces are subsequently weakened and allow the graphene planes to be separated with moderate sonication.<sup>12</sup> Using this method and graphite oxide as a precursor for graphene, it must be reduced through either thermal, electrochemical, or chemical methods to eliminate the oxygen functional groups and re-establish the  $\text{sp}^2$  structure.<sup>30</sup> The chemical method of reduction is most commonly used even though it will not remove all of the oxygen functional groups from the graphene.<sup>30</sup> As a result of the remaining functional groups, the resulting graphene displays physical properties very different from those of pristine graphene and may be desired based on the final application of the graphene produced.<sup>30</sup> The synthesis of graphene from graphite oxide is a widely used technique because it is scalable and produces graphene with unique electrical properties ideal for transducers and other electrochemical devices.<sup>30</sup>

Carbon nanotubes are often described “as rolled up graphene sheets” and are therefore a logical starting material for the top-down synthesis of graphene.<sup>34</sup> Graphene is produced from CNTs in a chemical process similar to the formation of graphite oxide as ions are intercalated between graphene layers and the induced stress causes the attractive forces of the molecule to

breakdown. One method of unzipping CNTs is through the Billups reduction protocol.<sup>55</sup> Through this sequence lithium and liquid NH<sub>3</sub> are intercalated between the layers of multi-walled carbon nanotubes (MWCNTs) and increase the inter-layer distance from 3.35 Å to 6.62 Å, enough strain to cause the walls of the CNTs break.<sup>34</sup> Graphene produced through this method can be described as graphene nanoribbons (GNRs), a graphene molecule with a large aspect ratio and a width of less than 10 nm.<sup>56</sup> GNRs are desirable because their band gap can be engineered through changes in the width of the molecules by selecting the appropriate CNT precursor.<sup>30</sup> The possibility of the mass production of GNRs with tunable band gaps makes graphene synthesized through this approach attractive to electronic applications.<sup>57</sup> One possible side-effect of this synthesis comes from the uses of a metal nanoparticle as a catalyst during the synthesis of CNTs. As a result metallic impurities will be present and persist in any graphene manufactured through this process and will impact the quality of the graphene produced.<sup>30</sup> Another side-effect of the way in which the graphene sheets are formed from CNTs is that many exposed edges are created which could be desirable for further chemical modification depending on the ultimate use of the graphene created.<sup>34</sup>

### **1.2.2 Bottom-up Methods**

Bottom-up methods make use of a catalyst to form the required chemical conditions for smaller organic molecules to be arranged into the sp<sup>2</sup> hybridized network of graphene. Bottom-up methods of graphene synthesis include organic synthesis,<sup>35</sup> epitaxial growth on SiC,<sup>36</sup> and CVD techniques.<sup>37-38</sup>

Organic synthesis is one method of bottom-up graphene production that has been reported in the literature.<sup>35,58</sup> Starting from a precursor monomer and using organic synthesis techniques,

graphene ribbons of 30 nm in length have been reported.<sup>35</sup> The organic methods involved in the production of graphene limit the potential size of graphene sheets produced through this approach to a few nanometers.<sup>30</sup> This limitation occurs because molecules larger than a few nanometers will no longer be soluble in organic solvents which enables undesirable side reactions and prevents further growth.<sup>30</sup> The largest graphene molecule reported through an organic synthetic route is 3.2 nm and contained 222 carbons.<sup>58</sup>

The epitaxial growth of graphene on SiC wafers is another well-established bottom-up synthetic route.<sup>36</sup> In this process the SiC substrate is heated to high temperatures (~1000°C) under ultrahigh vacuum (UHV) conditions.<sup>59</sup> Under these conditions, the Si atoms in the substrate sublime leaving a layer of carbon atoms that rearrange to form layers of epitaxial graphene.<sup>30</sup> Graphene produced through this method have electrical properties different than those obtained through mechanical exfoliation due to the manifestation of substrate-induced corrugations and nonstandard orientations of the layers.<sup>30</sup> Epitaxial growth on SiC shows substantial promise in the electronics industry because of its compatibility with current industry practices, however the high cost of the SiC substrate is prohibitive for industrial scale operations.<sup>30</sup>

CVD is a well-established nanofabrication technique that has been used in the synthesis of CNTs<sup>60</sup> that has been adapted to produce both single and few layer graphene.<sup>30</sup> During synthesis through this method, a carbon source is thermally decomposed in the presence of a catalyst, often a transition metal, and the carbon atoms deposit and orient themselves into the  $sp^2$  hybridized honeycomb structure.<sup>30</sup> In the synthesis of 1D CNTs, metal nanoparticles are used as the catalyst.<sup>60</sup> The technique has been adapted for the synthesis of graphene where the metal nanoparticles have been replaced by a larger metal surface on which the carbon atoms are deposited.<sup>30</sup> CVD typically makes use of methane, ethane, or propane<sup>61</sup> as the carbon source, however a plethora of exotic

carbon materials have been used including a Girl Scout cookie, polystyrene plastic, blades of grass and animal excrement<sup>62</sup> to show the robustness of the technique and the possibility of low cost precursors. Graphene has successfully been grown through CVD on a variety of metal substrates that include ruthenium,<sup>63</sup> platinum,<sup>64</sup> iridium,<sup>65</sup> nickel,<sup>37</sup> and copper<sup>66</sup> with nickel and copper being the most studied due to their availability and relatively low cost.<sup>67-68</sup> As important as the growth process via CVD is the transfer<sup>69</sup> of the graphene sheet from the metal catalyst to a suitable substrate as the quality of the graphene can be severely degraded in the transition.<sup>70</sup> There has been considerable research and excitement around the CVD synthesis of graphene because its low cost and efficiency make its use on an industrial scale a possibility.<sup>71</sup> Although the electrochemical properties of CVD produced graphene differ from mechanically exfoliated graphene possible applications are being explored in transistors,<sup>72</sup> electrodes,<sup>73</sup> and anti-corrosion coatings.<sup>74</sup>

### **1.3 GRAPHENE CHARACTERIZATION**

Since the isolation of pristine graphene in 2004,<sup>17</sup> the scientific community has developed new and adapted existing analytical techniques to characterize graphene and its physical properties. These techniques include, but are not limited to, optical microscopy,<sup>17</sup> ultraviolet-visible spectroscopy (UV-Vis),<sup>31</sup> scanning probe microscopies (atomic force microscopy (AFM)<sup>31</sup> and scanning tunneling microscopy (STM)<sup>30</sup>), electron microscopies (scanning electron microscopy (SEM)<sup>30</sup> and transmission electron microscopy (TEM)<sup>42</sup>), electron diffraction study,<sup>75</sup> x-ray photoelectron spectroscopy (XPS)<sup>76</sup>, and Raman spectroscopy.<sup>77</sup> As detailed below, UV-Vis, AFM, and Raman

spectroscopy techniques were chosen to identify and characterize graphene exfoliated through long-duration sonication.

### **1.3.1 Ultraviolet-Visible Spectroscopy**

UV-Vis is a useful technique to characterize graphene due to the relatively unstable  $\pi$  bonds of the  $sp^2$  hexagonal carbon lattice in graphene and their excitement from radiation in the ultraviolet and visible region of the electromagnetic spectrum.

Light in the visible region of the electromagnetic spectrum and has been formally studied since 1666 when Sir Isaac Newton used a prism to separate white light into individual colors and concluded that each color was bent differently by the prism.<sup>78</sup> The study of the visible spectrum and its interaction with matter continued over the centuries as line spectra were observed and emission spectra were used to characterize the elements. It was not until Niels Bohr reconciled the observed spectral lines with recently discovered quantum ideas in 1913 that the scientific community was introduced to the idea that electrons exist in defined states of energy and can only transition from one state to another.<sup>78</sup> He explained that the observed spectral lines are the result of electron transitions that emit or absorb exactly the amount of energy that defines the difference between the two states.<sup>78</sup> These ideas were further developed into the analytical technique of UV-Vis spectroscopy with the first commercial UV-Vis spectrometer, the Cary 11, being delivered to the Mellon Institute in 1947.<sup>79</sup>

UV-Vis spectroscopy is used to characterize graphene through the observed absorbance and its relationship to the concentration of the absorbing species. The Beer-Lambert law (equation 1), commonly referred to as Beer's Law, relates the measured absorbance to the concentration of graphene present in a sample.<sup>31</sup>

$$A = \alpha C_G \ell$$

**Equation 1.** Beer-Lambert Law.<sup>31</sup>

$A$  = Absorption;  $\alpha$  = absorption coefficient;  $C_G$  = concentration of graphene;  $\ell$  = path length

In the Beer-Lambert equation,  $A$  is the absorptivity of the absorbing species and is given in the units  $\text{L g}^{-1} \text{cm}^{-1}$ .<sup>80</sup> The absorption coefficient,  $\alpha$ , is a proportionality constant and expressed in  $\text{L mol}^{-1} \text{cm}^{-1}$ .<sup>80</sup> The path length,  $\ell$ , is the distance that the must travel through the sample and is reported in  $\text{cm}$ .<sup>80</sup> Finally,  $C_G$  represents the concentration of the absorbing species and is given in  $\text{mol L}^{-1}$ .<sup>80</sup>

### 1.3.2 Atomic Force Microscopy

AFM is a widely used characterization technique that is used to characterize both the size and the thickness of graphene flakes with atomic resolution.

AFM is a characterization technique that can be classified as a type of scanning probe microscopy (SPM). Optical microscopes cannot resolve features on the atomic level due to the wave nature of light and is limited to features one half of the wavelength of the incident light, the diffraction limit.<sup>81</sup> SPM is a branch of characterization techniques that have been developed to overcome the inherent limitations of optical microscopy and can generically be described as a technique that can obtain atomic resolution through rastering an atomically sharp tip across the sample's surface and measuring its interaction. The basic components common in SPM are the tip, laser, piezoelectric scanner, and feedback loop while the specific interaction with the surface is unique to each method of SPM. The field of scanning probe microscopy was pioneered by Gerd Binnig and Heinrich Rohrer who shared the 1986 Nobel Prize in Physics "for their design of the scanning tunneling microscope."<sup>82</sup> The invention of the scanning tunneling microscope (STM)<sup>83</sup> was the first SPM technique to be developed and was revolutionary in its resolution as well as the

possibilities that it offered. STM measures the tunneling current between an atomically sharp tip and a conducting sample. When the tip and sample are close (a few angstroms) the tip and sample electron wavefunctions overlap and when a bias is applied a tunneling current is created.<sup>84</sup> Since a tunneling current is measured in STM, only conductive samples can be studied.

AFM was developed as a complimentary technique to STM that can be used to image both conductors and insulators<sup>85</sup> but has since eclipsed STM as a more widely used characterization technique.<sup>86</sup> Figure 4(A) illustrates the basic components of an atomic force microscope. The topography of a sample is measured as the tip is rastered across the sample as illustrated by Figure 4(B). Interactions with the surface of the sample will cause movement of the tip and the laser being deflected off of the cantilever to be detected by a photodiode. The movement of the tip that is monitored is deflected according to Hooke's Law. The movement is both registered by the processing components as well as being part of a feedback loop that controls the piezoelectric stage that the sample is on. Manipulation of the piezoelectric crystals moves the sample to keep it the desired distance from the tip.

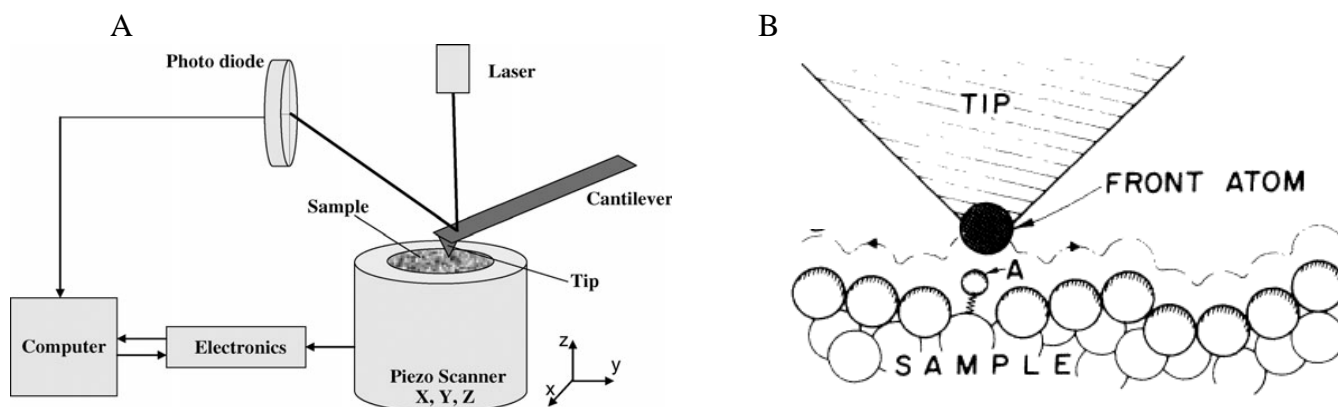


**Figure 4.** (A) Schematic diagram of an atomic force microscope.<sup>87</sup> (B) Close-up sketch of an AFM tip.<sup>85</sup>

(A) Reproduced from *Chem. Commun.*, **2008**, 1513-1532 with permission of The Royal Society of Chemistry.  
(B) Reprinted figure with permission from [Binnig, G.; Quate, C. F., *Phys. Rev. Lett.* 56 (9), 931. **1986.**]  
Copyright 1986 by the American Physical Society.

AFM can be used in three main modes of operation: contact, non-contact, and tapping. In contact mode the topography of the sample is measured with the tip in physical contact with the surface or is kept at a constant position through the feedback loop operated in the repulsive force regime.<sup>88</sup> Atomic resolution is achieved with a low loading force on the tip  $10^{-7}$  to  $10^{-11}$  N.<sup>89</sup> Contact mode can damage a sample if it is soft or too much force is applied to the tip.<sup>88</sup> In addition to surface damage, the image acquired from contact mode AFM is often poor due to lateral shear forces that can cause a stick-slip motion of the tip.<sup>88</sup> Non-contact mode eliminates the potential for surface damage to the sample as the tip does not contact the surface, but rather oscillates with a small amplitude ( $< 5$  nm) in the vicinity of the surface.<sup>88</sup> Despite protecting the sample, non-contact mode has several drawbacks that include a limited range where the oscillation amplitude is affected by the van der Waals interactions and the resolution is limited by its height above the surface.<sup>88</sup> Tapping mode, sometimes called AC mode, is designed as a compromise between contact and non-contact mode. During operation in tapping mode, the cantilever is oscillated near its resonant frequency (near 300 kHz) and strikes the surface once on each oscillation.<sup>88</sup> The oscillation amplitude is measured and the feedback system is designed to detect changes in the oscillation caused by intermittent contact with the surface.<sup>88</sup> The infrequent contact with the surface in tapping mode also eliminated most of the limits of contact mode caused by dragging the tip across the surface and results in high resolution images.<sup>88</sup> Tapping mode was used for the characterization of the solvent-exfoliated graphene.

Through its near atomic resolution, AFM is able to characterize both size and thickness of graphene. The thickness of graphene can be determined from AFM by determining the height of graphene above the substrate, once known the topographical information can be used to estimate the number of graphene layers present in a sample. Furthermore analysis of AFM images allows

for the measurement of graphene flakes to determine the average size and shape of the graphene present. An example of an atomic force microscopy image of graphene is presented in Figure 5.

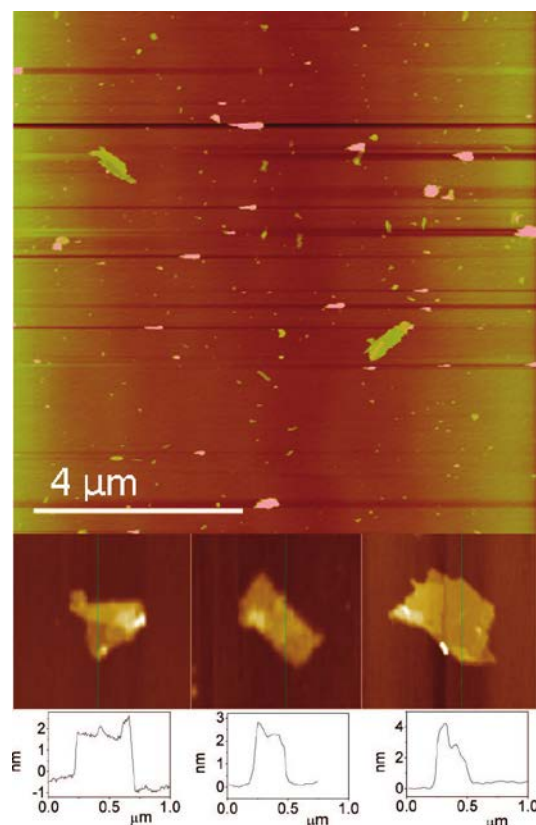


**Figure 5.** AFM image of graphene on silicon oxide substrate. Scale bar = 4 μm.<sup>90</sup>

Reprinted with permission from *J. Am. Chem. Soc.*, **2009**, 131 (10), pp 3611–3620.  
Copyright 2009 American Chemical Society.

### 1.3.3 Raman Spectroscopy

Raman spectroscopy is a fast and non-destructive technique used to observe the structural and electronic characteristics of graphene.<sup>91</sup> Raman spectroscopy is an ideal technique that is able to identify graphene from other graphitic material, characterize the number of layers present, and identify the quality of the graphene present with a faster throughput than other techniques such as AFM.

Raman spectroscopy relies on the observation of inelastic light scattering caused by rotational and vibrational transitions within a material.<sup>80</sup> The inelastic scattering of light that is now known as “Raman scattering” was first identified by Sir C. V. Raman in 1928,<sup>92</sup> a discovery for which he was awarded the Nobel Prize in 1930.<sup>80</sup> The technology of the era initially limited the use of Raman spectroscopy as an analytical technique because of the low intensity of light scattered through the Raman effect with the use of legacy radiation sources such as a low pressure mercury arc. Due to this limitation, analysis of a black material such as graphite through Raman spectroscopy was not always possible.<sup>93</sup> However with the advent of the laser as a powerful new source of radiation, Raman spectroscopy became a powerful tool in the characterization of graphite and eventually graphene.

After the introduction of the laser, Raman spectroscopy was used as a tool to study the structure of graphite long before the isolation of pristine graphene.<sup>93-94</sup> These early studies helped to define the Raman fingerprint of graphitic material and identified two bands, *G* band ( $\sim 1580\text{ cm}^{-1}$ ) and *D* band ( $\sim 1350\text{ cm}^{-1}$ ) that are common to all poly-aromatic hydrocarbons.<sup>95</sup> The *G* band is attributed to the bond stretching of  $\text{sp}^2$  atom pairs<sup>95</sup> ( $E_{2g}$  in-plane stretching).<sup>96</sup> The *D* band is assigned to the ring breathing modes of an aromatic ring.<sup>95</sup> Additionally all graphite materials have a third band at  $\sim 2700\text{ cm}^{-1}$ , a peak that has historically been labeled *G'* because it is the second largest band observed in graphite samples.<sup>94</sup> However, recent studies have revealed that the band at  $\sim 2700\text{ cm}^{-1}$  is unrelated to the *G* band and is more accurately labeled the *2D* peak as this band is the second order (overtone) of the *D* peak.<sup>97</sup> Figure 6 illustrates the Raman spectrum of a graphene edge and highlights the characteristic Raman bands present in graphene.

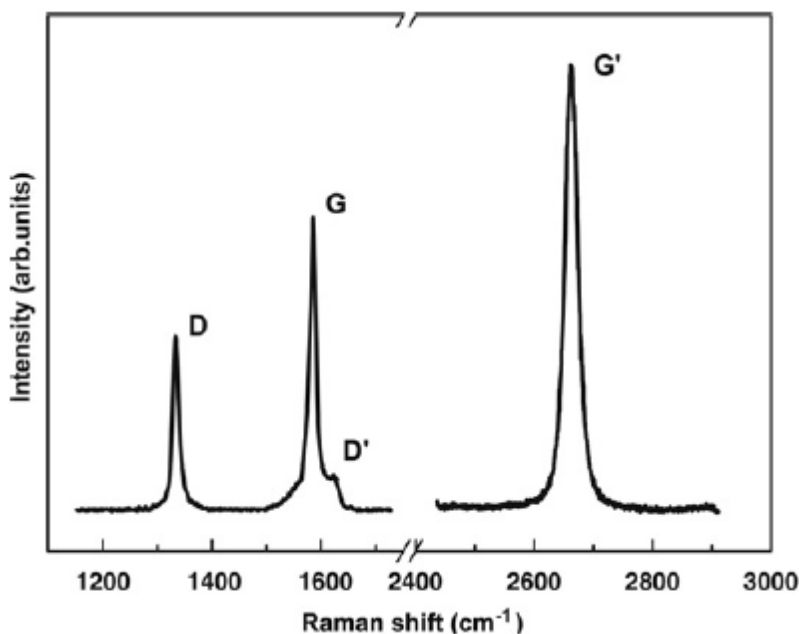


**Figure 6.** Raman spectrum of a graphene edge. Spectrum illustrates the characteristic bands of a graphitic compound. Characteristic bands include the *D* band (~1350 cm<sup>-1</sup>), *G* band (~1580 cm<sup>-1</sup>), and *G'* band (also known as the *2D* band) (~2700 cm<sup>-1</sup>).<sup>77</sup>

Reprinted from *Phys. Rep.*, 473 (5-6), Malard, L. M.; Pimenta, M. A.; Dresselhaus, G.; Dresselhaus, M. S., Raman spectroscopy in graphene, 54, Copyright 2009, with permission from Elsevier.

In addition to the common bands seen in the spectra of a graphitic material, graphene has a unique Raman fingerprint that can be used to differentiate graphene from other graphite based materials. As illustrated in Figure 7, graphene is distinguishable from graphite by the change in the shape of the *2D* band. The *2D* band of bulk graphite is composed of two smaller bands, *2D<sub>1</sub>* and *2D<sub>2</sub>* which are ¼ and ½ the height of the *G* band, respectively.<sup>95</sup> In contrast graphene has a single sharp *2D* band with approximately four times the intensity of the *G* band.<sup>97</sup> As the number of layers of graphene increase beyond five, the Raman spectra begins to resemble that of bulk graphite.<sup>97</sup>

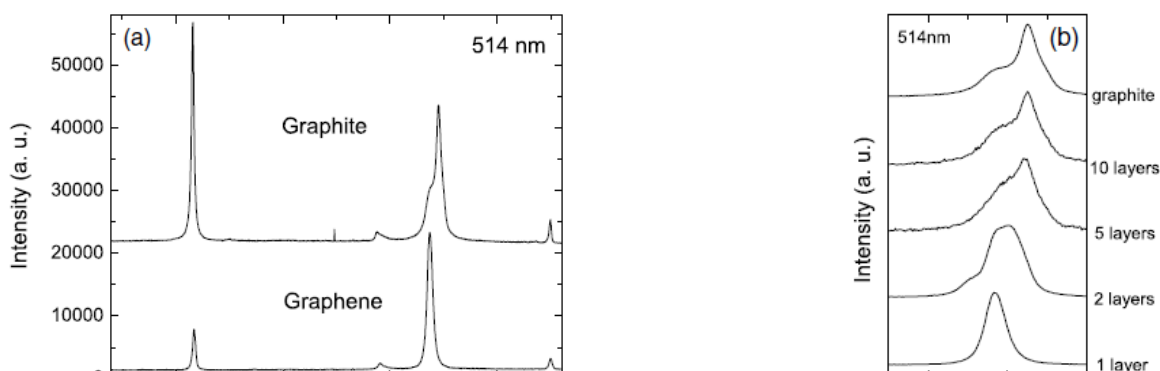


**Figure 7.** (A) Comparison of the Raman spectra of graphite and graphene at 514.5 nm. (B) Evolution of the  $2D$  peak with regard to the number of graphene layers present.<sup>97</sup>

Reprinted figures with permission from [Ferrari, A. C.; Meyer, J. C.; Scardaci, V.; Casiraghi, C.; Lazzeri, M.; Mauri, F.; Piscanec, S.; Jiang, D.; Novoselov, K. S.; Roth, S.; Geim, A. K., *Phys. Rev. Lett.*, 97 (18), 187401/2, 2006.] Copyright 2006 by the American Physical Society.

The  $2D$  band is a prominent feature used to differentiate graphene from graphite, but its inability to distinguish between the allotropes with more than five layers limits its usefulness in characterization. However, the  $G$  band also relays information about the thickness of a graphene sample and is useable as a measure beyond five layers. The intensity of the  $G$  band varies proportionally to the number of layers present in a sample and is therefore a useful indicator of the number of layers present up to the penetration depth of the laser.<sup>96</sup> Through analysis of the  $2D$  and  $G$  bands, Raman spectroscopy can therefore be used to distinguish the number of layers of graphene present.

The Raman spectra of graphene is also able to present information on the quality of the graphene under investigation. The  $D$  band, unlike the other characteristic bands of graphene is not always observed. The  $D$  band is typically observed at approximately  $1350\text{ cm}^{-1}$  but shifts to higher wavenumbers with an increase in incident radiation from the laser.<sup>94</sup> Additionally, the relative strength of the  $D$  band in comparison to the  $G$  band is dependent upon the amount of disorder or defects found in the material.<sup>93</sup> Therefore the  $D$  band is characteristic of scattering conditions only present with a disordered atomic arrangement and not observed in the Raman spectra of pristine

graphene.<sup>98</sup> As a result the presence of the *D* band indicates a defect and its intensity can be used to characterize the quality of the graphene.

With the use of modern instrumentation, the observation of Raman scattering through Raman spectroscopy has evolved into an important characterization technique in the study of graphene. The method allows for the rapid analysis of samples to identify graphene and comment on its quality. Therefore, due to its reliable and reproducible results Raman spectroscopy has become a standard characterization technique in the study of graphene.

## **1.4 OTHER CHARACTERIZATION TECHNIQUES**

Analytical chemistry is a branch of chemistry focused on both qualitatively and quantitatively identifying unknown substances.<sup>99</sup> Methods of analytical techniques are commonly grouped into classical “wet chemistry” techniques focused on the physical and chemical properties of an unknown compound and more modern instrumental techniques.<sup>100</sup> In this investigation the analytical techniques of high-performance liquid chromatography (HPLC), mass spectroscopy (MS), and nuclear magnetic resonance (NMR) spectroscopy were utilized to qualitatively investigate the possibility of contamination present in laboratory glassware.

### **1.4.1 High-Performance Liquid Chromatography**

From the Greek words *chroma*, “color” and *graphein*, “to write” chromatography is a term used to describe a wide variety of analytical separation techniques.<sup>101</sup> Separation techniques that fall under the broad definition of chromatography are utilized in modern analytical laboratories to

separate complex mixtures into their constituent components for further analysis. HPLC is one such method that is a powerful separation technique and useful in the identification of an unknown.

Although examples of naturally occurring separations can be traced back to the formation of the Earth itself,<sup>102</sup> the idea of modern analytical separations has its origins in the early 20<sup>th</sup> century with the work of Russian botanist M. S. Tswett.<sup>101</sup> In his early studies, Tswett developed a packed column technique to separate colored plant pigments.<sup>103-104</sup> Although his initial work was met with a lukewarm response, the study of separations science received a renaissance in interest in separating and purifying natural substances in the 1930s and reinvigorated the fledgling technique as it evolved into a laboratory staple.<sup>101</sup> Through continuous use, the technique developed with the introduction of open tubular chromatography, thin-layer chromatography, and ion-exchange methods that all advanced the usefulness of chromatography as an analytical technique.<sup>101</sup> The later found significant use during the Manhattan Project as a method of separating rare earth metals and is an example of how chromatography became a mainstream technique.<sup>105</sup> However it was not until the development of partition chromatography in 1941 by Martin and Synge,<sup>106</sup> an accomplishment that earned them the 1952 Nobel Prize in Chemistry, that chromatography became standard practice.<sup>107</sup> It was this development that truly showed the utility of chromatography and was the break through development that evolved into what are now modern chromatographic techniques. Partition chromatography grew into gas chromatography after Golay introduced the open tubular (capillary columns)<sup>108</sup> which has become a standard practice in many industrial applications. Partition chromatography also evolved into liquid chromatography by initially utilizing a polar stationary phase within the columns and a non-polar mobile phase. In a system with these components, retention generally increases with the polarity of the analyte as the more polar molecules are retained by the polar stationary phase, for historical reasons this

convention became known as normal-phase chromatography. The introduction of reversed-phase chromatography where the stationary phase is less polar than the mobile phase made liquid chromatography much more efficient.<sup>109</sup> Reverse phase chromatography also allowed the development of gradient elution<sup>110</sup> where the polarity of the mobile phase is changed during the separation to further increase the efficiency of a separation. These developments that built upon the theory of partition chromatography evolved to become what is now known as HPLC and has become a standard analytical technique in the identification of unknown compounds.

A modern HPLC instrument is modular in nature and is customizable dependent upon the goals of the operator. As such, specific components are assembled to produce the desired separation but in general a HPLC instrument typically includes a solvent source, a pump, a sample injection mechanism, a column, a detector, and a data processing system (Figure 8).

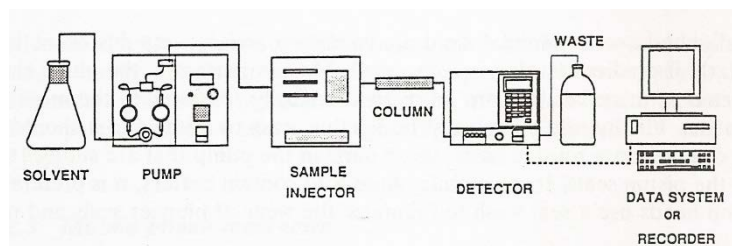


**Figure 8.** Block diagram of a HPLC instrument.<sup>101</sup>

Reprinted from *Principles and Practice of Modern Chromatographic Methods*, Robards, K., Haddad, P. R., and Jackson, P. E., "High-performance Liquid Chromatography – Instrumentation and Techniques," Pg. 229, Copyright 2004, with permission from Elsevier.

Unlike gas chromatography which utilizes an inert gas as a mobile phase, the selection of a solvent (mobile phase) in HPLC will have a large impact on the quality of the separation as it will interact with both the analyte and the stationary phase. The primary purpose of the pump is to supply the mobile phase to the system in the most reproducible manner possible. Pumps for HPLC are typically designed to deliver the mobile phase at a constant pressure and are typically run with a flow-rate between 0-10 ml min<sup>-1</sup> although some columns may require a substantially higher flow-

rate.<sup>101</sup> In an HPLC system the sample is injected into the moving mobile phase prior to the column and is not a trivial detail in system design.<sup>101</sup> The injection needs to minimize the disruption to the flow of the mobile phase as well as be quick enough to minimize band broadening.<sup>101</sup> Sample injection can be carried out manually or through the use of an auto-sampler. In addition to the selection of the mobile phase, the selection of the column will have the most impact on the speed and quality of the separation. The size of the column, packing material, size of the particles, and configuration of the column are a few of the many attributes of the column that can be selected and will impact the speed and the quality of the separation. The detector used in an HPLC instrument is selected based on the purpose of the separation. Some typical detectors include UV-Vis detectors, fluorescence detectors, refractive index detectors, conductivity detectors, and MS.<sup>100</sup> Modern instruments will also include some sort of electrical data collection and processing system to analyze the data acquired through the separation. In this investigation, HPLC was utilized with a reverse phase column to isolate suspected contaminants through analysis with mass spectroscopy.

#### **1.4.2 Mass Spectroscopy**

Mass spectroscopy is a form of atomic mass spectroscopy that is often utilized as the detector for an analytical separation to provide qualitative information about the identity of an unknown. The origins of mass spectroscopy can be traced to the early 20<sup>th</sup> century and physicist J. J. Thomson's work on cathode rays which first measured the charge-to-mass ratio of an electron and served as the theoretical basis of MS.<sup>111</sup> Thomson's work was expanded upon by one of his students, Francis Aston, who is credited with building the first mass spectrometer designed to measure the mass of a charged atom.<sup>111</sup> The technique saw rapid development during the following decades and

became recognized as a standard analytical technique after widespread use in the Manhattan Project to identify elemental isotopes.<sup>111</sup> MS has since become a highly commercialized analytical instrument and is a common fixture in modern analytical laboratories.

A generic MS instrument, as seen in Figure 9, is typically connected directly to the separation method and is composed of three major components: an ion source, a mass filter, and an ion collector.<sup>112</sup>

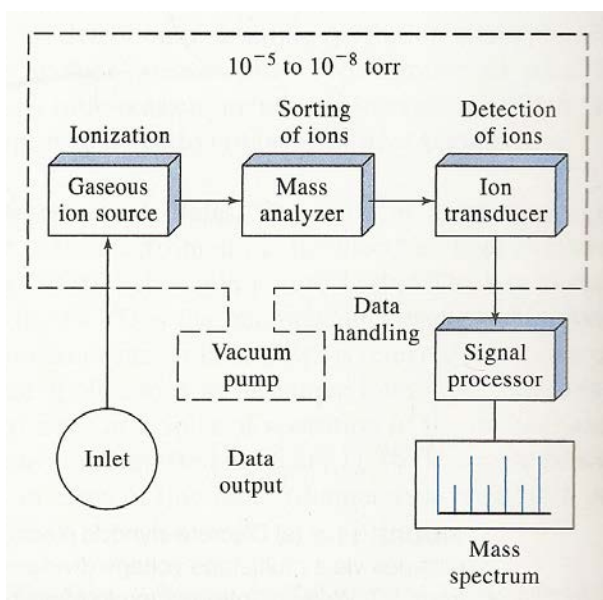
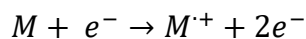


**Figure 9.** Block diagram of a Mass Spectrometer.<sup>100</sup>

Reprinted with permission from Cengage Learning SO.

Common sample ionization sources include electron impact, chemical ionization, electrospray ionization, and field ionization.<sup>100</sup> Electron impact is historically the most common ionization method<sup>100</sup> however the electrospray technique has gained widespread acceptance since its introduction in the 1980's.<sup>113</sup> To produce ions for mass analysis, the electron impact method produces a molecular mist by heating the sample and then uses an electron beam to bombard the sample to cause fragmentation and ionization as summarized by Equation 2.<sup>100</sup>



**Equation 2.** Primary reaction of electron-impact ionization.  
 $M$  = analyte molecule;  $e^{-}$  = electron;  $M^{+}$  = molecular ion of the analyte

In contrast to the electron impact method of ionization, electrospray ionization introduces a droplet of the sample into a gas stream through a high voltage bias to form a dispersion of ions.<sup>113</sup> Once formed the ions are allowed to expand into a vacuum through a supersonic free jet and introduced to the mass filter.<sup>113</sup> Electrospray ionization has found widespread use in the analysis of biological samples as a soft ionization technique and its development earned John Fenn a portion of the 2002 Nobel Prize in Chemistry.<sup>114</sup> Electrospray ionization is the method of ionization utilized in this investigation.

After ionization, the mass filter is used to select the ions of interest by their mass-to-charge ratio ( $m/z$ ). Magnetic sector analyzers, quadrupole mass spectrometers, and time-of-flight mass analyzers are typical types of mass filters used in modern MS instruments,<sup>100</sup> a quadrupole was used as the mass filter for this experiment. A quadrupole mass spectrometer consists of four parallel metallic rods.<sup>100</sup> Opposite rods are electronically linked and connected to a variable DC power source with one pair connected to the positive terminal and the other pair to the negative connection.<sup>100</sup> Each pair of rods is also connected to variable radio-frequency AC sources that are 180° out of phase.<sup>100</sup> During operation the ions are accelerated into the quadrupole with a 5 to 10 V potential difference while the DC and AC voltages are simultaneously increased.<sup>100</sup> The difference in polarity between the rods of the quadrupole interact with the ions and cause all but the those with the  $m/z$  of interest to impact the rods or be ejected from the filter.<sup>100</sup> Through this technique, a quadrupole mass filter is capable of resolving ions that differ by only one mass unit.<sup>100</sup> The final portion of the MS is a transducer that is capable of detecting the separated ions to be

recorded and processed electronically. The analysis of an unknown analyte through MS produces a spectrum that consists of a fragmentation pattern, reported in  $m/z$ , of the analyte.<sup>100</sup>

As an analytical technique, MS is useful in providing evidence to support the identity of an unknown through a compound specific fragmentation pattern. The fragmentation pattern can serve as a fingerprint of the unknown by presenting the molecular weight of the compound as well as identifying the functional groups present. During ionization, the analyte is fragmented into smaller molecules that when assembled are unique to a specific compound. Of note in the fragmentation pattern are the molecular peak and the base peak. The molecular peak is associated with the molecular mass of the compound while the base peak is the most intense peak and therefore identified as the most abundant ion in the compound, these peaks are not always co-located. In modern investigations the analysis of mass spectra is accomplished electronically by comparing the experimental spectra to one of many databases of known compounds such as the one maintained by the National Institute of Standards and Technology.<sup>115</sup> The information obtained through MS analysis is able to provide qualitative evidence for the identity of an unknown compound. In this investigation MS was used as a detector to identify contaminants isolated through HPLC.

### **1.4.3 Nuclear Magnetic Resonance**

Nuclear Magnetic Resonance is an analytical technique used to characterize an unknown through the magnetic properties of the selected atomic nuclei. NMR measures the absorption of electromagnetic radiation by atomic nuclei in the radio frequency range of the electromagnetic spectrum, between 4 to 900 MHz.<sup>100</sup> The energy states required for the absorption measured by NMR are created through exposing the sample to an intense magnetic field.<sup>100</sup> NMR is useful as

an analytical technique because the resonance frequency of each proton is dependent upon its chemical environment within the molecule and returns a unique spectrum. The spectra acquired through NMR can provide evidence to the identity of an unknown and have become a widely used analytical technique in the investigation of organic molecules.

NMR is based on the principles of electronic spin and the magnetic moment that were established in the 1920s through a series of investigations such as the Stern-Gerlach experiment<sup>116</sup> and the work of Pauli that suggested the atomic properties of spin and a magnetic moment that can interact with a magnetic field to split their energy levels.<sup>100</sup> Isidor Rabi expanded upon these early investigations by making the first observation of the NMR phenomenon by passing a stream of hydrogen atoms through a magnetic field and recording the absorption and the deflection of the hydrogen beam.<sup>117</sup> These observations earned Rabi the 1944 Nobel Prize in Physics “for his resonance method for recording the magnetic properties of atomic nuclei.”<sup>118</sup> The technique was further expanded in 1946 when Bloch<sup>119</sup> at Stanford and Purcell<sup>120</sup> at the Massachusetts Institute of Technology independently and through different experimental routes reported the observation of NMR in bulk materials. Their discovery earned the 1952 Nobel Prize in Physics “for their development of new methods for nuclear magnetic precision measurements and discoveries in connection therewith”<sup>121</sup> and unlocked NMR for the quantitative and qualitative analysis of a wide variety of materials.

Modern NMR techniques have evolved beyond the first commercially available 30 MHz NMR instruments in the 1950’s in both resolution and computing power.<sup>122</sup> The most powerful instruments available today boast a 1 GHz magnet and enhance the capability of the technique to analyze more complex molecules, most notably proteins, that could not previously be resolved.<sup>122</sup> Most NMR investigations are focused on the  $^1\text{H}$  and  $^{13}\text{C}$  nuclei and used in many routine organic

investigations however, modern techniques allow for more than 200 isotopes that have magnetic moments to be studied through NMR techniques.<sup>100</sup> The development of more powerful instruments and advanced data processing techniques have allowed NMR to delve deeper into the biological sciences as more complex compounds can be analyzed. In this investigation <sup>1</sup>H NMR was utilized to characterize the contaminants suspected to impact the colloidal stability of graphene.

## 1.5 COLLOIDAL STABILIZATION

A colloid is a system in which the molecules dispersed in a medium are microscopically heterogeneous and have at least one of its dimensions between 1 nm and 1  $\mu$ m.<sup>123</sup> A colloid differs from a solution by the size of the suspended particles. Similar to a solution, the particles in a colloid are indistinguishable to the naked eye but unlike a solution the particles in a colloid are large enough to scatter light.<sup>99</sup> The properties of the nanoparticles present in a colloid can be altered through the colloid's preparation and handling making the treatment of the colloid important to the final use of the nanoparticles.<sup>123</sup> Graphene prepared through solution-based exfoliation meets this definition of a colloid and therefore the properties of the graphene and its final use are partially dependent upon the quality of the colloidal solution produced.

In a colloidal suspension, graphene particles are subjected to Brownian motion and van der Waal's interactions with other particles. Brownian motion is the free and random movement of particles in a colloidal system caused by collisions with the molecules of the medium.<sup>124</sup> Due to the kinetic energy of each individual graphene particle suspended in a solvent, each graphene sheet is allowed to both translate and rotate freely within the colloid.<sup>125</sup> Due to this movement, it is

appropriate to model graphene particles as spheres which allows the Brownian motion to be described by Fick's first law (Equation 3).<sup>125</sup> This approximation does not account for intercolloid interactions.<sup>125</sup>

$$J_{1i}^{diff}(r) = -D_1 \frac{dN_1}{dr}$$

**Equation 3.** Fick's First Law.<sup>125</sup>

$J_{1i}^{diff}$  = diffusive flux as a function of the radius,  $r$ , from the reference  $i$ -layer of graphene;  $N_1$  = concentration (number of single-layer graphene sheets per unit volume);  $D_1$  = diffusivity of a single-layer graphene sheet in the solvent.

As molecules within a colloidal suspension are diffusing according to the random movement of Brownian motion, they will occasionally pass within close proximity to each other. If there is no repulsive force present, these molecules will agglomerate due to the attractive van der Waal's forces present between the molecules and the suspension will lose its stability. The term "van der Waals forces" is a collective term that refers to an assortment of interactions between particles. These forces include: London dispersion interaction between the electron clouds on each particle, dipole-dipole (Keesom) interaction, and dipole-induced dipole (Debye) interactions.<sup>123</sup> The dipole-dipole interactions are only present when both molecules have a permanent dipole moment and are not considered in a colloidal graphene solution.<sup>123</sup> Although the vdW forces (0.004 - 0.04 eV) are weaker than hydrogen bonds (0.05 - 0.3 eV) as well as covalent and ionic bonds (2 - 10 eV), they begin to interact at a relatively long range ( $\sim 1$  nm) when compared to the stronger bonds that interact much close ( $\sim 1$  Å).<sup>123</sup> Therefore, vdW forces are a major force behind the stability of colloidal graphene.

Estimating the vdW forces present in a colloidal suspension will give insight into the stability of the suspension. In general, the vdW forces vary as  $d^{-n}$  where  $d$  is the distance between the molecules and  $n$  is  $\sim 2$  for equal spheres,<sup>123</sup> which is an appropriate assumption for graphene flakes.<sup>125</sup> Furthermore, since the major contribution to the vdW forces of graphene flakes in a

colloid are attributed to the London dispersion interaction, they can be estimated by the electromagnetic interaction caused by the fluctuation dipole (Equation 4).

$$\phi = -\frac{3}{2} \left( \frac{h\nu_1 h\nu_2}{h\nu_1 + h\nu_2} \right) \frac{\alpha_1 \alpha_2}{r^6} = \frac{\lambda_{12}}{r^6}$$

**Equation 4.** Estimation of the London dispersion force.<sup>123</sup>  
 $\phi$  = potential energy;  $h\nu$  = characteristic energy of the molecule (subscript identifies the molecule);  
 $\alpha$  = polarizability;  $\lambda_{12}$  = London constant;  $r$  = distance between the molecules.

The estimation of the London dispersion interaction can be further simplified for similar molecules through Equation 5.

$$\phi = -\frac{\lambda_{11}}{r^6}$$

**Equation 5.** Simplification of the London dispersion force for two like molecules.<sup>123</sup>  
 $\phi$  = potential energy;  $\lambda_{11}$  = London constant;  $r$  = distance between the molecules.

The estimated potential energy of the vdW forces between two molecules can be represented graphically in a method introduced by John Lennard-Jones.<sup>126</sup> Often referred to as the Lennard-Jones potential and summarized in equation 6, this estimation relates the attractive and repulsive forces acting on a two molecule system.

$$\phi(r) = 4\phi_o \left[ \left( \frac{x_o}{r} \right)^{12} - \left( \frac{x_o}{r} \right)^6 \right]$$

**Equation 6.** Lennard-Jones potential.<sup>123</sup>  
 $\phi(r)$  = potential energy separated by a distance,  $r$ ;  $\phi_o$  = minimum value of  $\phi$  which occurs at  $r_o$ ;  $x_o$  = distance that corresponds to an intermolecular potential between the two particles of zero (often annotated as  $\sigma$ ).

The Lennard-Jones potential is often presented in graphical form (Figure 10) in an easily understood format that conveys the relationship between the attractive and repulsive forces as well as their relationship to the distance between the particles. As shown in Figure 10, the repulsive forces dominate at small distances between the particles where a large amount of energy would be required to overcome them and force aggregation. Alternatively, the attractive forces that scale to the sixth power are the prevailing forces at larger distances. One feature of note is the potential

well that forms as a localized minimum within the graph. The depth of the well is related to the attraction between the two particles where a deeper well indicates a stronger interaction.<sup>127</sup> The radius value that corresponds to the minimum value of the potential well indicates the distance at which the repulsive and attractive forces are in equilibrium.<sup>127</sup>

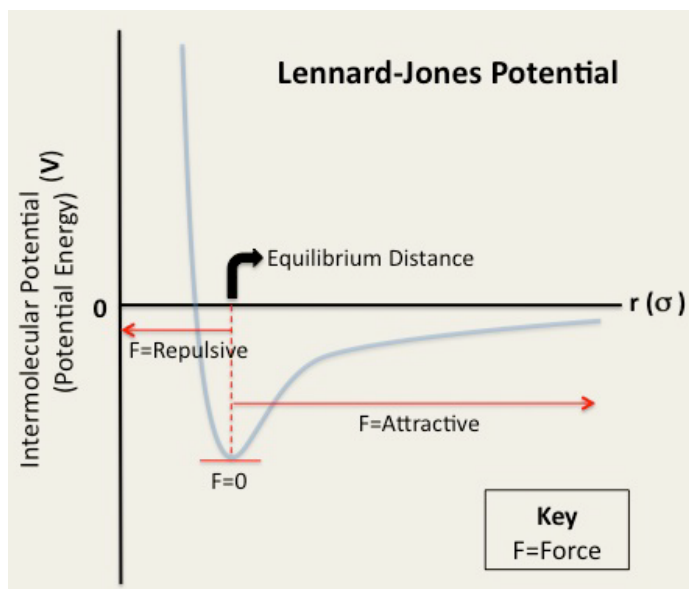


**Figure 10.** Lennard-Jones Potential. Graphical depiction of the potential energy between two molecules.<sup>128</sup>

Reprinted in accordance with the Creative Commons Attribution-Noncommercial-Share Alike 3.0 United States License (CC BY-NC-SA 3.0 US).

Forces that work to alter the potential well and alter the stability of a colloidal solution can be divided between electrostatic and steric methods of stabilization.

### 1.5.1 Electrostatic Stabilization

A molecule can become electrostatically stabilized in an aqueous solution through the formation of an electric double layer. An electric double layer is formed when counterions become adsorbed to a molecule's surface and interact with polarized water molecules to form a layer called the Stern layer.<sup>123</sup> When this charged layer interacts with the diffuse counterions within the liquid

surrounding the molecule, a double layer is formed.<sup>123</sup> When the double layers of two particles approach each other, they repel and there is stability added to the system.<sup>123</sup>

### 1.5.2 Steric Stabilization

Steric stabilization of a colloidal suspension is accomplished through adding a polymer or surfactant molecules to the suspension.<sup>123</sup> Stabilization is achieved by making aggregation thermodynamically unfavorable in terms of the Gibbs energy (Equation 7).<sup>123</sup>

$$\Delta G = \Delta H - \Delta S$$

**Equation 7.** Gibbs Energy.<sup>123</sup>

$\Delta G$  = total change in Gibbs energy;  $\Delta H$  = total change in enthalpy;  $\Delta S$  = total change in entropy

An unfavorable increase in Gibbs energy is produced as the molecules of the stabilizing surfactant or polymer interact with each other. As the stabilizing molecules interpenetrate, they begin to become constrained in the conformations that they can adopt because their movements are hindered by their neighbor molecules. The restricted movement of the intercalated molecules decrease the configurational entropy of the system.<sup>123</sup> Additionally, enthalpy increases as the molecules become more closely packed and are at a higher energy state than when they are only exposed to other similar molecules.<sup>123</sup> Therefore a negative entropy and positive enthalpy result in an increase to the Gibbs energy which is unfavorable to mixing and causes stability in the system.

### 1.5.3 Stabilization of Solvent-Exfoliated Graphene in NMP

One explanation for the stability of solvent-exfoliated graphene in a colloidal suspension is a similarity in the surface energy between NMP and graphite.<sup>129</sup> Surface energy,  $\gamma$ , is defined as the

energy associated with the surface atoms of a molecule and differs from the energy of atoms in the bulk of the material.<sup>123</sup> Surface energy can be estimated by multiplying the number of bonds broken,  $N_b$ , by half of a bond energy,  $\varepsilon$  (Equation 8).<sup>123</sup>

$$\gamma = N_b \left( \frac{1}{2} \varepsilon \right)$$

**Equation 8.** Surface energy.<sup>123</sup>  
 $\gamma$  = surface energy;  $N_b$  = number of broken bonds;  $\varepsilon$  = bond energy

The surface energy of graphite is defined as the energy per unit area that is needed to overcome the vdW forces between two graphene layers.<sup>39</sup> This value has been conveyed in the literature as being approximately 70 – 80 mJ m<sup>-2</sup>.<sup>129</sup> The surface energy of the solvent used in this study, NMP, can be calculated from its surface tension and has been reported as 41.26 mJ m<sup>-2</sup>.<sup>130</sup> Therefore, the surface energy of graphite is relatively close to that of NMP and results in a minimal energy cost to overcome the vdW forces between the molecules.<sup>129</sup> This energy match contributes directly to the effectiveness of NMP as a solvent for the solution-based exfoliation of graphene as well as the stability of the colloidal solution that is created.

The importance between the close surface energies of the solvent and graphene and its impact on the exfoliation can be described through the enthalpy of mixing (Equation 9).

$$\frac{\Delta H_{mix}}{V_{mix}} \approx \frac{2}{T_{flake}} (\delta_G - \delta_{sol})^2 \phi$$

**Equation 9.** Enthalpy of Mixing per unit volume.  $\Delta H_{mix}$  = Entalpy of Mixing;  $V_{mix}$  = volume;  $T_{flake}$  = thickness of a graphene flake;  $\phi$  = graphene volume fraction.<sup>39</sup>

As illustrated in Equation 9, the enthalpy of mixing is reliant upon the surface energies of both graphene and the solvent. When the difference between the surface energies is small, the energy cost for exfoliation is minimized and is possible through low-powered techniques such as sonication.<sup>39</sup> Additionally, the efficiency of graphene exfoliation with minimal differences in surface energy suggests that the primary interactions between the solvent and graphite is through

vdW forces instead of stronger covalent bonds, again allowing for exfoliation with minimal energy.<sup>39</sup> Through their research Hernandez and co-workers concluded that the optimal surface energy of a solvent for the exfoliation of graphene is between 40 and 50 mJ m<sup>-2</sup>, a range that includes NMP.<sup>39</sup>

In addition to increasing the efficiency of the exfoliation, the surface energy match between the solvent and graphene impacts the stability of the colloidal solution. In the solution, the solvent counteracts the vdW forces between the graphene sheets and consequently stabilizes the solution.<sup>125</sup> The specific mechanism of interaction between the solvent molecules and graphene is unknown, however an understanding of the behavior of graphene in a colloidal suspension is well documented.<sup>125</sup>

Through a series of molecular dynamics simulations Shih *et al.* investigated the interactions of parallel graphene sheets with NMP.<sup>125</sup> Through these simulations, the researchers calculated the potential of mean force (PMF) between the two graphene sheets that corresponds to the energy needed to desorb a confined layer of NMP molecules between the graphene sheets.<sup>125</sup> The results of the simulation are depicted in Figure 11 where the researchers concluded that the major barrier between aggregation is the desorption of the final layer of confined solvent molecules.<sup>125</sup> As depicted in the graph, the interaction between the graphene sheets is attractive when the distance is relatively large (7.6 Å – 8.4 Å) and becomes repulsive as the solvent molecules become more confined (6.6 Å – 7.6 Å).<sup>125</sup> The behavior noted below an inter-plane distance of 6.6 Å is dominated by the vdW forces between the graphene sheets as it is no longer favorable for the solvent molecules to be confined.<sup>125</sup>

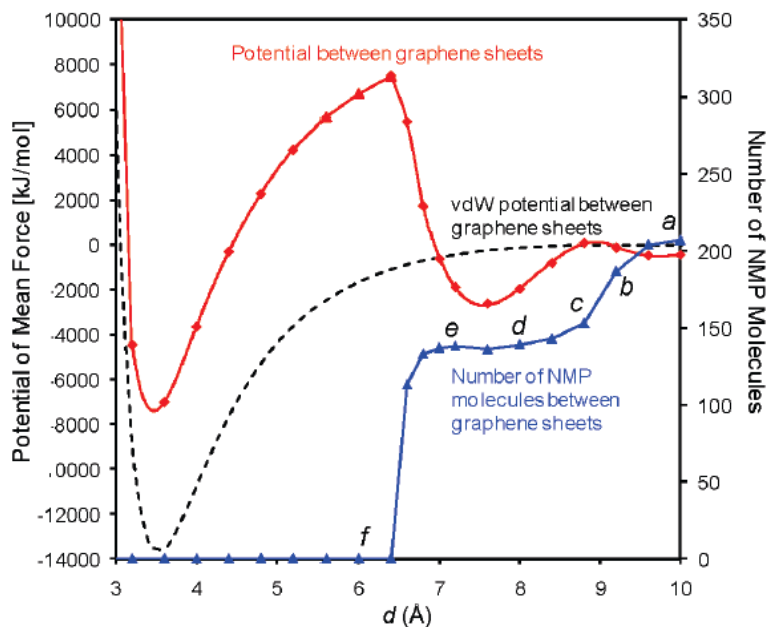


**Figure 11.** Simulated potential mean force (PMF) between two parallel single-layer graphene flakes in NMP. Red line: PMF between the graphene sheets. Blue line: Number of NMP molecules between the graphene sheets. Black line: Lennard-Jones potential between two graphene sheets in the absence of a solvent.<sup>125</sup> Note that the minimum of the potential well is  $\sim 3.5$  Å, the interlayer distance between graphene sheets in bulk graphite.<sup>125</sup>

Reprinted with permission from *J. Am. Chem. Soc.*, **2010**, 132 (41), pp 14638–14648.  
Copyright (2010) American Chemical Society.

From the calculated behavior of graphene sheets with NMP, it is shown that NMP stabilizes the colloidal suspension by introducing a high energy barrier to aggregation and decreasing the potential well. By minimizing the potential well the aggregation of graphene flakes becomes a kinetically controlled event.<sup>125</sup> This conclusion was reached to describe the reaction because the higher energy barrier caused by the solvent lowered the aggregation rate while the smaller potential well resulted in a larger equilibrium concentration of graphene flakes.<sup>125</sup> Additionally, because of the energetically favorable confinement of the solvent molecules, the solvent has a higher affinity for graphene than it does for other like molecules, further increasing the stability.<sup>125</sup> Therefore, it was found that the stability of a colloidal graphene solution is dependent upon solvent interactions that can alter the vdW forces between graphene sheets. It was found that the final layer of solvent molecules dominates the stability of graphene sheets,  $d < 9$  Å, as it can hinder the attractive forces

between graphene sheets and alter the stability of a colloidal solution through a kinetically controlled interaction.

The kinetics of the interaction between graphene sheets and solvent molecules plays a role in the stability of the colloidal suspension because it is not a static system. Through Brownian motion the molecules are in constant random motion that can cause collisions between the molecules in solution. Therefore it is important to understand the frequency of these collisions and how they may impact the overall stability of the suspension. The frequency of collisions between the molecules present in a colloidal solution can be calculated through Equation 10 which is derived from Fick's first law and the Stokes-Einstein relationship.<sup>125</sup>

$$Z_{1i} = \frac{4\pi D_1 N_{b1}}{\int_{r_0}^{\infty} \frac{\exp\left[\frac{V_{1i}(r)}{k_B T}\right]}{r^2} dr}$$

**Equation 10.** Collision frequency between graphene sheets.<sup>125</sup>

$Z_{1i}$  = collision frequency;  $D_1$  = diffusivity of a single layer graphene sheet in the solvent;  $N_{b1}$  = bulk concentration of  $i$ -layer graphene sheets;  $V_{1i}$  = interaction potential;  $k_B$  = Boltzmann's Constant;  $T$  = absolute temperature;  $r$  = radial distance from the reference  $i$ -layer graphene sheet.

Collisions within the colloid are important to understanding its stability because graphene flakes will favor combining to form multi-layer graphene when the distance between them is 3.5 Å (Figure 11). In order for the graphene particles to aggregate, they must first overcome the energy barrier created by the final layer of confined solvent molecules. Through its motion individual graphene sheets can possess a kinetic energy greater than the barrier imposed by the solvent and therefore cause aggregation when a collision occurs. Therefore overtime, a colloidal graphene solution will aggregate despite the stabilizing effect of a solvent such as NMP (Figure 12).

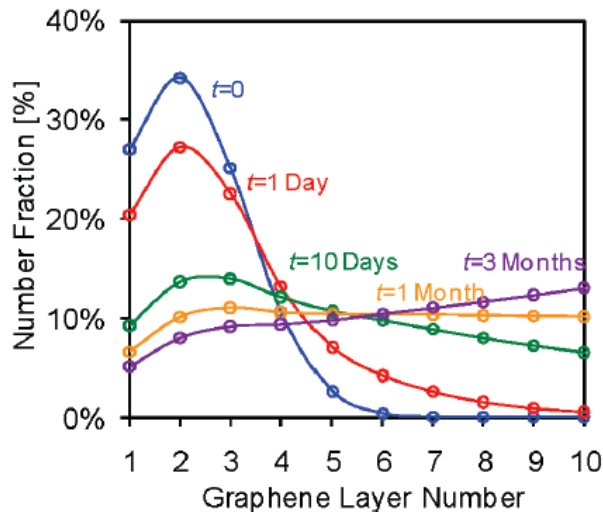


**Figure 12.** Predicted distributions of graphene sheet thickness over time.<sup>125</sup>

Reprinted with permission from *J. Am. Chem. Soc.*, **2010**, 132 (41), pp 14638–14648.  
Copyright (2010) American Chemical Society.

## 1.6 SPECIFIC AIMS

The goal of this project was to develop an understanding of the physical and chemical properties of graphene as well as the standard synthetic methods used in preparing and charactering the 2D allotrope of carbon. Furthermore, an appreciation of the stabilization forces present in a colloidal graphene solution was developed. These principles were used to investigate the observed stabilization of a colloidal graphene solution in common laboratory glassware attributed to an unknown source of contamination. Through experimental and instrumental methods the stabilizing effect was scrutinized for potential scientific and industrial value.

The specific aims of this project include:

Specific Aim I: To exfoliate few layer graphene sheets through a modification of the solution-based synthetic protocol published by Khan *et al.*<sup>42</sup>

Specific Aim II: Characterize the graphene synthesized through solution-based exfoliation with standard instrumental techniques.

Specific Aim III: Identify the contamination observed in common laboratory glassware.

Specific Aim IV: Confirm the effect of contaminants on a colloidal graphene solution and identify possible mechanisms for the changes in stability.

## 2.0 EXPERIMENTAL

The initial focus of this investigation was to exfoliate graphene through a solvent-based method with the goal of maximizing the concentration of graphene produced. The graphene was then characterized through UV-Vis, AFM, and Raman techniques. In the course of this investigation solvent exchange was utilized as a technique to remove the solvent. During the solvent exchange an unexpected stabilization effect was noticed in certain glassware that sparked a secondary investigation to identify the source of the added stability.

## 2.1 MATERIALS

### 2.1.1 Graphene Synthesis

The solvent-based exfoliation was carried out using graphite flakes and 1-methyl-2-pyrrolidione (NMP) purchased from Sigma-Aldrich (St. Louis, MO). The solvent exchange utilized acetone purchased from Fisher Scientific (Waltham, MA) and methanol ( $\geq 99.8\%$  A.C.S. reagent), ethanol, chloroform, formamide, dichloromethane, 2-propanol supplied by Sigma-Aldrich. Additionally methanol supplied by OmniSolv, a sub-brand of Fisher Scientific as also utilized.  $18\text{ M}\Omega\cdot\text{cm}$   $\text{H}_2\text{O}$  was prepared with a ThermoScientific MicroPure system. Piranha solution was prepared using hydrogen peroxide and sulfuric acid from Sigma Aldrich.

The glassware utilized included Fisherbrand (Vials, Screw Thread) with Cap, Attached 25 x 95 mm, 8 dram (USA) (Item # FS60910A8), Fisherbrand (Vials, Screw Thread) with Cap,

Attached 21 x 70 mm, 4 dram (China) (Item # FS60910A4), and Kimble-Chase 60910L-1 15x45 mm Screw Thread Vial, 1 dram (USA) (Item # 60910A1) which were all purchased through Fisher Scientific. Additionally, Qorpak Clear Borosilicate Sample Vials with caps, 10 dram (Item # GLC04893) and Fisherbrand 9" disposable Pasteur pipets were supplied by Fisher Scientific and were utilized in the preparation and handling of the colloidal graphene solution.

To complete the characterization of the exfoliated graphene Thermal Oxide Silicon wafers (University Wafer) and 13 mm Whatman® Anodisc 13 filter membranes with a 0.1  $\mu\text{m}$  pore size were utilized. Additionally the solvent-based exfoliation was carried out utilizing a VWR Ultrasonic Cleaner (Model #97043-988), Buchler parasitotic pump, Oakton pH6 Acorn Series pH/mV/ $^{\circ}\text{C}$  meter, and Eppendorf Centrifuge 5804.

### **2.1.2 Colloidal Stabilization**

In addition to the reagents, glassware, and equipment previously mentioned, chloroform-d for NMR (99.8 atom %D in 0.75 mL ampules) and isoprene (98%, stabilized) were purchased from ACRO Organics (Geel, Belgium). The isoprene was washed using sodium hydroxide (Certified ACS pellets) and calcium chloride, anhydrous (pellets, 4-20 mesh) from Fisher Scientific. Acetonitrile was acquired from Sigma-Aldrich and a 500 MHz NMR tube was purchased from Fisher Scientific. Additionally a Lab-line Imperial II Radiant Heat Oven was utilized to treat the glassware.

## 2.2 SAMPLE PREPARATION

### 2.2.1 Graphene Synthesis

Graphene was prepared through the solution-based exfoliation of graphite through a synthetic protocol based on the work of Khan *et al.*<sup>42</sup> Graphene synthesis was carried out on a 1/8 scale of that reported in the literature where 0.825g graphite flakes was sonicated for 168 hours (7 days) in 250-mL of 1-methyl-2-pyrrolidone (NMP). Sonication was carried out in a VWR Ultrasonic Cleaner (Model #97043-988). The water level was maintained through the use of a Buchler peristaltic pump equipped with a 2000-mL water reservoir. The temperature of the bath was routinely monitored with the use of an Oakton pH6 Acorn Series pH/mV/°C meter and maintained between 20°C - 50°C by replacing water with ice as needed. The experimental set-up is depicted in Figure 13.



**Figure 13.** Experimental Set-up for Graphene Synthesis. 500-mL round-bottom flask reaction vessel suspended in VWR Ultrasonic Cleaner (Model #97043-988). Buchler peristaltic pump and 2000-mL water reservoir used to maintain level of water bath. Also shown Oakton pH6 Acorn Series pH/mV/°C meter used to monitor sonication bath temperature.

Prior to characterizing or use, the 168 hour solvent-exfoliated graphene was centrifuged at 2000 RPM for 60 minutes to separate the un-exfoliated graphite particles from the colloidal solution. The graphene solution was then decanted from the vials after centrifugation.

### **2.2.1.1 UV-Vis Spectroscopy**

UV-Vis was used to evaluate the concentration of the graphene produced through sonication in a method described by Khan and co-workers.<sup>42</sup> The concentration of graphene ( $C_G$ ) can be determined through UV-Vis by using the relationship illustrated in Beer's Law (Equation 1). The absorption coefficient ( $\alpha$ ) reported by Khan *et al.* at 660 nm ( $\alpha = 3620 \text{ mL mg}^{-1} \text{ m}^{-1}$ ) was used to approximate the concentration of graphene produced.<sup>42</sup> The absorption ( $A$ ) of graphene was obtained using a both a ThermoScientific GENESYS 10S UV-Vis and a ThermoScientific NanoDrop 2000c Spectrophotometer. Prior to analysis, the graphene samples went through a series of dilutions (from 2x to 64x) in NMP.

### **2.2.1.2 Atomic Force Microscopy**

Samples for characterization through AFM were prepared on silicon wafers (thermal oxide wafers (100), 301 nm average oxide layer thickness: University Wafer) as a substrate. Prior to use, the wafers were cleaned in piranha solution (7 mL  $\text{H}_2\text{SO}_4$ , 3 mL  $\text{H}_2\text{O}_2$  and heated to 30°C for 30 minutes).

*Warning: Piranha solution presents an explosive danger and is a strong oxidant.*

*All work with piranha should be done in a fume hood. Handle with extreme caution.*

Graphene was deposited on the Si wafers through drop casting and dried by spin coating at a velocity of  $\sim 2,000$  rpm. Graphene utilized in AFM images was separated from NMP through

solvent exchange (Section 2.2.2) with methanol and redispersed in solution through an hour of sonication prior to use.

### **2.2.1.3 Raman Spectroscopy**

A sample for analysis through Raman spectroscopy was prepared by filtering 100  $\mu\text{L}$  of the centrifuged 168 hour exfoliated graphene solution through a 13 mm Whatman® Anodisc 13 filter membrane with a 0.1  $\mu\text{m}$  pore size via vacuum filtration. The graphene solution was introduced to the filter membrane in 10  $\mu\text{L}$  aliquots and allowed to dry overnight.

## **2.2.2 Solvent Exchange**

Although NMP is a widely used solvent for the exfoliation of graphene, its high boiling point (204.3°C)<sup>131</sup> makes it difficult to remove for the characterization of the exfoliated graphene. A solvent exchange regiment similar to that described by Zhang *et al.*<sup>132</sup> was adopted to replace the NMP with methanol (boiling point: 64.7°C).<sup>133</sup> To accomplish the solvent exchange 7.5-mL of the 168- hour solution was mixed with 7.5-mL methanol and allowed to separate. The mixture was then centrifuged at 2000 RPM for 60 minutes. After centrifugation, the supernatant was removed and 10-mL of methanol was added to the precipitated graphitic material. The process of centrifugation, decanting, and adding fresh methanol was repeated for a total of four cycles. After the solvent exchange, the graphene was re-dispersed into solution through 1 hour of sonication.

### **2.2.3 Colloidal Stabilization**

During the investigation of contamination present in the 8 dram Fisherbrand Vials, the vials were used in two conditions: “New” and “Cleaned.” A “New” vial was removed from the original packaging and used as is. A “Cleaned” vial was prepared from a new vial by cleaning with powdered soap and water, rinsed with de-ionized water, rinsed with acetone, blown dry with nitrogen, and baked at ~ 90°C in a Lab-line Imperial II Radiant Heat Oven until used.

#### **2.2.3.1 Benchtop Observations**

Samples for benchtop observations were prepared in “new” and “cleaned” 8 dram vials with 10 mL of centrifuged 168 hour graphene solution and 10 mL of methanol. After mixing, the vials were stirred to avoid contact with the closure. Isoprene, in varying volumes (10  $\mu$ L, 25  $\mu$ L, 50  $\mu$ L, 100  $\mu$ L, 1000  $\mu$ L), was then added to cleaned vials through an auto-pipet. Prior to use, isoprene was washed in 0.1 M NaOH to remove the stabilizer, tert-butylcatechol, in a method described by Armarego and Chai.<sup>134</sup> Following the separation, the cleaned isoprene was dried over CaCl<sub>2</sub> and isolated through vacuum filtration. The isoprene was confirmed dry through FT-IR analysis (Nicolet 6700 FT-IT; ThermoScientific OMNIC Software Version 8.3) and the absence of a broad peak between 3200 – 3600 cm<sup>-1</sup> which is characteristic of the O-H stretching in water.<sup>100</sup>

#### **2.2.3.2 HPLC – MS**

A “new” and a “cleaned” vial were used to prepare samples for analysis through HPLC. Samples were prepared by mixing 250  $\mu$ L of 18.20 M $\Omega$  H<sub>2</sub>O with 250  $\mu$ L acetonitrile in each of the vials. Samples were stirred within the vials, but not shaken to avoid contact with the threaded caps.

### **2.2.3.3 Nuclear Magnetic Resonance Spectroscopy**

A NMR sample was prepared by agitating 0.75 mL of ACROS Organics Chloroform-d for NMR (99.8 atom %D) in a “new” vial with a vortex shaker for approximately 60 seconds. After agitation, the sample was introduced to a 500 MHz NMR tube using a disposable syringe with a metal needle.

### **2.2.4 Colloidal Stabilization – Isoprene**

Isoprene, the monomer of the suspected contaminant, is a readily available through commercial sources and was investigated as a substitute for polyisoprene. It was suspected that as the monomer the stabilization effect will be decreased over that caused by the longer carbon chain of the polymer.

#### **2.2.4.1 Benchtop Observations**

To observe the colloidal suspension over time a set of seven samples were prepared simultaneously. Six of the samples were prepared in “cleaned” 8 dram vials while the final sample was prepared in a “new” vial to illustrate the effects of the unknown contamination. Each sample contained 10 mL of methanol and 10 mL of the centrifuged 168 hour graphene solution. Finally, isoprene (10  $\mu$ L, 25  $\mu$ L, 50  $\mu$ L, 100  $\mu$ L, and 1000  $\mu$ L) was added to the remaining samples through auto-pipet. Stirring of the samples was kept to a minimum after mixing to ensure that the sample did not come into contact with the cap. After preparation, the samples were isolated on the benchtop for observation.

#### **2.2.4.2 UV-Vis Spectroscopy – Kinetic**

Sample preparation for the UV-Vis Kinetics study was accomplished in the same manner as the samples prepared for the Benchtop Observations of the colloidal stability. After the sample was prepared in an 8 dram vial, an aliquot of the solution was removed for analysis in a quartz cuvette.

#### **2.2.5 Colloidal Stabilization – Polyisoprene**

An ideal experiment to confirm the stabilizing effect of the suspected contaminant, polyisoprene, on the colloidal graphene solutions would be to repeat the benchtop and UV-Vis Kinetic studies described with a low-molecular weight sample of polyisoprene. Although this method was researched it was not accomplished for several practical reasons. Several reliable synthetic routes exist to polymerize isoprene. These include the use of benzyl diethyldithiocarbamate as an iniferter<sup>135</sup> and a radical polymerization scheme using the reversible addition-fragmentation chain transfer (RAFT) technique.<sup>136</sup> The RAFT technique appeared to be the most promising method available because it allowed for the precise control of the molecular weight of the product however the non-availability of the initiators through commercial sources made the technique impractical. Moreover, the physical properties of isoprene, most notably a low boiling point of 34 °C,<sup>137</sup> required advanced and time consuming organic chemistry techniques along with specialized equipment that was not readily available. Polyisoprene is commercially available in the molecular weight range (800 – 1000) desired, however a sample was not able to be acquired within the time constraints of this project. Therefore the benchtop and kinetic experiments remain an avenue of investigation for follow-on studies.

## **2.3 CHARACTERIZATION METHODS**

### **2.3.1 Graphene Synthesis**

#### **2.3.1.1 UV-Vis Spectroscopy**

Graphene samples were characterized after dilution through UV-Vis spectroscopy using both a ThermoScientific GENESYS 10S UV-Vis and a ThermoScientific NanoDrop 2000c Spectrophotometer with quartz cuvettes. The GENESYS 10S instrument utilized a Xenon flash lamp and collected data over the wavelength range of 190 – 1100 nm. The NanoDrop 2000c instrument also utilized a Xenon flash lamp as its light source and scanned the wavelength range 190 – 840 nm. For concentration calculations the absorption at 660 nm was recorded.

#### **2.3.1.2 Atomic Force Microscopy**

The AFM samples as previously described were analyzed on an Asylum MFP-3D Atomic Force Microscope by tapping mode in air with HQ:NSC15/Al BS  $\mu$ masch AFM probes (325 kHz, 40 N/m) purchased from NanoAndMore USA. Images were analyzed utilizing Asylum Research Igor Pro (Version 6.3.7.2) software.

#### **2.3.1.3 Raman Spectroscopy**

The Raman sample prepared as described through vacuum filtration was characterized through Raman spectroscopy using a Nikon microscope. The sample was analyzed using a 532 nm single longitudinal mode solid state laser with a 40x objective (NA: 0.60) which produced a spot size of  $\sim 1 \mu\text{m}$ . Measurements were taken at two different power settings and exposure times. The higher power setting used provided 3.1 mW of power and was integrated for 30 seconds. A second

measurement was taken using 0.13 mW of power and was integrated for 10 minutes. The instrumental results were analyzed using Andor SOLIS for Spectroscopy (Solis Version 4.16.30003.0; SDK Version 2.88.30003.0) software.

## **2.3.2 Laboratory Contamination Studies**

### **2.3.2.1 Benchtop Observations**

To confirm the presence of a contamination effect during solvent exchange, a series of systematic benchtop observations were made. In the series of experiments as many variables as possible were analyzed. The series of observations were designed to determine if the contamination came from the vial, cap, or was unique to a specific shipment from which the vials were acquired. Once the experiments were designed, observations were taken at regular intervals and photographed to observe trends in the separations. All observations were taken in ambient lab conditions. Results were documented in the laboratory notebook and through photography with a Samsung Galaxy S5 equipped with a 16 megapixel camera and a Canon EOS Rebel T1i (15.50 megapixel) digital camera.

### **2.3.2.2 High-Performance Liquid Chromatography**

To isolate the contaminants present in the “new” 8 dram vials, samples prepared as described were separated using HPLC. The separation was completed using a modular ThermoScientific Ultimate 3000 instrument. The instrument was equipped with a reverse phase C<sub>18</sub> Hypersil GOLD column (100 x 2.1 mm; 1.9 μm particles). Samples were introduced to the column through the use of an auto-sampler with an injection volume of 5.0 μL. The column temperature was set to 30°C and the separation carried out through a gradient elution scheme where %B was increased from

10% to 90% over 23 minutes (Solvent A = water; Solvent B = acetonitrile) at a constant flowrate of 0.2 mL min<sup>-1</sup>.

### **2.3.2.3 Mass Spectroscopy**

Analysis through mass spectroscopy was carried out immediately following separation through HPLC as the instruments were attached in tandem. MS analysis was completed with a ThermoScientific Q Exactive instrument utilizing electrospray ionization and operating in positive mode. The analytes were analyzed over the range of 133.4 to 2000 *m/z* with a resolution of 70,000. Analysis was completed using the included Thermo Xcaliber Qual Browser (Version 3.0.63).

### **2.3.2.4 Nuclear Magnetic Resonance Spectroscopy**

The presence of contamination was probed through NMR using a Bruker Ultrashield 500 Plus instrument. The equipment utilized a liquid helium cooled 500 MHz magnet. The sample prepared as previously described was analyzed in a 500 MHz NMR tube with CDCl<sub>3</sub> as the solvent. <sup>1</sup>H NMR Data acquisition utilized 16 scans taking a total time of 11.48 minutes. The data acquired was analyzed using the Bruker TopSpin (Version 2.1) software suite.

## **2.3.3 Colloidal Stabilization - Isoprene**

### **2.3.3.1 Benchtop Observations**

A series of benchtop observations were made to observe the visual changes of the colloidal suspensions overtime. The experiments were designed so that a side-to-side comparison could be made to contrast different experimental conditions. Results were documented in the laboratory

notebook from observations and through photography with a Samsung Galaxy S5 equipped with a 16 megapixel camera and a Canon EOS Rebel T1i (15.50 megapixel) digital camera.

### **2.3.3.2 UV-Vis Spectroscopy – Kinetic**

The stability of the colloidal graphene samples were characterized through UV-Vis spectroscopy using a ThermoScientific NanoDrop 2000c Spectrophotometer with quartz cuvettes. The kinetic studies were automatically completed using the ThermoScientific NanoDrop 2000/2000c control software (Version 1.6.198) and set to take a measurement every five minutes for 12 hours. Each measurement scanned the wavelength range 190 – 840 nm. Additionally the absorption at 660 nm was recorded during each measurement for later analysis of the reaction kinetics.

## 3.0 RESULTS AND DISCUSSION

### 3.1.1 Graphene Synthesis

#### 3.1.1.1 UV-Vis Spectroscopy

Graphene prepared through the protocol previously described and diluted was analyzed through the use of UV-Vis spectroscopy. Figure 14 shows a typical UV-Vis spectrum acquired from a diluted sample of solvent-exfoliated graphene prepared during this investigation.

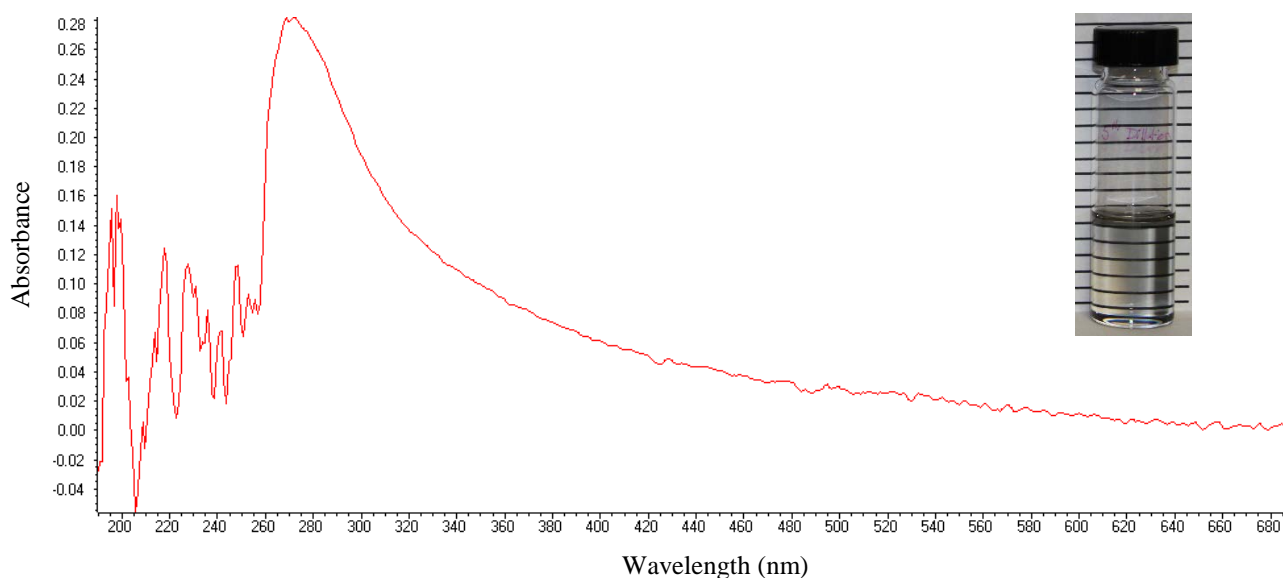


**Figure 14.** UV-Vis spectrum of the sixth serial dilution (64x) of solvent-exfoliated graphene.  
Inset: Image of diluted graphene sample.

The main feature of the spectrum is an absorption peak around 270 nm. This peak is characteristic of a graphene UV-Vis sample and the  $\pi \rightarrow \pi^*$  transition of the  $sp^2$  hybridized bonds of an aromatic ring.<sup>138</sup> The full instrument range was scanned during each measurement with the absorbance at 660 nm recorded to calculate the concentration.

In order to determine the concentration of solvent exfoliated graphene, Khan *et al.* presented a technique in which the absorption coefficient ( $\alpha$ ) of graphene is experimentally determined so that Beer's Law (equation 1) can be applied.<sup>31</sup> To accomplish this calculation, the researchers measured the absorbance for multiple graphene samples from a range of sonication times and centrifugation rates at 660 nm.<sup>31</sup> Additionally, they acquired the mass of each sample through filtration and weighing.<sup>31</sup> With this information they were able to report that the average value of  $\alpha$  (660nm) is 3620 mL mg<sup>-1</sup> m<sup>-1</sup>.<sup>31</sup> The method of graphene synthesis used in this investigation is a variant of the method pioneered by Khan and co-workers,<sup>42</sup> therefore the literature reported value of  $\alpha$  (660nm) was utilized to calculate an estimate of concentration of the graphene produced. Through Beer's Law and the methodology described, the concentration of graphene produced was calculated as 0.545 mg mL<sup>-1</sup>, slightly lower than the literature value of 0.8 mg mL<sup>-1</sup>.<sup>42</sup>

### **3.1.1.2 Atomic Force Microscopy**

The previously described graphene samples prepared on thermal oxide silicon wafers were characterized using AFM. On the samples a low density of plate like structures were observed in all areas of the sample that were analyzed, a representative image is displayed in Figure 15(A).

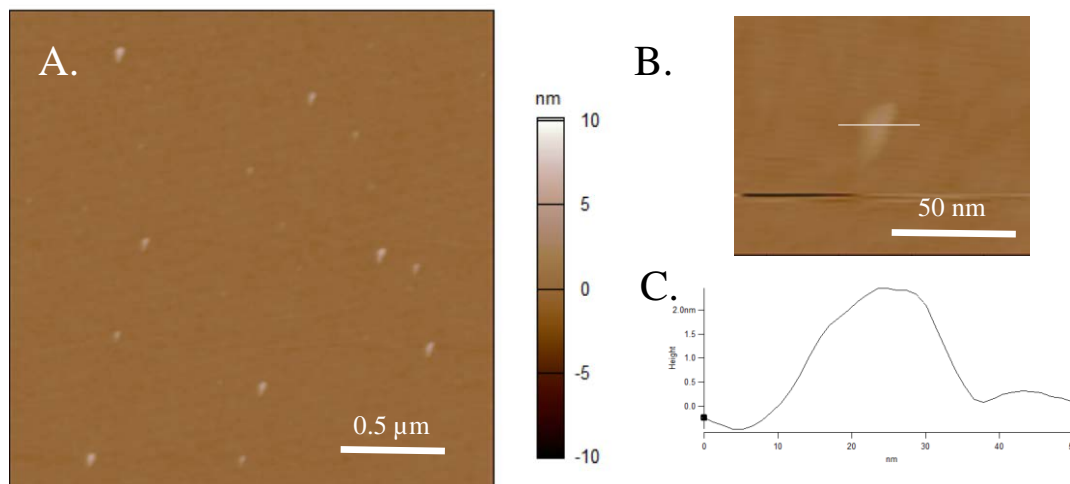


**Figure 15.** AFM images of experimentally prepared graphene samples on thermal oxide silicon wafer substrate, images obtained using tapping mode (A) Image of  $6.25 \mu\text{m}^2$  section of sample showing dispersion of graphene flakes on the substrate. Scale bar =  $0.5 \mu\text{m}$  (B) Image of single graphene flake. Scale bar =  $50 \text{ nm}$  (C) Cross section of single flake in image (B).

Figure 15(B) is a representative image of the individual graphene flakes that were observed. The flakes varied in length from approximately  $45 \text{ nm}$  to  $250 \text{ nm}$  and are  $2 \text{ nm}$  to  $12 \text{ nm}$  in height. Therefore the graphene flakes observed were smaller than the average flake size ( $1 \mu\text{m} \times 0.5 \mu\text{m}$ ) reported by Khan *et al.* prepared by the parent procedure.<sup>42</sup>

### 3.1.1.3 Raman Spectroscopy

The thin film graphene sample prepared through vacuum filtration was characterized with Raman spectroscopy as previously described. The Raman spectrum acquired (Figure 16) displays the three characteristic bands (*D*, *G*, and *2D* bands) of a graphitic material. The experimental Raman spectrum does not show evidence of single layer graphene (Figure 7), but is consistent with that of few layer graphene.

The *D* band is not observed in the Raman spectrum of pristine graphene.<sup>97</sup> Therefore, the clearly defined *D* band observed in the experimentally obtained spectrum at  $\sim 1380 \text{ cm}^{-1}$  indicates that there is the presence of defects within the sample. The blue-shift of the *D* band from the expected  $1350 \text{ cm}^{-1}$  is most likely a bi-product of the higher laser intensity used in acquiring the

measurement.<sup>94</sup> The most likely source of the defects within the sample are the edges of the individual graphene flakes. The edges are the suspected source of the disorder for several reasons. First, the spot size of the excitation laser used was  $\sim 1 \mu\text{m}$ , this is several times larger than the average size of the graphene flakes analyzed and it is likely that the laser was incident to several graphene edges during the measurement. Furthermore, the unbroadened G band indicates that the source of disorder is likely the flake edges rather than a structural defect.<sup>129</sup> Another probable cause of the observed disorder is random stacking of the graphene flakes. Through the preparation of the sample and aggregation, it is likely that the flakes randomly stacked or formed multi-layer graphene and reflected disorder during the Raman measurement. Finally, the intensity of the *D* band indicates that the edges of the graphene flakes are most likely in the armchair configuration as edges in the zig-zag configuration result in the observation of little to no *D* band in a Raman spectrum.<sup>139</sup> Therefore, since the edges of a graphene flake act as a defect the presence of the *D* band is consistent with a sample of graphene exfoliated through solvent-based methods with a small flake size.<sup>39</sup>

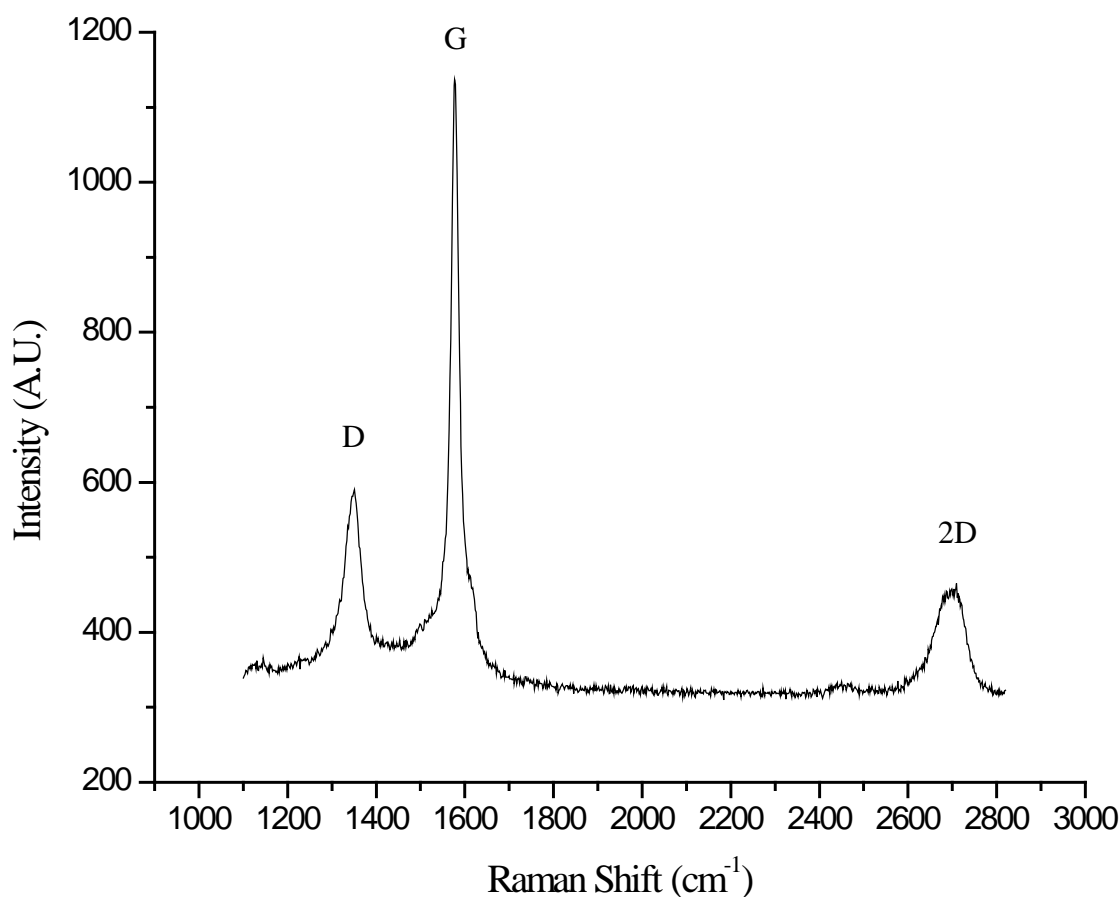


**Figure 16.** Raman spectrum of graphene prepared through solvent-based exfoliation. The characteristic *D* band ( $\sim 1380\text{ cm}^{-1}$ ), *G* band ( $\sim 1580\text{ cm}^{-1}$ ), and *2D* band ( $\sim 2700\text{ cm}^{-1}$ ) of graphene are present. The measurement was taken with a laser intensity of 3.1 mW and integrated for 30 seconds.

The characteristic *G* band ( $\sim 1580\text{ cm}^{-1}$ ), which is a result of the Raman active  $E_{2g}$  vibrational mode of graphite, and the *2D* band ( $\sim 2700\text{ cm}^{-1}$ ) are both present in the spectra and are always included in the Raman spectra of graphene.<sup>139</sup> In a pristine sample of graphene a sharp *2D* band is expected to be approximately four times the intensity of the *G* band.<sup>95</sup> Although this relationship was not observed experimentally, the presence of few layer graphene is suspected because of the shape of the *2D* band. Most notably, the *2D* band is nearly symmetric in shape and absent of the *2D*<sub>1</sub> shoulder peak present in the Raman spectra of graphite (Figure 7).<sup>95</sup> Additionally, the observed *2D* band is not a single sharp peak but is a broadened symmetric peak.

The broadening effect seen in bi-layer graphene (Figure 17A) is a byproduct of the 2D band splitting during excitation into four components in multi-layer graphene before evolving into two components and the distinct shape of the graphite 2D band.<sup>95</sup> Comparison between the reported 2D band of bi-layer graphene (Figure 17A)<sup>95</sup> and the experimentally obtained spectra (Figure 16) strongly support the presence of few layer graphene.

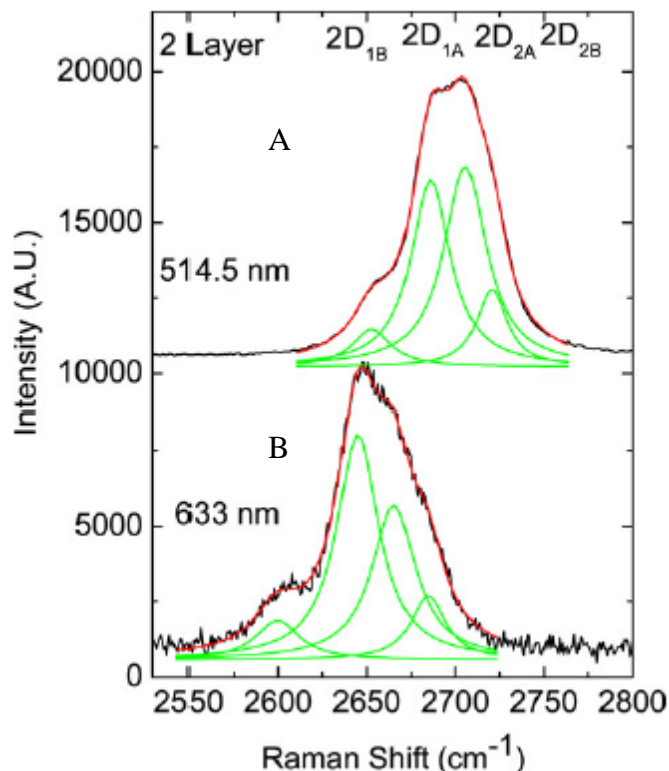


**Figure 17.** Shape of 2D band in bi-layer graphene. (A) 514.5 nm laser excitation (B) 633 nm laser excitation.<sup>95</sup>

Reprinted from *Solid State Commun.*, 143 (1-2), Ferrari, A. C., Raman spectroscopy of graphene and graphite: Disorder, electron-phonon coupling, doping and nonadiabatic effects, 52, Copyright 2007, with permission from Elsevier.

### 3.1.2 Laboratory Contamination Studies

The presence of laboratory contamination was first uncovered through benchtop observations during the solvent exchange process. Solvent exchange was determined to be necessary due to the undesirable properties of NMP and the difficulty in working with the graphene solution when

dispersed in NMP. To identify an appropriate solvent for the exchange, a selection of eight different solvents that were found to be miscible with NMP were tested by mixing amounts of each solvent with the 168 hour graphene solution in 1 dram vials. Daily observations were then made to identify the solvent that caused precipitation to occur the quickest (Figure 18).

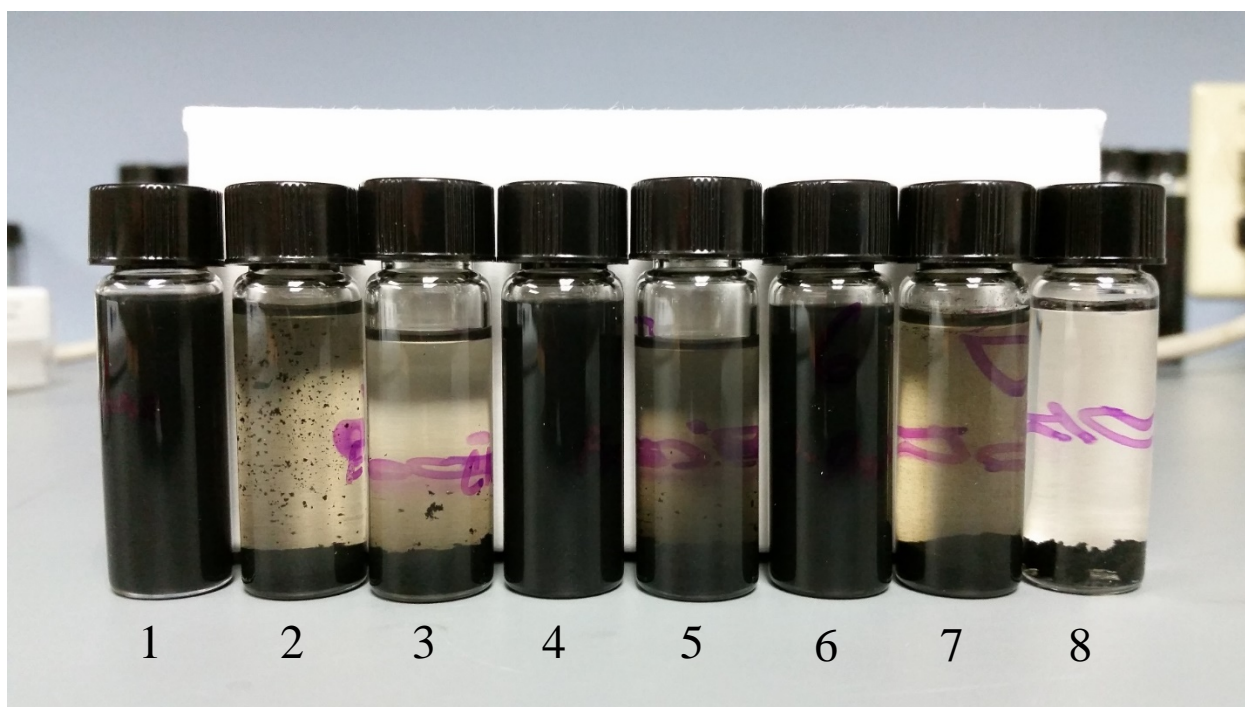


**Figure 18.** Solvents miscible with NMP mixed with 168 hour graphene solution after 8 days of observation. (1) acetone (2) ethanol (3) chloroform (4) formamide (5) dichloromethane (6) 2-propanol (7) DI H<sub>2</sub>O (8) methanol.

As clearly seen in Figure 18, methanol performed the best and was selected for the solvent exchange. This experimental result is consistent with the work of Zhang and co-workers who suggested ethanol for the technique but indicated that methanol and dichloromethane would also give satisfactory results.<sup>132</sup>

When the solvent exchange was scaled up from 1 dram to 8 dram vials, it was noticed that the 1:1 ratio of the 168-hour graphene suspension and methanol separated differently in different sized vials (Figure 19). This observation sparked a secondary investigation into what was causing the added stability of the colloid suspension within the larger vials.

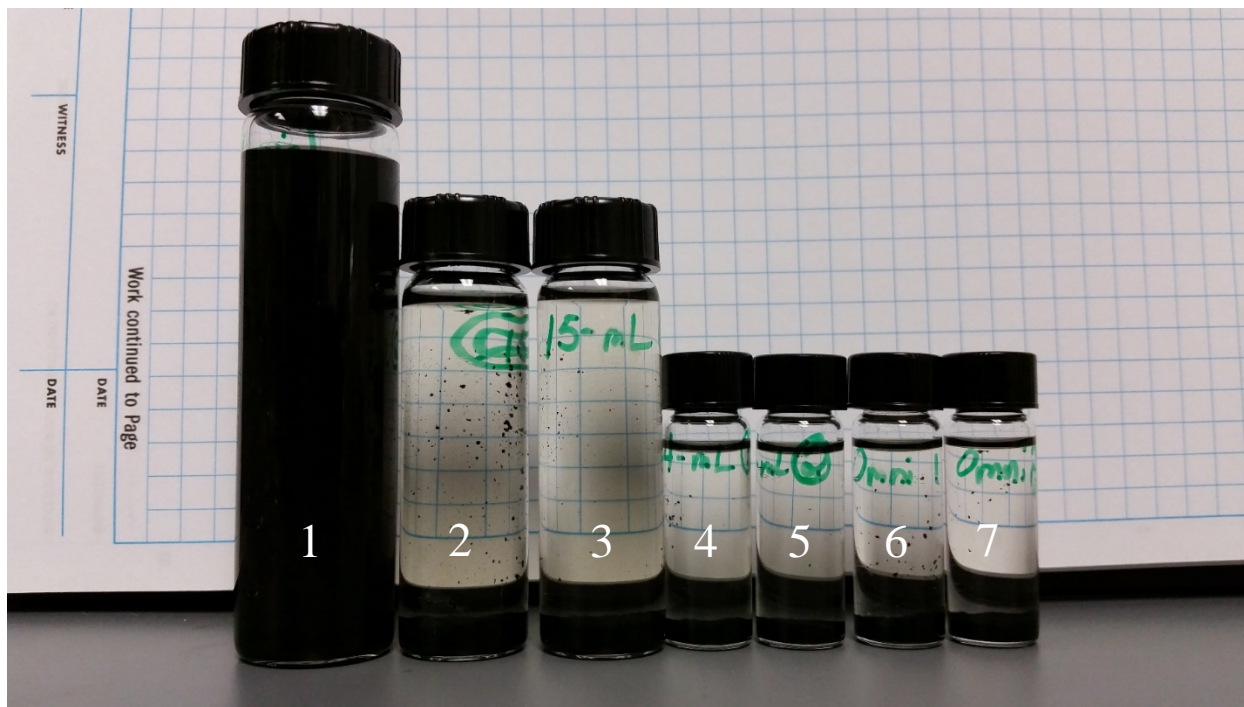


**Figure 19.** Solvent exchange was scaled-up up to 8 dram vials with a 1:1 mixture of 168-hour graphene solution and methanol to confirm the stabilization effect. Image taken after 68 hours. (1) 8 dram vial (2 and 3) duplicate 4 dram vials (4 and 5) duplicate 1 dram vials (6 and 7) duplicate 1 dram vials using Omnisolv methanol to determine if the solvent was the source of the disparity in performance.

### 3.1.2.1 Benchtop Observations

A series of benchtop observations were made to both confirm the disparity in separation quality between different sized vials and to try to isolate the condition that was causing the behavior.

Through the observations it was determined that if the vial was “cleaned” or “new” had the largest impact on the stability of the solution. Figure 20 illustrates the dramatic differences in behavior noted in some of the benchtop observations. Contact with the cap, different lots of vials, and centrifugation were all evaluated and found to have no impact on stability. The only other action that had a noticeable impact on the stability of the solution besides cleaning was whether after mixing it was “shaken” (violently shaken to ensure contact of the liquid with the vial’s cap) or “stirred” (mixed with a glass Pasteur pipet). Although a difference between “shaken” and “stirred” samples was noted, it is attributed to the possible difference in the quality of mixing

between the samples, not a stabilization effect. Therefore, from the benchtop observations made, it was concluded that the contamination was likely present in the vials from the manufacturer.

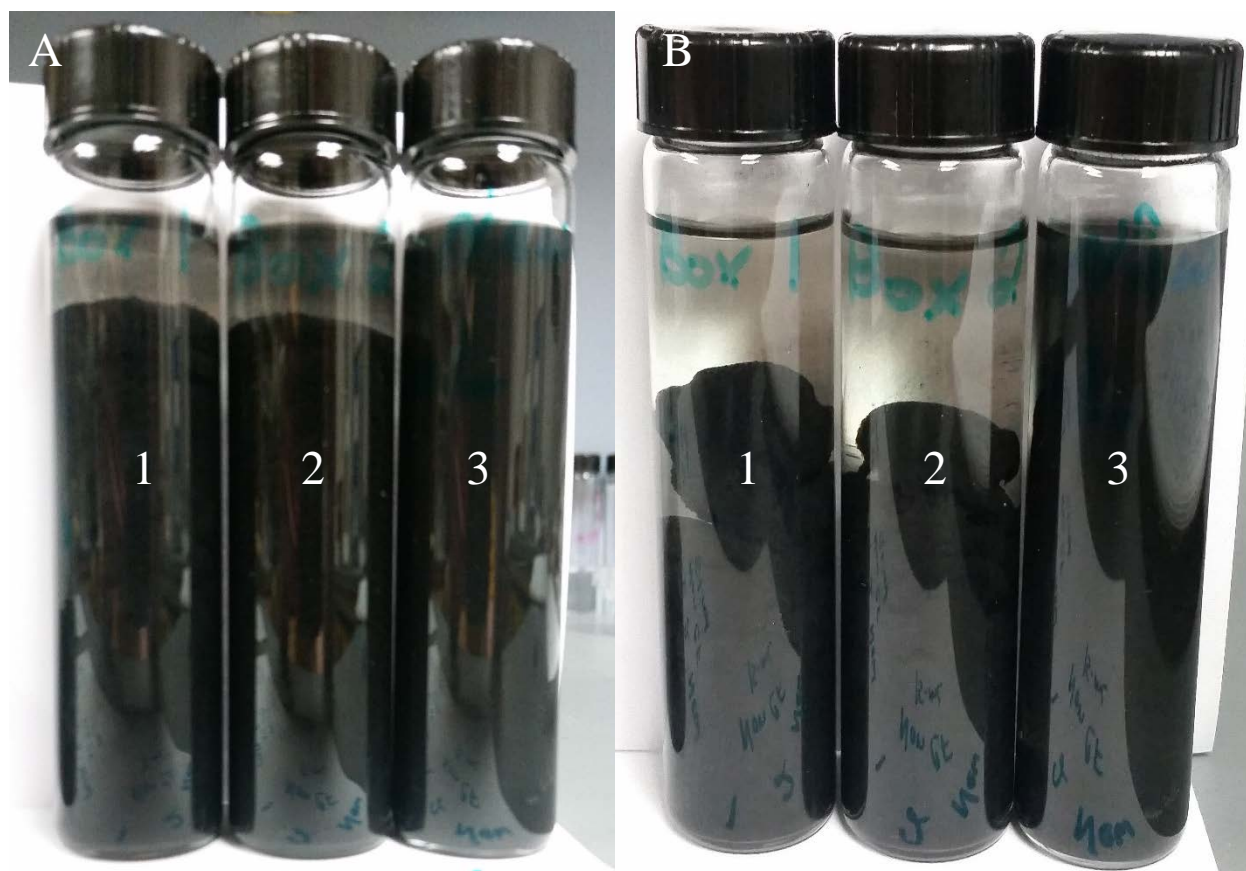


**Figure 20.** Benchtop observations. Vials 1 and 2 are both “cleaned” but from different packages and lots. Vial 3 is a “new” 8 dram vial. (A) One hour after mixing. (B) 2 hours 10 minutes after mixing.

Fisher Scientific was contacted about this concern and contacted the manufacturer on the researcher’s behalf. The manufacturer (unnamed supplier in the United States) reported “that there is no coating in the interior of the vial.”<sup>140</sup> As a result, further analysis through HPLC-MS and NMR were needed to identify the suspected contamination within the vials.

### **3.1.2.2 High-Performance Liquid Chromatography**

An HPLC investigation through the procedure previously described was accomplished to isolate any possible contaminants within a “new” 8 dram vial. Figure 21 summarizes these results.

Through comparison of the control “cleaned” vial chromatogram, Figure 21(A), and the chromatogram acquired from “new” vial, Figure 21(B), four peaks were highlighted as possible differences and warranted further investigation. The difference in the appearance between the two chromatograms is due to the scale used by the analysis software. The y-axis is displayed in “relative abundance” instead of absolute values so that a direct comparison could not be made. Therefore chemical intuition and the expertise of the technicians completing the separation were relied on to identify the peaks of interest. Additionally, the noise observed beyond a 20 minute retention time is attributed to contaminants in the column used for the separation and do not show any meaningful differences between the two chromatograms worthy of investigation.

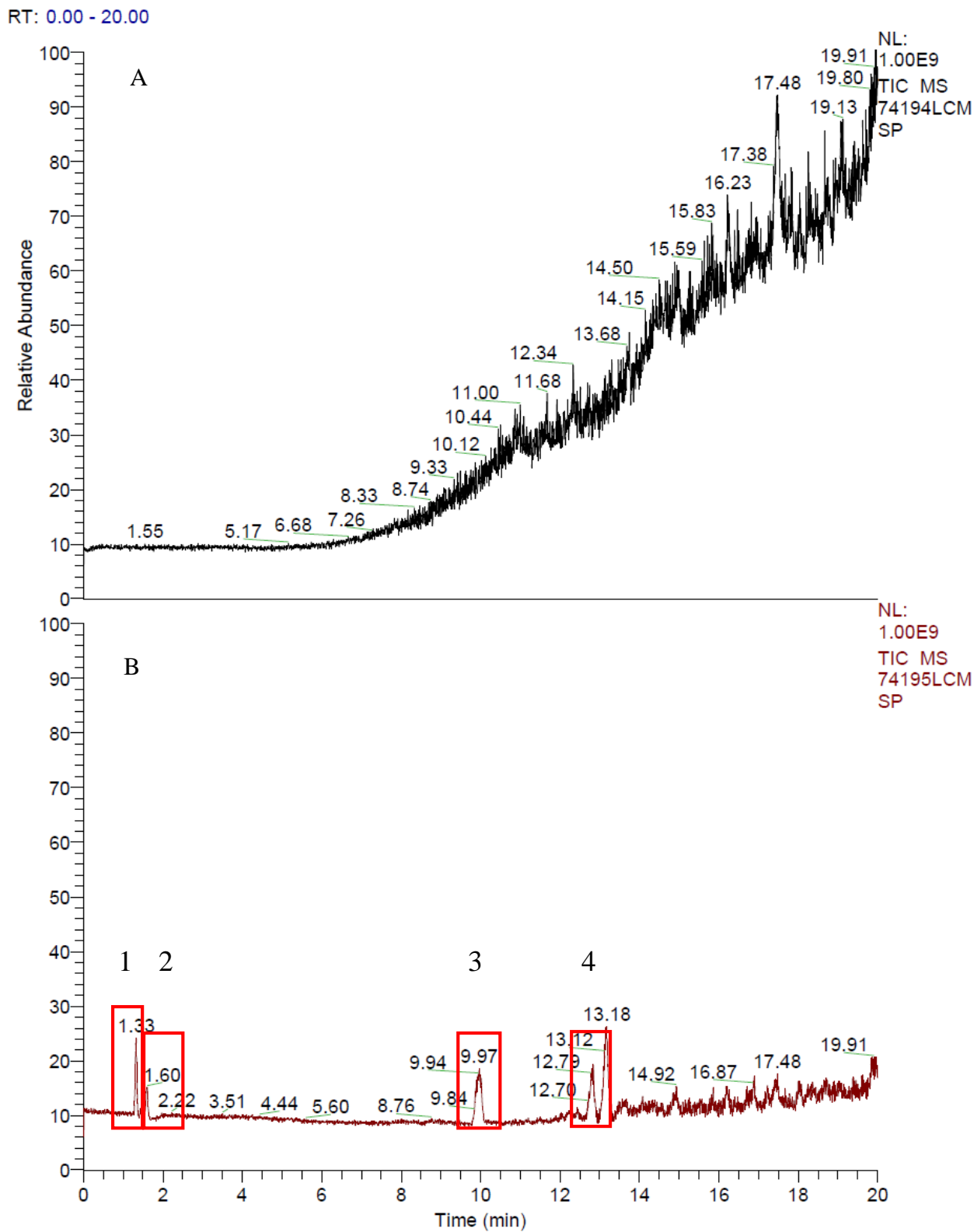


**Figure 21.** HPLC chromatograms from (A) “cleaned” vial and (B) “new” vial. Highlighted red boxes indicate interpreted differences between the two separations.

### 3.1.2.3 Mass Spectroscopy

Mass spectroscopy was utilized to analyze the four peaks that were identified for further investigation through HPLC.

The mass spectrum for the first peak of interest identified through HPLC (Figure 21, peak 1) is shown in Figure 22. The identity of this compound was not readily identified through comparison of the spectra to databases of known compounds, but the fragmentation pattern yielded some important clues to a possible identity. The most noticeable feature is the repeating pattern of fragmentation with a spacing of 68  $m/z$ . The repeating fragmentation pattern is indicative of a polymer with a repeating unit that has a mass of 68. One possible combination of atoms for the repeating unit is  $C_5H_8$ . Research revealed that isoprene, a component of natural rubber, is a possible molecule that meets this criteria.

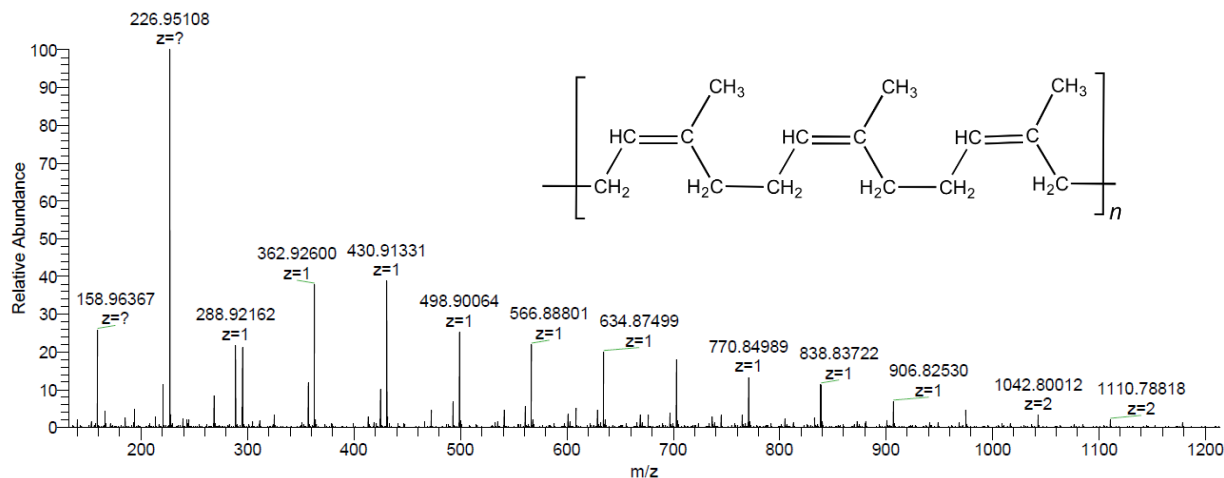


**Figure 22.** Spectrum obtained from MS analysis of peak with a retention time between 1.26 – 1.36 minutes.  
Inset: Chemical structure of suspected molecule, polyisoprene ( $C_5H_8$ ).

Isoprene, hailed as “one of nature’s favorite building blocks” is found in many compounds isolated from animal and plant products.<sup>141</sup> In its polymer form, polyisoprene, it is used as a plasticizer in rubber compounds and in the manufacturing process of rubber goods.<sup>142</sup> When revealed that the cap of the 8 dram vials being investigated is a “black phenolic screw-top closure with polyvinyl-faced pulp liner” and that the vials were almost certainly exposed to machinery during the

manufacturing process, it would be very plausible that they were exposed to polyisoprene during their manufacturing or shipment.<sup>143</sup>

Despite the initial analytical evidence, the presence of polyisoprene does not explain all of peaks observed in the mass spectrum of the unknown. Most notably the initial peak displayed with a  $m/z$  of 159 is inconsistent with polyisoprene. It is suspected that this fragmentation peak corresponds to an unknown end group. There are additionally two other instances in the spectrum where the repeating  $m/z$  of 68 breaks down and are likely from the presence of a functional group attached to the polymer chain. It is highly likely that if the contaminant is naturally occurring or its presence is otherwise unintended, that it would not be pure and therefore have some type of functionalization or other defect present. Additionally, it is likely that the end group or other functional groups within the contaminant are polar. Evidence to support the polarity of this unknown group is provided from the HPLC chromatogram (Figure 21) where the unknown eluted first from the column with a retention time near 1.3 minutes. In reverse phase chromatography, a nonpolar molecule such as polyisoprene would be expected to interact more favorably with the nonpolar stationary phase and be retained longer.<sup>100</sup> The opposite effect was observed with the suspected polymer eluting first, suggesting a polar component in the molecule. Therefore it is suspected that the identity of the compound with a retention time between 1.26 and 1.36 minutes is a low molecular weight ( $\sim 1000$ ) copolymer consisting mostly of polyisoprene (Figure 22, inset).

The remaining peaks of interest highlighted through HPLC were not readily identified through a high confidence match with the instrument's electronic database, nor did they contain any readily identifiable features to guide the investigation. Therefore they remain as unknowns

and possible leads for further investigation if polyisoprene is determined not to be the contaminant and the source of the colloidal stability.

### 3.1.2.4 Nuclear Magnetic Resonance Spectroscopy

The identity of the unknown contaminant was further investigated through NMR spectroscopy.

The  $^1\text{H}$  NMR spectrum obtained from the investigation is depicted in Figure 23.

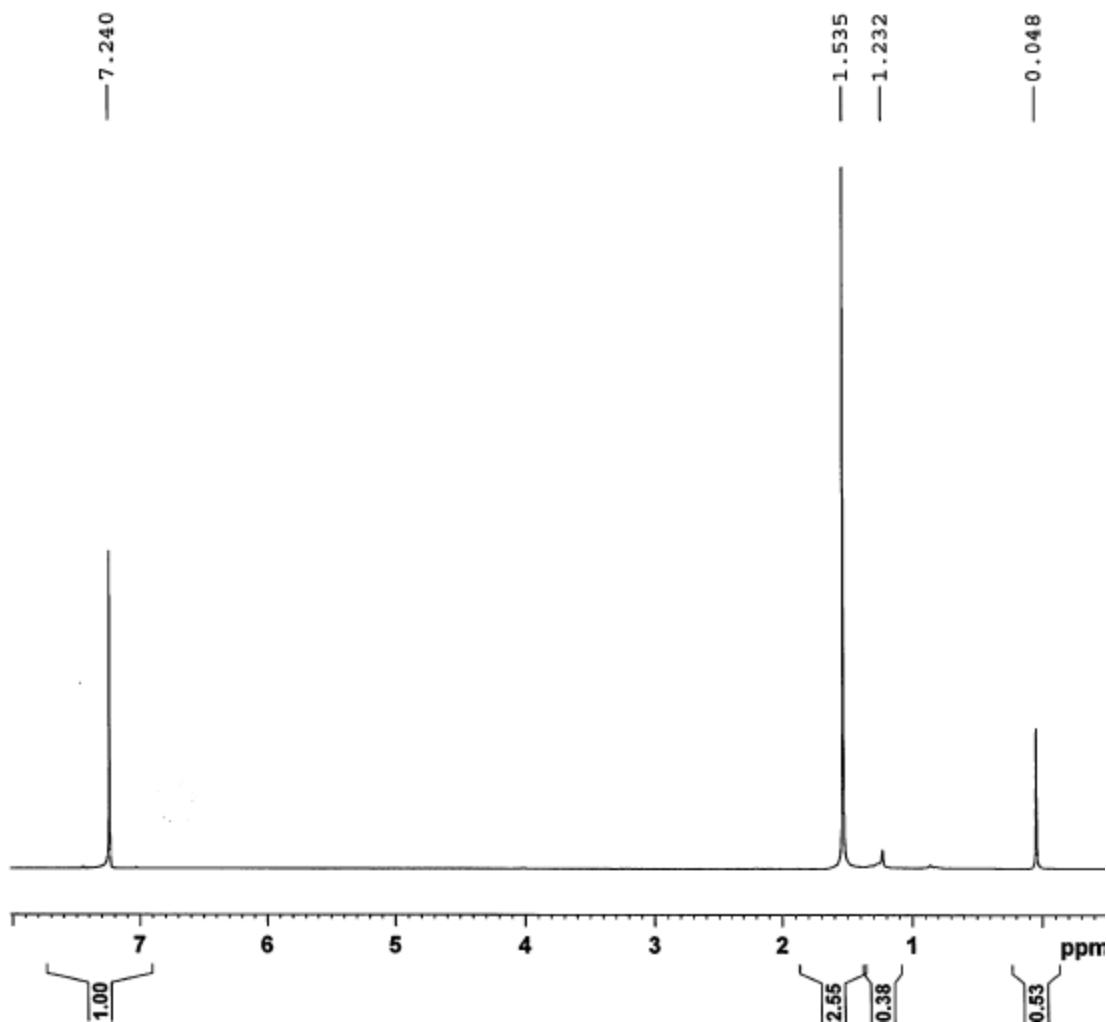


**Figure 23.**  $^1\text{H}$  NMR spectrum obtained from contaminated vial. Spectrum obtained using 16 scans on a 500 MHz NMR with  $\text{CDCl}_3$  as the solvent.

Analysis of the spectrum was completed through the TopSpin software and focused on identifying the observed peaks. The peak at 7.240 is expected and is the  $^1\text{H}$  NMR solvent peak for

$\text{CDCl}_3$ , it is readily identifiable and was used to calibrate the remaining peaks. The most dominant peak in the spectrum, a singlet at 1.535, is most likely from  $\text{H}_2\text{O}$  contamination. Gottlieb *et al.* identified this location for the signal corresponding to the instrument response from the symmetric hydrogens in  $\text{H}_2\text{O}$ .<sup>144</sup> It is not a surprise to see a signal from  $\text{H}_2\text{O}$  as atmospheric contamination is the likely source as no special precautions to dry the sample were made. It is suspected that the singlet peaks at 1.232 and 0.048 are from common laboratory contaminants that may or may not have come from the contaminated vial. The peak at 1.232 is characteristic of grease from a long chain linear aliphatic hydrocarbon, this could have been acquired through the sample preparation and is a possible lead for identifying the remaining three unknown compounds identified through HPLC.<sup>144</sup> Additionally the peak at 0.048 could also be from grease contamination and is characteristic of poly(dimethyl siloxane).<sup>144</sup> This contaminant has a unit mass of 74 and therefore does not match the mass spectrum of a polymer that was previously identified but could possibly be from the sample preparation or NMR tube. Therefore, a peak corresponding to isoprene could not be assigned from this NMR analysis. Although evidence was not acquired to substantiate the identity of polyisoprene as the contaminant, it also does not eliminate it due to the high detection limit of the  $^1\text{H}$  NMR technique. It is suspected that the contaminant in the vials is at a very low concentration and therefore could not be detected through  $^1\text{H}$  NMR.

### **3.1.3 Colloidal Stabilization – Isoprene**

The effect of isoprene on the stability of the colloidal graphene solution was probed through observation and a kinetics study completed with UV-Vis spectroscopy. To qualify the impact of isoprene on the stability varying concentrations of the monomer were added to the samples.

In an effort to understand the interaction of the monomer with the graphene flakes, the theoretical surface coverage of the graphene flakes by isoprene was calculated at different concentrations. To do so, a series of assumptions were made. First, the graphene flakes were assumed to be monolayer and that the area on both sides of the flake are available to interact with the isoprene molecules. The area of the graphene flakes were calculated using the average dimensions (1  $\mu\text{m}$  x 0.5  $\mu\text{m}$ ) reported by Khan *et al.* as an approximation as this research was based in part on their procedure.<sup>42</sup> Finally to determine the number of graphene flakes present in the solution, the experimentally determined concentration from the UV-Vis investigation was utilized.

To calculate the surface area of isoprene available to interact with the graphene in the sample an area known as the solvent accessible surface area (Figure 24) was utilized. Unlike the graphene flakes, which were assumed to be atomically flat rectangles, the chemical structure of isoprene does not allow for all of its surface area to be available for interactions with neighboring molecules. Due mainly to structural hindrances, and defined by its chemical properties, the solvent accessible surface area has become a common value to describe the surface area of the molecule. First proposed by Michael Connolly, the solvent assessable area is calculated from the locus of the center of a sphere that is representative of a solvent molecule.<sup>145</sup> The sphere is then rolled along the surface of the outside of the molecule, defined as the van der Waal's surface, to determine the area that a solvent molecule can access.<sup>146</sup> The modern method of making this calculation is through computational software. CambridgeSoft Chem3D 15.0 was utilized to calculate the solvent accessible area for this investigation. The software utilized a computational method designed by Connolly to compliment his earlier work.<sup>147</sup> Through this method, the calculated

solvent accessible area of isoprene is  $100.536 \text{ \AA}^2$  which was used to calculate the possible surface coverage in the colloidal solution. The results of these calculations are summarized in Table 1.

**Table 1.** Surface Coverage ( $\Theta$ ) of Graphene Flakes with Isoprene.

Isoprene ( $\mu\text{L}$ )	Concentration of Isoprene (ppm)	Surface Area of Isoprene ( $\text{\AA}^2$ )	$\Theta$ (%)
<b>10</b>	340	$6.05 \times 10^{21}$	423
<b>25</b>	850	$1.51 \times 10^{22}$	1058
<b>50</b>	1700	$3.03 \times 10^{22}$	2115
<b>100</b>	3400	$6.05 \times 10^{22}$	4231
<b>1000</b>	34000	$6.05 \times 10^{23}$	42311

**Assumptions:** Mono-layer flakes of graphene with the average dimensions of  $1 \mu\text{m} \times 0.5 \mu\text{m}$ . Total surface area of graphene available in 10 mL sample =  $1.43 \times 10^{21} \text{ \AA}^2$ .

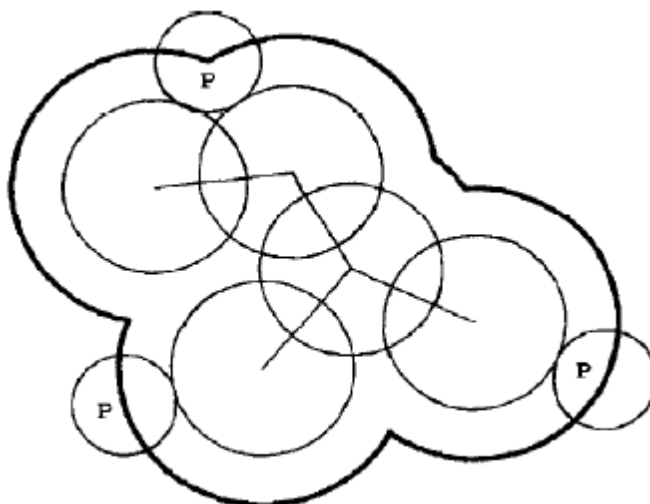


**Figure 24.** Solvent Accessible Area.<sup>148</sup>

Bold line represents the solvent accessible area; thin line represents the van der Waals surface; spheres labeled with a “P” represent the probe sphere.

Reprinted from *Computers & Chemistry*, 18 (4), Pacios, L. F., ARVOMOL/CONTOUR: Molecular surface areas and volumes on personal computers, 378, Copyright 1994, with permission from Elsevier.

### 3.1.3.1 Benchtop Observations

Observations were made every 30 minutes during the first 6 hours and hourly thereafter until 12 hours had elapsed. A final observation was made at 24 hours. During the observations no change was visually noticed in the stability of the colloid until the one hour mark where the clean vial began to show signs of sedimentation. All of the samples began to show signs of separation by

one and a half hours with sample 1 showing the most, closely followed by 2 and 3. At this time samples 4-7 were indistinguishable with very little separation. As the observations were continued, a trend in separation related to the concentration of isoprene developed around two and a half hours (Figure 25).



**Figure 25.** Colloidal stability observation taken at 2.5 hours. (1) Clean (2) New (3) 10  $\mu\text{L}$  (4) 25  $\mu\text{L}$  (5) 50  $\mu\text{L}$  (6) 100  $\mu\text{L}$  (7) 1000  $\mu\text{L}$ .

The trend in separation between the vials continued over time with vial 1 becoming the first to completely settle out at four hours. After ten hours all but vials 4, 5, and 7 were completely separated. After 24 hours the vials were indistinguishable.

From Figure 25 it is noticeable that the 100  $\mu\text{L}$  sample does not conform to the trend in stability associated with the concentration of isoprene. The advanced precipitation seen in the 100  $\mu\text{L}$  vial is attributed to additional agitation that the other vials did not receive. The additional treatment to vial six was accidental and illustrates the effect of mixing on the stability of the colloidal solution. Zhang and coworkers documented this effect in their study of solvent exchange noting that centrifugation can shorten the amount of time needed for the procedure.<sup>132</sup>

### 3.1.3.2 UV-Vis Spectroscopy – Kinetic

In an effort to quantify the change in stability over time and confirm the results of the benchtop observations, a series of UV-Vis measurements were made to observe the change in absorbance. These observations were made every five minutes over a 12 hour period producing 144 unique spectrum that detail the change in the colloidal stability over time. Figures 26 and 27 are representative of the measurements and show the most dramatic differences in behavior.

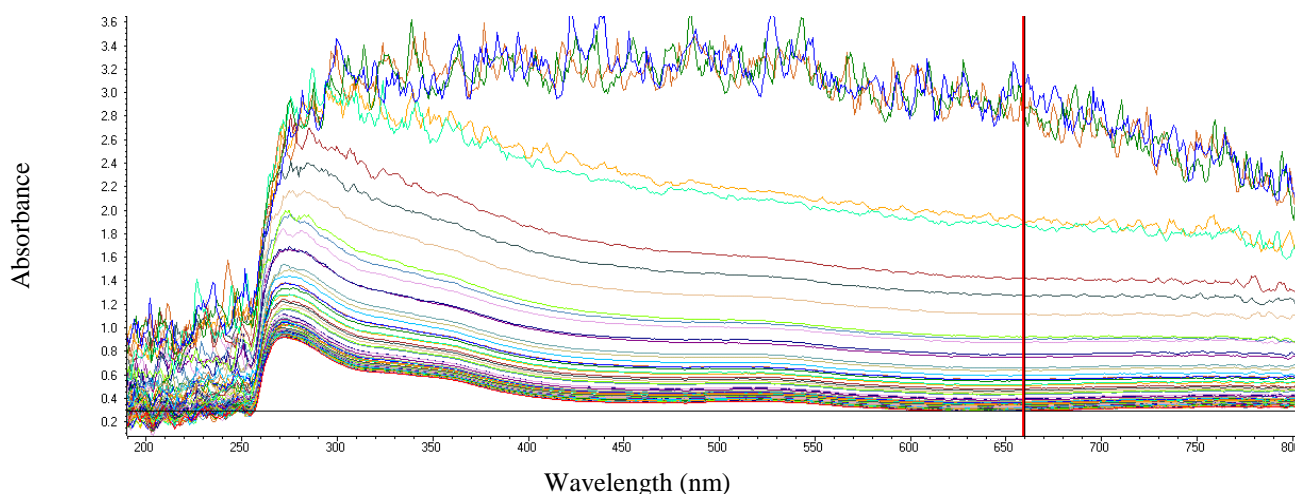


**Figure 26.** Composite depiction of the UV-Vis spectra collected during the kinetics study of the colloidal graphene solution in a “Clean” 8 dram vial. A measurement was taken every 5 minutes over a 12 hour period.

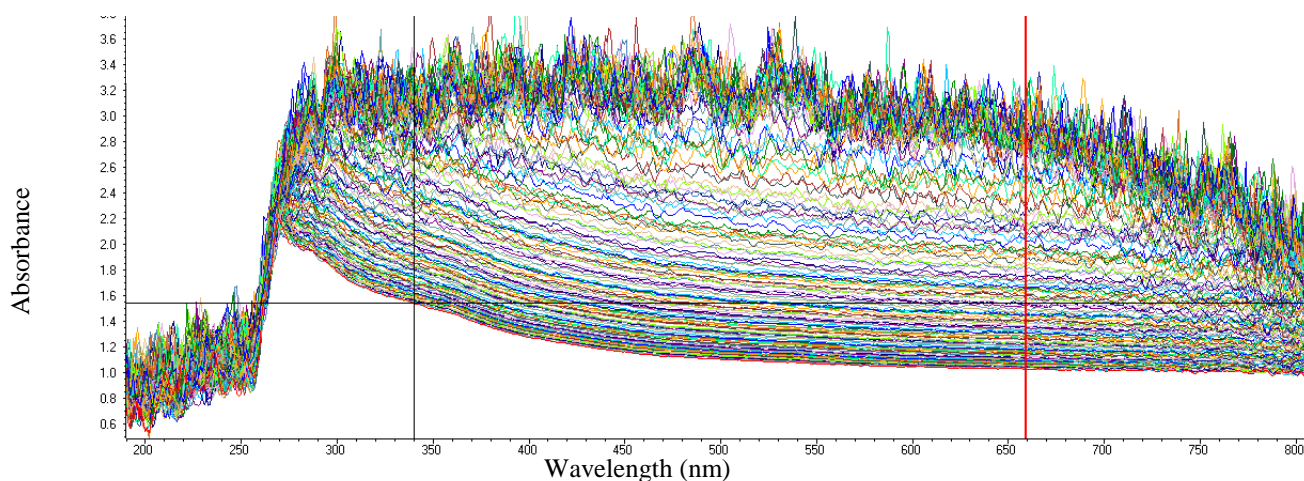


**Figure 27.** Composite depiction of the UV-Vis spectra collected during the kinetics study of the colloidal graphene solution in a “Clean” 8 dram vial stabilized with 1000  $\mu\text{L}$  of isoprene. A measurement was taken every 5 minutes over a 12 hour period.

As noted in Figure 26 the colloidal solution is stable only for a relatively short period of time, as indicated by the small number of spectra with a high absorbance value. Once the solution begins to settle out, the spectra reveal that it is a fairly fast process given the large gaps between sequential spectra. Additionally, the large concentration of spectral lines at low absorbance values indicate that most of the observations occurred after the solution had settled. In contrast, the sample that was stabilized with 1000  $\mu\text{L}$  of isoprene showed a large concentration of spectra with a high absorbance, indicating a delay in precipitation. Additionally, the small gaps between the measurements during the loss of stability indicate it was a slower process than that seen in the clean sample. To directly compare the results of all of the measurements, the absorbance value at 660 nm were plotted for each measurement during each of the experimental sequences (Figure 28).

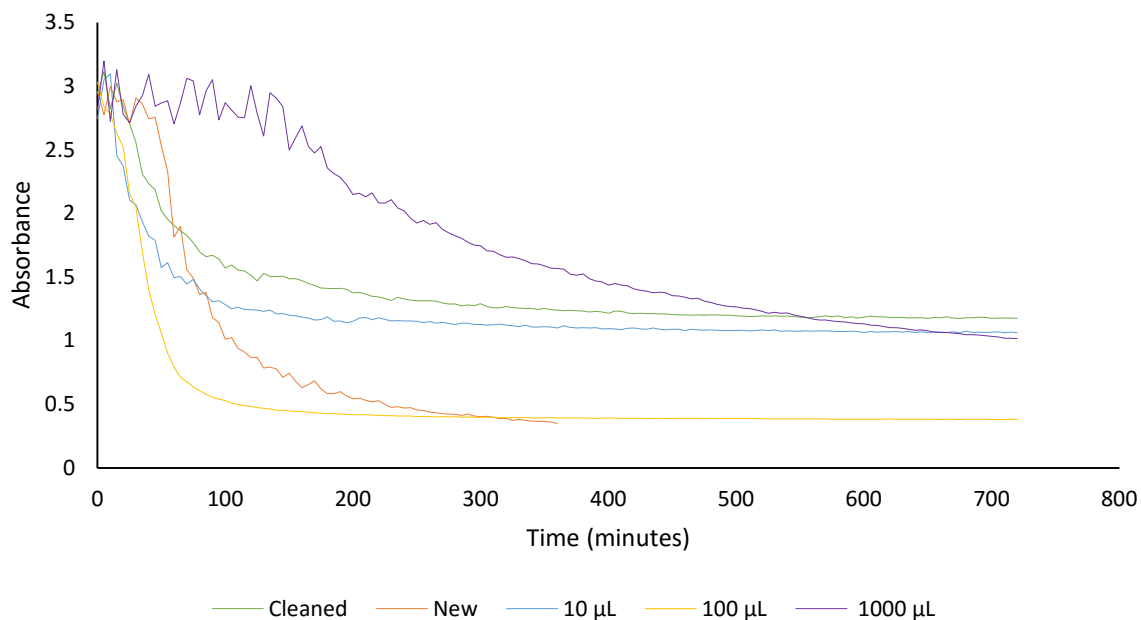


**Figure 28.** Absorbance values over time. The absorbance at 660 nm was plotted for each measurement to graphically depict the stability of each sample over time.

As illustrated in Figure 28, the kinetics study results do not directly match those taken through observations. Similar to the benchtop observations all of the samples showed signs of

separation in the first hour and a half with a decrease in absorption. Also the sample with 1000  $\mu\text{L}$  of isoprene shows the most stability as was experimentally observed. The kinetic results do not confirm the order of separation that was visually observed, although it does confirm that they all have similar stabilities. The reason for the disparity could stem from several sources. The quartz cuvettes used have a tapered shape that allows a smaller volume of analyte to be used. While this allowed for less of a sample to be used, the sample may not have been representative of the larger volume. Additionally with the confined space in the cuvettes, it was observed that particles were still suspended after twelve hours when they would have settled out in the 8 dram vials, this effect may be caused by the confinement and effect the results of the measurements. Additionally, there may have been some heating effects from the instrument. The NanoDrop 2000c used to complete the measurements is equipped with a Xenon flash lamp that takes each measurement in less than 3 seconds. In order to make rapid measurements, the instrument uses between 12-18 W of power, an intensity that may heat the sample and with only 5 minutes in between measurements may not be fully dissipated prior to the next iteration. It is unknown why the data reflects two distinct baselines, however this effect may also be related to the cuvettes. The instrument is focused at 8.5 mm from the bottom of the cuvette for each measurement. Given the behavior of the sample in the confined cuvettes, it is possible that some portion of an aggregated flake was suspended near where the measurements were taken and reflected in the results.

Although the kinetic results did not completely mirror the laboratory observations, they do illustrate a difference in behaviors between the low concentration samples and the high concentration sample. A better sample preparation method to ensure a representative sample and a different cuvette might increase the reliability of future measurements.

## 4.0 CONCLUSION AND FUTURE DIRECTIONS

Through the solvent-based exfoliation of graphite flakes, in a procedure that was adapted from Khan and co-workers,<sup>42</sup> few-layer graphene was successfully produced. The graphene produced was characterized through several of the standard techniques widely used in the study of graphene and included UV-Vis, AFM, and Raman spectroscopy. Together these techniques were able to relay information about the concentration, size, and thickness of the exfoliated graphene. The UV-Vis analysis revealed that the concentration of graphene produced was  $0.545 \text{ mg mL}^{-1}$ . AFM was utilized to investigate the morphology of the flakes that were found to be between 45 and 250 nm in length and less than 12 nm high. Finally, the results of analysis with Raman spectroscopy identified the graphene produced to be few-layer ( $< 5$  layer). In comparison to the parent procedure, which produced few-layer layer graphene at a concentration of  $0.8 \text{ mg mL}^{-1}$  with an average size of  $1 \text{ }\mu\text{m} \times 0.5 \text{ }\mu\text{m}$ , the scaled down experimental procedure detailed above was not as efficient.

After the preparation of graphene it was desirable to replace the solvent, NMP, with a solvent that is more easily manipulated in ambient conditions. Through an experimental process, methanol was selected as the replacement solvent and utilized in a solvent exchange scheme. When the solvent exchange process was scaled up, added stability was noticed within the 8 dram vials that were being used. After several observations, it was determined that this effect was reproducible and sparked a new route for the investigation.

A series of experiments were then carried out to try and isolate the source of the stability. From these observations the greatest difference in stability was seen between the “new” and “cleaned” vials, therefore the possibility of contamination from the manufacturing process was

investigated. To isolate a possible contaminant, HPLC was used to isolate any potential compounds unique to the “new” vials and were subsequently analyzed through MS. This investigation revealed four potential compounds of interest where three were inconclusively identified. The remaining compound is suspected of being a low-molecular weight copolymer consisting mostly of polyisoprene and was investigated further. A  $^1\text{H}$  NMR study was also completed to find additional evidence as to the identity of the contaminant. The results of the  $^1\text{H}$  NMR did not offer any further evidence that polyisoprene was present, however since the contamination is expected to exist at very low concentrations it is suspected that if present it was below the instrument’s detection limit. Based on the analytical evidence acquired it is suspected that a low-molecular weight ( $\sim 1000$ ) copolymer consisting mostly of polyisoprene is the contaminant in the 8 dram vials. The most likely source of this contamination is either the polyvinyl-faced pulp liner of the phenolic screw-top closures supplied with each vial or some other contact with polyisoprene or a natural rubber derivative during the manufacturing process.

In an effort to further understand the stabilization effect of the suspected contaminant on the colloidal graphene solution, a series of observations and a UV-Vis kinetics study were completed. Over a twelve hour observation period a dramatic difference in the stability rates were observed visually. The observations showed that the clean vial precipitated first followed by the new vial and the isoprene samples maintaining their stability the longest. The samples that contained isoprene appeared to have increasing stability roughly proportional to the concentration of the monomer present. These observations were partially confirmed through UV-Vis spectroscopy as the absorbance was measured at regular intervals over a twelve hour period. The most dramatic differences were seen between the sample exposed to  $1000\ \mu\text{L}$  of isoprene and the

other samples. Therefore, the repeatable stabilization effect was observed to be somewhat related to the concentration of the contaminant present.

A mechanism for the stability of a colloidal graphene solution in NMP was suggested by the researchers in Coleman's group at Trinity University as being related to the similarity in surface energy between graphene and the solvent.<sup>129</sup> The importance of similar surface energies was further explored theoretically by Shih and co-workers at the Massachusetts Institute of Technology who suggested that this energy match led to a confined layer of solvent molecules between graphene flakes and added stability.<sup>125</sup> Through this lens, some insight into the behavior of the stability of the colloidal solution and its interaction with a contaminant can be gained.

The solution of graphene prepared in NMP through sonication results in a very stable colloidal solution. It has been reported in the literature that this stability has lasted several months.<sup>39</sup> The stability of this colloidal solution can be explained by the similarity in surface energy between NMP and graphene (Figure 29, green line). In solution the NMP molecules adsorb to the available graphene surfaces and become confined between layers, because of the energy match this arrangement is thermodynamically favorable and the graphene flakes are kept outside the radius where the vdW forces dominate to cause aggregation. The stability will be lost over time as the Brownian motion within the solution will cause the graphene flakes to randomly collide with each other. When the force of these collisions are great enough to dislodge a solvent molecule, the graphene particles will approach each other and the vdW forces will cause aggregation over time.

The solvent exchange scheme was possible because the addition of methanol disrupted the stability of the colloidal system. Solvents such as methanol are useful for the solvent exchange because its surface energy is drastically lower than that of NMP or graphene (Figure 29, red line).

Due to this disparity, when the solution is diluted with methanol it is energetically favorable for the graphene flakes to aggregate rather than bind with methanol. Therefore the rapid loss of stability in the solvent exchange process can be attributed to the change in surface energies.

While the mechanism of stabilization through contamination with polyisoprene is unknown, it is suspected that it can at least partially be explained through a discussion of similar surface energies and steric stability. The surface energy of polyisoprene is reported between 31-34  $\text{mJ m}^{-2}$  (Figure 29, blue line),<sup>149</sup> a value that lies within the range of values reported for the surface energy of graphene.<sup>39</sup> Therefore, it is suspected that the polyisoprene molecules would readily adsorb to the graphene flakes and lower their surface energy over the energetically mismatched methanol molecules. Additionally, the suspected contaminant is a polymer comprised of a chain of repeat units. Even at the low molecular weights suspected as a contaminant, it is likely that the polymers consisted of at least a dozen such repeat units, adding a length far greater than the van der Waals radius of graphene to the affected flake's surface. Therefore it is suspected that these polymer chains added a small degree of steric stability to the solution. At the concentrations observed (Table 1) the stabilization effect is fleeting as the natural motion within the solution will quickly disrupt the polyisoprene stabilization and allow the aggregation of the graphene flakes during the solvent exchange.

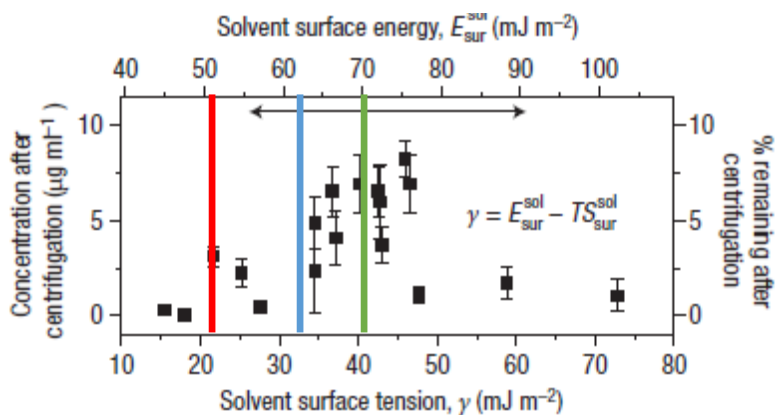


**Figure 29.** Plot of graphite concentration reported by Hernandez *et al.* after centrifugation for a range of solvents versus solvent surface tension.<sup>39</sup> The arrow at the top of the figure shows the approximate range of graphite surface energy as reported in the literature.<sup>39</sup> The red line was added to highlight the surface tension of methanol (22.6 mJ m<sup>-2</sup>).<sup>150</sup> The blue line identifies the surface tension of poly(isoprene) (31-34 mJ m<sup>-2</sup>).<sup>149</sup> The green line identifies the surface tension of NMP (41.26 mJ m<sup>-2</sup>).<sup>130</sup>

Adapted by permission from Macmillan Publishers Ltd: *Nat. Nanotechnol.* **2008**, 3 (9), 563-568, copyright (2008).

In this investigation the monomer isoprene was utilized as a substitute for polyisoprene and a dramatic impact on stability was recorded both through observation and UV-Vis kinetics. It is suspected that the mechanism of stabilization was related to that suggested for polyisoprene, however it is expected that there was much less of a steric effect because of the molecule's smaller size. It is therefore possible to suspect that other small molecules found as laboratory contaminants with a similar surface energy may have a stabilizing effect on a colloidal graphene solution.

The most obvious future direction for the research presented is to accomplish the stability studies with polyisoprene. Through altering the molecular weight it would be possible to quantify the amount of contamination within the "new" vials and also further investigate the theory that steric stabilization is part of the stabilization mechanism observed. Additionally it would be of value to investigate other sources of common laboratory contamination to observe their effect on stability. Such an investigation may lend more evidence to the theory that the surface energy of the contaminant may impact the stability. Such an investigation may be useful to identifying new stabilization methods for a colloidal graphene mixture that may have desirable properties.

As the scientific community continues to answer the call for new and more efficient methods of solvent-based graphene exfoliation to alter the physical properties of the graphene produced as well as scale production for industrial applications, methods of efficiently processing the material will also be needed. A group of organic solvents have been identified as efficient solvents for exfoliation but they have physical properties that make them difficult to handle and limit their industrial application. Solvent exchange has become one such method of removing the high boiling point solvents, but severely reduces the stability of the colloidal stability. For certain uses, the stability of the colloid may be important to the final use of the graphene. Therefore there is a need to gain some understanding of the stabilization mechanism within the colloidal graphene solution. The observations presented in this investigation offer one potential source of added stability and a possible route of investigation to uncover new methods to control the stability of a colloidal graphene mixture.

## REFERENCES

1. National Institute of Standards & Technology., Specifications, Tolerances, and Other Technical Requirements for Weighing and Measuring Devices. 2012 Edition ed.; United States Department of Commerce.
2. Fowler, W. A., Experimental and theoretical nuclear astrophysics: the quest for the origin of the elements. *Rev. Mod. Phys.* **1984**, *56* (2, pt. 1), 149-80.
3. Roebroeks, W.; Villa, P., On the earliest evidence for habitual use of fire in Europe. *Proc. Natl. Acad. Sci. U. S. A.* **2011**, *108* (13), 5209-5214, S5209/1-S5209/30.
4. Jordan, D. K. Ancient Metallurgy. <http://pages.ucsd.edu/~dkjordan/arch/metallurgy.html> (accessed October 19, 2015).
5. Avogadro, A., Essay on a Manner of Determining the Relative Masses of the Elementary Molecules of Bodies, and the Proportions in Which They Enter into These Compounds. *Journal de Physique* **1811**, *73*, 58-76.
6. De Volder, M. F. L.; Tawfick, S. H.; Baughman, R. H.; Hart, A. J., Carbon Nanotubes: Present and Future Commercial Applications. *Science (Washington, DC, U. S.)* **2013**, *339* (6119), 535-539.
7. Kroto, H. W.; Heath, J. R.; O'Brien, S. C.; Curl, R. F.; Smalley, R. E., C<sub>60</sub>: buckminsterfullerene. *Nature (London)* **1985**, *318* (6042), 162-3.
8. Kroto, H. W.; Allaf, A. W.; Balm, S. P., C<sub>60</sub>: Buckminsterfullerene. *Chem. Rev.* **1991**, *91* (6), 1213-35.
9. Iijima, S., Helical microtubules of graphitic carbon. *Nature (London)* **1991**, *354* (6348), 56-8.
10. Pugno, N. M.; Bosia, F.; Carpinteri, A., Multiscale stochastic simulations for tensile testing of nanotube-based macroscopic cables. *Small* **2008**, *4* (8), 1044-52.
11. Katsnelson, M. I., Graphene: carbon in two dimensions. *Mater. Today (Oxford, U. K.)* **2007**, *10* (1-2), 20-27.
12. Dreyer, D. R.; Ruoff, R. S.; Bielawski, C. W., From Conception to Realization: An Historical Account of Graphene and Some Perspectives for Its Future. *Angew. Chem., Int. Ed.* **2010**, *49* (49), 9336-9344.
13. Wallace, P. R., The Band Theory of Graphite. *Physical Review* **1947**, *71* (9), 622-634.
14. Boehm, H. P.; Clauss, A.; Fischer, G. O.; Hofmann, U., The adsorption behavior of very thin carbon films. *Z. Anorg. Allg. Chem.* **1962**, *316*, 119-27.
15. Boehm, H. P.; Setton, R.; Stumpp, E., Nomenclature and terminology of graphite intercalation compounds. *Carbon* **1986**, *24* (2), 241-5.
16. Boehm, H.-P.; Setton, R.; Stumpp, E., Nomenclature and terminology of graphite intercalation compounds. *Pure Appl. Chem.* **1994**, *66* (9), 1893-901.
17. Novoselov, K. S.; Geim, A. K.; Morozov, S. V.; Jiang, D.; Zhang, Y.; Dubonos, S. V.; Grigorieva, I. V.; Firsov, A. A., Electric Field Effect in Atomically Thin Carbon Films. *Science (Washington, DC, U. S.)* **2004**, *306* (5696), 666-669.
18. Nobelprize.org The Nobel Prize in Physics 2010. [http://www.nobelprize.org/nobel\\_prizes/physics/laureates/2010/](http://www.nobelprize.org/nobel_prizes/physics/laureates/2010/) (accessed August 14, 2015).

19. Novoselov, K. S.; Geim, A. K.; Morozov, S. V.; Jiang, D.; Katsnelson, M. I.; Grigorieva, I. V.; Dubonos, S. V.; Firsov, A. A., Two-dimensional gas of massless Dirac fermions in graphene. *Nature (London, U. K.)* **2005**, *438* (7065), 197-200.
20. Ahn, J.-H.; Hong, B. H., Graphene for displays that bend. *Nat. Nanotechnol.* **2014**, *9* (10), 737-738.
21. Liu, J., Charging graphene for energy. *Nat. Nanotechnol.* **2014**, *9* (10), 739-741.
22. De, S.; Coleman, J. N., Are There Fundamental Limitations on the Sheet Resistance and Transmittance of Thin Graphene Films? *ACS Nano* **2010**, *4* (5), 2713-2720.
23. Nair, R. R.; Blake, P.; Grigorenko, A. N.; Novoselov, K. S.; Booth, T. J.; Stauber, T.; Peres, N. M. R.; Geim, A. K., Fine Structure Constant Defines Visual Transparency of Graphene. *Science (Washington, DC, U. S.)* **2008**, *320* (5881), 1308.
24. Bohm, S., Graphene against corrosion. *Nat. Nanotechnol.* **2014**, *9* (10), 741-742.
25. Tsetseris, L.; Pantelides, S. T., Graphene: An impermeable or selectively permeable membrane for atomic species? *Carbon* **2014**, *67*, 58-63.
26. Joshi, R. K.; Carbone, P.; Wang, F. C.; Kravets, V. G.; Su, Y.; Grigorieva, I. V.; Wu, H. A.; Geim, A. K.; Nair, R. R., Precise and Ultrafast Molecular Sieving Through Graphene Oxide Membranes. *Science (Washington, DC, U. S.)* **2014**, *343* (6172), 752-754.
27. Surwade, S. P.; Mahurin, S. M.; Smirnov, S. N.; Vlassiuk, I. V.; Unocic, R. R.; Veith, G. M.; Dai, S., Water desalination using nanoporous single-layer graphene. *Nat Nanotechnol* **2015**.
28. Kostarelos, K.; Novoselov, K. S., Graphene devices for life. *Nat. Nanotechnol.* **2014**, *9* (10), 744-745.
29. Siochi, E. J., Graphene in the sky and beyond. *Nat. Nanotechnol.* **2014**, *9* (10), 745-747.
30. Ambrosi, A.; Chua, C. K.; Bonanni, A.; Pumera, M., Electrochemistry of graphene and related materials. *Chem. Rev. (Washington, DC, U. S.)* **2014**, *114* (14), 7150-7188.
31. Khan, U.; O'Neill, A.; Lotya, M.; De, S.; Coleman, J. N., High-Concentration Solvent Exfoliation of Graphene. *Small* **2010**, *6* (7), 864-871.
32. Su, C.-Y.; Lu, A.-Y.; Xu, Y.; Chen, F.-R.; Khlobystov, A. N.; Li, L.-J., High-quality thin graphene films from fast electrochemical exfoliation. *ACS Nano* **2011**, *5* (3), 2332-2339.
33. Marcano, D. C.; Kosynkin, D. V.; Berlin, J. M.; Sinitskii, A.; Sun, Z.; Slesarev, A.; Alemany, L. B.; Lu, W.; Tour, J. M., Improved Synthesis of Graphene Oxide. *ACS Nano* **2010**, *4* (8), 4806-4814.
34. Cano-Marquez, A. G.; Rodriguez-Macias, F. J.; Campos-Delgado, J.; Espinosa-Gonzalez, C. G.; Tristan-Lopez, F.; Ramirez-Gonzalez, D.; Cullen, D. A.; Smith, D. J.; Terrones, M.; Vega-Cantu, Y. I., Ex-MWNTs: Graphene Sheets and Ribbons Produced by Lithium Intercalation and Exfoliation of Carbon Nanotubes. *Nano Lett.* **2009**, *9* (4), 1527-1533.
35. Yang, X.; Dou, X.; Rouhanipour, A.; Zhi, L.; Raeder, H. J.; Muellen, K., Two-dimensional graphene nanoribbons. *J. Am. Chem. Soc.* **2008**, *130* (13), 4216-4217.
36. Wu, Z.-S.; Ren, W.; Gao, L.; Liu, B.; Jiang, C.; Cheng, H.-M., Synthesis of high-quality graphene with a pre-determined number of layers. *Carbon* **2009**, *47* (2), 493-499.
37. Reina, A.; Jia, X.; Ho, J.; Nezich, D.; Son, H.; Bulovic, V.; Dresselhaus, M. S.; Kong, J., Large Area, Few-Layer Graphene Films on Arbitrary Substrates by Chemical Vapor Deposition. *Nano Lett.* **2009**, *9* (1), 30-35.
38. Somani, P. R.; Somani, S. P.; Umeno, M., Planer nano-graphenes from camphor by CVD. *Chem. Phys. Lett.* **2006**, *430* (1-3), 56-59.

39. Hernandez, Y.; Nicolosi, V.; Lotya, M.; Blighe, F. M.; Sun, Z.; De, S.; McGovern, I. T.; Holland, B.; Byrne, M.; Gun'Ko, Y. K.; Boland, J. J.; Niraj, P.; Duesberg, G.; Krishnamurthy, S.; Goodhue, R.; Hutchison, J.; Scardaci, V.; Ferrari, A. C.; Coleman, J. N., High-yield production of graphene by liquid-phase exfoliation of graphite. *Nat. Nanotechnol.* **2008**, *3* (9), 563-568.
40. Blake, P.; Brimicombe, P. D.; Nair, R. R.; Booth, T. J.; Jiang, D.; Schedin, F.; Ponomarenko, L. A.; Morozov, S. V.; Gleeson, H. F.; Hill, E. W.; Geim, A. K.; Novoselov, K. S., Graphene-Based Liquid Crystal Device. *Nano Lett.* **2008**, *8* (6), 1704-1708.
41. Hernandez, Y.; Lotya, M.; Rickard, D.; Bergin, S. D.; Coleman, J. N., Measurement of Multicomponent Solubility Parameters for Graphene Facilitates Solvent Discovery. *Langmuir* **2010**, *26* (5), 3208-3213.
42. Khan, U.; Porwal, H.; O'Neill, A.; Nawaz, K.; May, P.; Coleman, J. N., Solvent-Exfoliated Graphene at Extremely High Concentration. *Langmuir* **2011**, *27* (15), 9077-9082.
43. Valles, C.; Drummond, C.; Saadaoui, H.; Furtado, C. A.; He, M.; Roubeau, O.; Ortolani, L.; Monthieux, M.; Penicaud, A., Solutions of negatively charged graphene sheets and ribbons. *J. Am. Chem. Soc.* **2008**, *130* (47), 15802-15804.
44. Varrla, E.; Paton, K. R.; Backes, C.; Harvey, A.; Smith, R. J.; McCauley, J.; Coleman, J. N., Turbulence-assisted shear exfoliation of graphene using household detergent and a kitchen blender. *Nanoscale* **2014**, *6* (20), 11810-11819.
45. Lotya, M.; King, P. J.; Khan, U.; De, S.; Coleman, J. N., High-Concentration, Surfactant-Stabilized Graphene Dispersions. *ACS Nano* **2010**, *4* (6), 3155-3162.
46. Ricardo, K. B.; Sendeki, A.; Liu, H., Surfactant-free exfoliation of graphite in aqueous solutions. *Chem. Commun. (Cambridge, U. K.)* **2014**, *50* (21), 2751-2754.
47. Green, A. A.; Hersam, M. C., Solution Phase Production of Graphene with Controlled Thickness via Density Differentiation. *Nano Lett.* **2009**, *9* (12), 4031-4036.
48. Wang, L.; Ambrosi, A.; Pumera, M., Could Carbonaceous Impurities in Reduced Graphenes be Responsible for Some of Their Extraordinary Electrocatalytic Activities? *Chem. - Asian J.* **2013**, *8* (6), 1200-1204.
49. Wang, G.; Wang, B.; Park, J.; Wang, Y.; Sun, B.; Yao, J., Highly efficient and large-scale synthesis of graphene by electrolytic exfoliation. *Carbon* **2009**, *47* (14), 3242-3246.
50. Alanyalioglu, M.; Segura, J. J.; Oro-Sole, J.; Casan-Pastor, N., The synthesis of graphene sheets with controlled thickness and order using surfactant-assisted electrochemical processes. *Carbon* **2012**, *50* (1), 142-152.
51. Low, C. T. J.; Walsh, F. C.; Chakrabarti, M. H.; Hashim, M. A.; Hussain, M. A., Electrochemical approaches to the production of graphene flakes and their potential applications. *Carbon* **2013**, *54*, 1-21.
52. Brodie, B. C., On the atomic weight of graphite. *Philosophical Transactions of the Royal Society of London* **1859**, 249-259.
53. Staudenmaier, L., Preparation of graphitic acid. *Ber.* **1898**, *31*, 1481-7.
54. Hummers, W. S., Jr.; Offeman, R. E., Preparation of graphitic oxide. *J. Am. Chem. Soc.* **1958**, *80*, 1339.
55. Stephenson, J. J.; Sadana, A. K.; Higginbotham, A. L.; Tour, J. M., Highly Functionalized and Soluble Multiwalled Carbon Nanotubes by Reductive Alkylation and Arylation: The Billups Reaction. *Chem. Mater.* **2006**, *18* (19), 4658-4661.

56. Chen, L.; Hernandez, Y.; Feng, X.; Muellen, K., From Nanographene and Graphene Nanoribbons to Graphene Sheets: Chemical Synthesis. *Angew. Chem., Int. Ed.* **2012**, *51* (31), 7640-7654.
57. Wu, J.; Pisula, W.; Muellen, K., Graphenes as potential material for electronics. *Chem. Rev. (Washington, DC, U. S.)* **2007**, *107* (3), 718-747.
58. Cai, J.; Ruffieux, P.; Jaafar, R.; Bieri, M.; Braun, T.; Blankenburg, S.; Muoth, M.; Seitsonen, A. P.; Saleh, M.; Feng, X.; Muellen, K.; Fasel, R., Atomically precise bottom-up fabrication of graphene nanoribbons. *Nature (London, U. K.)* **2010**, *466* (7305), 470-473.
59. Berger, C.; Song, Z.; Li, T.; Li, X.; Ogbazghi, A. Y.; Feng, R.; Dai, Z.; Marchenkov, A. N.; Conrad, E. H.; First, P. N.; de Heer, W. A., Ultrathin epitaxial graphite: two-dimensional electron gas properties and a route toward graphene-based nanoelectronics. *J. Phys. Chem. B* **2004**, *108* (52), 19912-19916.
60. Yudasaka, M.; Kikuchi, R.; Matsui, T.; Ohki, Y.; Yoshimura, S.; Ota, E., Specific conditions for Ni catalyzed carbon nanotube growth by chemical vapor deposition. *Appl. Phys. Lett.* **1995**, *67* (17), 2477-9.
61. Wassei, J. K.; Mecklenburg, M.; Torres, J. A.; Fowler, J. D.; Regan, B. C.; Kaner, R. B.; Weiller, B. H., Chemical Vapor Deposition of Graphene on Copper from Methane, Ethane and Propane: Evidence for Bilayer Selectivity. *Small* **2012**, *8* (9), 1415-1422.
62. Ruan, G.; Sun, Z.; Peng, Z.; Tour, J. M., Growth of graphene from food, insects, and waste. *ACS Nano* **2011**, *5* (9), 7601-7607.
63. Sutter, P. W.; Flege, J.-I.; Sutter, E. A., Epitaxial graphene on ruthenium. *Nat. Mater.* **2008**, *7* (5), 406-411.
64. Vitchev, R.; Malesevic, A.; Petrov, R. H.; Kemps, R.; Mertens, M.; Vanhulsel, A.; van Haesendonck, C., Initial stages of few-layer graphene growth by microwave plasma-enhanced chemical vapour deposition. *Nanotechnology* **2010**, *21* (9), 095602/1-095602/7.
65. Coraux, J.; N'Diaye, A. T.; Busse, C.; Michely, T., Structural Coherency of Graphene on Ir(111). *Nano Lett.* **2008**, *8* (2), 565-570.
66. Li, X.; Cai, W.; An, J.; Kim, S.; Nah, J.; Yang, D.; Piner, R.; Velamakanni, A.; Jung, I.; Tutuc, E.; Banerjee, S. K.; Colombo, L.; Ruoff, R. S., Large-Area Synthesis of High-Quality and Uniform Graphene Films on Copper Foils. *Science (Washington, DC, U. S.)* **2009**, *324* (5932), 1312-1314.
67. Kim, K. S.; Zhao, Y.; Jang, H.; Lee, S. Y.; Kim, J. M.; Kim, K. S.; Ahn, J.-H.; Kim, P.; Choi, J.-Y.; Hong, B. H., Large-scale pattern growth of graphene films for stretchable transparent electrodes. *Nature (London, U. K.)* **2009**, *457* (7230), 706-710.
68. Bae, S.; Kim, H.; Lee, Y.; Xu, X.; Park, J.-S.; Zheng, Y.; Balakrishnan, J.; Lei, T.; Kim, H. R.; Song, Y. I.; Kim, Y.-J.; Kim, K. S.; Oezylmaz, B.; Ahn, J.-H.; Hong, B. H.; Iijima, S., Roll-to-roll production of 30-inch graphene films for transparent electrodes. *Nat. Nanotechnol.* **2010**, *5* (8), 574-578.
69. Kang, J.; Shin, D.; Bae, S.; Hong, B. H., Graphene transfer: key for applications. *Nanoscale* **2012**, *4* (18), 5527-5537.
70. Zhu, X.; Yuan, H.; Hight Walker, A. R.; Liu, Z.; Peng, L.-m.; Richter, C. A.; w, Toward Clean and Crackless Transfer of Graphene. *ACS Nano* **2011**, *5* (11), 9144-9153.
71. Novoselov, K. S.; Fal'ko, V. I.; Colombo, L.; Gellert, P. R.; Schwab, M. G.; Kim, K., A roadmap for graphene. *Nature (London, U. K.)* **2012**, *490* (7419), 192-200.

72. Farmer, D. B.; Chiu, H.-Y.; Lin, Y.-M.; Jenkins, K. A.; Xia, F.; Avouris, P., Utilization of a Buffered Dielectric to Achieve High Field-Effect Carrier Mobility in Graphene Transistors. *Nano Lett.* **2009**, *9* (12), 4474-4478.
73. Li, X.; Zhu, Y.; Cai, W.; Borysiak, M.; Han, B.; Chen, D.; Piner, R. D.; Colombo, L.; Ruoff, R. S., Transfer of Large-Area Graphene Films for High-Performance Transparent Conductive Electrodes. *Nano Lett.* **2009**, *9* (12), 4359-4363.
74. Chen, S.; Brown, L.; Levendorf, M.; Cai, W.; Ju, S.-Y.; Edgeworth, J.; Li, X.; Magnuson, C. W.; Velamakanni, A.; Piner, R. D.; Kang, J.; Park, J.; Ruoff, R. S., Oxidation resistance of graphene-coated Cu and Cu/Ni alloy. *ACS Nano* **2011**, *5* (2), 1321-1327.
75. Meyer, J. C.; Geim, A. K.; Katsnelson, M. I.; Novoselov, K. S.; Obergfell, D.; Roth, S.; Girit, C.; Zettl, A., On the roughness of single- and bi-layer graphene membranes. *Solid State Commun.* **2007**, *143* (1-2), 101-109.
76. Coleman, J. N., Liquid exfoliation of defect-free graphene. *Acc. Chem. Res.* **2013**, *46* (1), 14-22.
77. Malard, L. M.; Pimenta, M. A.; Dresselhaus, G.; Dresselhaus, M. S., Raman spectroscopy in graphene. *Phys. Rep.* **2009**, *473* (5-6), 51-87.
78. Thomas, N. C., The early history of spectroscopy. *J. Chem. Educ.* **1991**, *68* (8), 631-4.
79. Varian, US-Vis Varian Cary 50 Series Spectrometer.
80. Ingle, J. D.; Crouch, S. R., *Spectrochemical Analysis*. Prentice Hall: Englewood Cliffs, NJ, 1988; p 590.
81. Ashkenaz, D. E.; Paige Hall, W.; Haynes, C. L.; Hicks, E. M.; McFarland, A. D.; Sherry, L. J.; Stuart, D. A.; Wheeler, K. E.; Yonzon, C. R.; Zhao, J.; Godwin, H. A.; Van Duyne, R. P., Coffee Cup Atomic Force Microscopy. *J. Chem. Educ.* **2010**, *87* (3), 306-307.
82. Nobelprize.org The Nobel Prize in Physics 1986.  
[http://www.nobelprize.org/nobel\\_prizes/physics/laureates/1986/](http://www.nobelprize.org/nobel_prizes/physics/laureates/1986/) (accessed August 21, 2015).
83. Binnig, G.; Rohrer, H.; Gerber, C.; Weibel, E., Surface studies by scanning tunneling microscopy. *Phys. Rev. Lett.* **1982**, *49* (1), 57-61.
84. Chen, C. J., *Introduction to scanning tunneling microscopy*. Oxford University Press: 2008.
85. Binnig, G.; Quate, C. F., Atomic Force Microscope. *Phys. Rev. Lett.* **1986**, *56* (9), 930-933.
86. Giessibl, F. J., AFM's path to atomic resolution. *Mater. Today (Oxford, U. K.)* **2005**, *8* (5), 32-41.
87. Barattin, R.; Voyer, N., Chemical modifications of AFM tips for the study of molecular recognition events. *Chem. Commun. (Cambridge, U. K.)* **2008**, (13), 1513-1532.
88. Zhong, Q.; Inniss, D.; Kjoller, K.; Elings, V. B., Fractured polymer/silica fiber surface studied by tapping mode atomic force microscopy. *Surf. Sci.* **1993**, *290* (1-2), L688-L692.
89. Rugar, D.; Hansma, P., Atomic force microscopy. *Phys. Today* **1990**, *43* (10), 23-30.
90. Lotya, M.; Hernandez, Y.; King, P. J.; Smith, R. J.; Nicolosi, V.; Karlsson, L. S.; Blighe, F. M.; De, S.; Wang, Z.; McGovern, I. T.; Duesberg, G. S.; Coleman, J. N., Liquid Phase Production of Graphene by Exfoliation of Graphite in Surfactant/Water Solutions. *J. Am. Chem. Soc.* **2009**, *131* (10), 3611-3620.
91. Wang, Y. Y.; Ni, Z. H.; Shen, Z. X.; Wang, H. M.; Wu, Y. H., Interference enhancement of Raman signal of graphene. *Appl. Phys. Lett.* **2008**, *92* (4), 043121/1-043121/3.
92. Raman, C. V.; Krishnan, K. S., A new type of secondary radiation. *Nature (London, U. K.)* **1928**, *121*, 501-2.
93. Tuinstra, F.; Koenig, J. L., Raman spectrum of graphite. *J. Chem. Phys.* **1970**, *53* (3), 1126-30.

94. Vidano, R. P.; Fischbach, D. B.; Willis, L. J.; Loehr, T. M., Observation of Raman band shifting with excitation wavelength for carbons and graphites. *Solid State Commun.* **1981**, 39 (2), 341-4.
95. Ferrari, A. C., Raman spectroscopy of graphene and graphite: Disorder, electron-phonon coupling, doping and nonadiabatic effects. *Solid State Commun.* **2007**, 143 (1-2), 47-57.
96. Graf, D.; Molitor, F.; Ensslin, K.; Stampfer, C.; Jungen, A.; Hierold, C.; Wirtz, L., Spatially Resolved Raman Spectroscopy of Single- and Few-Layer Graphene. *Nano Lett.* **2007**, 7 (2), 238-242.
97. Ferrari, A. C.; Meyer, J. C.; Scardaci, V.; Casiraghi, C.; Lazzeri, M.; Mauri, F.; Piscanec, S.; Jiang, D.; Novoselov, K. S.; Roth, S.; Geim, A. K., Raman Spectrum of Graphene and Graphene Layers. *Phys. Rev. Lett.* **2006**, 97 (18), 187401/1-187401/4.
98. Casiraghi, C.; Hartschuh, A.; Qian, H.; Piscanec, S.; Georgi, C.; Fasoli, A.; Novoselov, K. S.; Basko, D. M.; Ferrari, A. C., Raman Spectroscopy of Graphene Edges. *Nano Lett.* **2009**, 9 (4), 1433-1441.
99. Atkins, P.; Jones, L., *Chemical Principles: The Quest for Insight*. Freeman: New York, NY, 1998.
100. Skoog, D. A.; Holler, F. J.; Crouch, S. R., *Principles of Instrumental Analysis*. 6th ed.; Thomson Brooks/Cole: Canada, 2007.
101. Robards, K.; Haddad, P. R.; Jackson, P. E., *Principles and Practice of Modern Chromatographic Methods*. Elsevier Academic Press: San Deiego, CA, 2004.
102. Giddings, J. C., *Unified Separation Science*. John Wiley & Sons: New York, NY, 1991.
103. Tswett, M., Physical-chemical studies on chlorophyll. Adsorptions. *Ber. Dtsch. Bot. Ges.* **1906**, 24, 316-323.
104. Tswett, M., Adsorption analysis and chromatographic methods. Application to chlorophyll chemistry. *Ber. Dtsch. Bot. Ges.* **1906**, 24, 384-393.
105. Spedding, F. H.; Fulmer, E. I.; Butler, T. A.; Gladrow, E. M.; Gobush, M.; Porter, P. E.; Powell, J. E.; Wright, J. M., The separation of rare earths by ion exchange. III. Pilot plant scale separations. *J. Am. Chem. Soc.* **1947**, 69, 2812-18.
106. Martin, A. J. P.; Synge, R. L. M., A new form of chromatogram employing two liquid phases. I. A theory of chromatography. II. Application to the microdetermination of the higher monoamino acids in proteins. *Biochem. J.* **1941**, 35, 1358-68.
107. Nobelprize.org The Nobel Prize in Chemistry 1952.  
[http://www.nobelprize.org/nobel\\_prizes/chemistry/laureates/1952/](http://www.nobelprize.org/nobel_prizes/chemistry/laureates/1952/) (accessed October 23, 2015).
108. Golay, M. J. E., Vapor-phase chromatography and the telegrapher's equation. *Anal. Chem.* **1957**, 29, 928-32.
109. Howard, G. A.; Martin, A. J. P., Separation of the C12-C18 fatty acids by reversed-phase partition chromatography. *Biochem. J.* **1950**, 46, 532-8.
110. Alm, R. S.; Williams, R. J. P.; Tiselius, A., Gradient elution analysis. I. A general treatment. *Acta Chem. Scand.* **1952**, 6, 826-36.
111. Griffiths, J., A brief history of mass spectrometry. *Anal. Chem. (Washington, DC, U. S.)* **2008**, 80 (15), 5678-5683.
112. Cafiso, D. S. Intro to Mass Spectrometry.  
<http://orgchem.colorado.edu/Spectroscopy/MS/inletsys.html> (accessed September 30, 2015).
113. Yamashita, M.; Fenn, J. B., Electrospray ion source. Another variation on the free-jet theme. *J. Phys. Chem.* **1984**, 88 (20), 4451-9.

114. Nobelprize.org The Nobel Prize in Chemistry 2002.  
[http://www.nobelprize.org/nobel\\_prizes/chemistry/laureates/2002/](http://www.nobelprize.org/nobel_prizes/chemistry/laureates/2002/) (accessed November 9, 2015).
115. National Institute of Standards & Technology., NIST Chemistry WebBook.  
<http://webbook.nist.gov/chemistry/> (accessed October 17, 2015).
116. Gerlach, W.; Stern, O., Der experimentelle Nachweis der Richtungsquantelung im Magnetfeld. *Z. Physik* **1922**, 9 (1), 349-352.
117. Becker, E. D., A Brief History of Nuclear Magnetic Resonance. *Analytical Chemistry* **1993**, 65 (6), 295A-302A.
118. Nobelprize.org The Nobel Prize in Physics 1944.  
[http://www.nobelprize.org/nobel\\_prizes/physics/laureates/1944/](http://www.nobelprize.org/nobel_prizes/physics/laureates/1944/) (accessed October 13, 2015).
119. Bloch, F.; Hansen, W. W.; Packard, M., Nuclear Induction. *Physical Review* **1946**, 69 (3-4), 127-127.
120. Purcell, E. M.; Torrey, H. C.; Pound, R. V., Resonance absorption by nuclear magnetic moments in a solid. *Phys. Rev.* **1946**, 69, 37-8.
121. Nobelprize.org The Nobel Prize in Physics 1952.  
[http://www.nobelprize.org/nobel\\_prizes/physics/laureates/1952/](http://www.nobelprize.org/nobel_prizes/physics/laureates/1952/) (accessed October 13, 2015).
122. Bhattacharya, A., Chemistry: Breaking the billion-hertz barrier. *Nature (London, U. K.)* **2010**, 463 (7281), 605-606.
123. Agrawal, D. C., *Introduction to Nanoscience and Nanomaterials*. World Scientific: Singapore, 2013.
124. IUPAC., Brownian motion. <http://goldbook.iupac.org/B00748.html> (accessed October 25, 2015).
125. Shih, C.-J.; Lin, S.; Strano, M. S.; Blankschtein, D., Understanding the Stabilization of Liquid-Phase-Exfoliated Graphene in Polar Solvents: Molecular Dynamics Simulations and Kinetic Theory of Colloid Aggregation. *Journal of the American Chemical Society* **2010**, 132 (41), 14638-14648.
126. Jones, J. R., The determination of molecular fields (II) From the equation of state of a gas. *Proc. R. Soc. London, Ser. A* **1924**, 106, 463-77.
127. Naeem, R. Lennard-Jones Potential.  
[http://chemwiki.ucdavis.edu/Physical\\_Chemistry/Physical\\_Properties\\_of\\_Matter/Intermolecular\\_Forces/Lennard-Jones\\_Potential](http://chemwiki.ucdavis.edu/Physical_Chemistry/Physical_Properties_of_Matter/Intermolecular_Forces/Lennard-Jones_Potential) (accessed October 31, 2015).
128. Naeem, R. Lennard-Jones Potential.  
[http://chemwiki.ucdavis.edu/Physical\\_Chemistry/Physical\\_Properties\\_of\\_Matter/Intermolecular\\_Forces/Lennard-Jones\\_Potential](http://chemwiki.ucdavis.edu/Physical_Chemistry/Physical_Properties_of_Matter/Intermolecular_Forces/Lennard-Jones_Potential) (accessed November 8, 2015).
129. Wang, J.; Hernandez, Y.; Lotya, M.; Coleman, J. N.; Blau, W. J., Broadband Nonlinear Optical Response of Graphene Dispersions. *Adv. Mater. (Weinheim, Ger.)* **2009**, 21 (23), 2430-2435.
130. Garcia-Abuin, A.; Gomez-Diaz, D.; Navaza, J. M.; Vidal-Tato, I., Surface Tension of Aqueous Solutions of Short N-Alkyl-2-pyrrolidinones. *J. Chem. Eng. Data* **2008**, 53 (11), 2671-2674.
131. Sigma-Aldrich 1-Methyl-2-pyrrolidinone.  
<http://www.sigmaaldrich.com/catalog/product/sial/328634?lang=en&region=US> (accessed August 29, 2015).

132. Zhang, X.; Coleman, A. C.; Katsonis, N.; Browne, W. R.; van Wees, B. J.; Feringa, B. L., Dispersion of graphene in ethanol using a simple solvent exchange method. *Chem. Commun. (Cambridge, U. K.)* **2010**, 46 (40), 7539-7541.
133. Sigma-Aldrich Methanol. <http://www.sigmaaldrich.com/chemistry/solvents/methanol-center.html> (accessed August 29, 2015).
134. Armarego, W.; Chai, C., *Purification of Laboratory Chemicals*. 7th ed.; Elsevier: United States, 2013.
135. Kongkaew, A.; Wootthikanokkhan, J., Polymerization of isoprene by using benzyl diethyldithiocarbamate as an iniferter. *ScienceAsia* **1999**, 25 (1), 35-41.
136. Jitchum, V.; Perrier, S., Living Radical Polymerization of Isoprene via the RAFT Process. *Macromolecules* **2007**, 40 (5), 1408-1412.
137. National Center for Biotechnology Information., Isoprene. <http://pubchem.ncbi.nlm.nih.gov/compound/isoprene#section=Information-Sources> (accessed November 3, 2015).
138. Li, D.; Mueller, M. B.; Gilje, S.; Kaner, R. B.; Wallace, G. G., Processable aqueous dispersions of graphene nanosheets. *Nat. Nanotechnol.* **2008**, 3 (2), 101-105.
139. Cancado, L. G.; Pimenta, M. A.; Neves, B. R. A.; Dantas, M. S. S.; Jorio, A., Influence of the Atomic Structure on the Raman Spectra of Graphite Edges. *Phys. Rev. Lett.* **2004**, 93 (24), 247401/1-247401/4.
140. Hale, L., Fisher Customer Service Inquiry. Kurpiel, C., Ed. 2015.
141. Schoenberg, E.; Marsh, H. A.; Walters, S. J.; Saltman, W. M., Polyisoprene. *Rubber Chem. Technol.* **1979**, 52 (3), 526-604.
142. Rozentsvet, V. A.; Kozlov, V. G.; Ziganshina, E. F.; Boreiko, N. P.; Kostjuk, S. V., Cationic polymerization of isoprene using zinc halides as co-initiators: towards well-defined oligo(isoprene)s under mild conditions. *Polym. Int.* **2013**, 62 (5), 817-826.
143. Scientific, F. Fisherbrand™ Class B Clear Glass Threaded Vials with Closures Attached Fisherbrand™ Class B Clear Glass Threaded Vials with Closures Attached <https://www.fishersci.com/shop/products/fisherbrand-class-b-clear-glass-threaded-vials-closures-attached-12/p-204692#tab2> (accessed October 31, 2015).
144. Gottlieb, H. E.; Kotlyar, V.; Nudelman, A., NMR chemical shifts of common laboratory solvents as trace impurities. *J. Org. Chem.* **1997**, 62 (21), 7512-7515.
145. Connolly, M. L., Solvent-accessible surfaces of proteins and nucleic acids. *Science (Washington, D. C., 1883-)* **1983**, 221 (4612), 709-13.
146. Connolly, M. L., Analytical molecular surface calculation. *J. Appl. Crystallogr.* **1983**, 16 (5), 548-58.
147. Connolly, M. L., The molecular surface package. *J. Mol. Graphics* **1993**, 11 (2), 139-41.
148. Pacios, L. F., ARVOMOL/CONTOUR: Molecular surface areas and volumes on personal computers. *Computers & Chemistry* **1994**, 18 (4), 377-385.
149. Diversified Enterprises., Surface Energy Data - Assorted Polymers. 2015.
150. Methanol Institute., Properties of Methanol. <http://www.methanol.org/Technical-Information/Properties-of-Methanol.aspx> (accessed October 28, 2015).